

DYNAMICAL APPROACH STUDY OF SPURIOUS STEADY-STATE NUMERICAL SOLUTIONS OF NONLINEAR DIFFERENTIAL EQUATIONS II. GLOBAL ASYMPTOTIC BEHAVIOR OF TIME DISCRETIZATIONS*

H. C. YEE

*Fluid Dynamics Division, NASA Ames Research Center,
Moffett Field, CA, 94035, USA*

P. K. SWEBY[†]

*Department of Mathematics, University of Reading,
Whiteknights, Reading RG6 2AX, England*

(Received 19 August 1993; in final form 10 February 1994)

SUMMARY

The global asymptotic nonlinear behavior of 11 explicit and implicit time discretizations for four 2×2 systems of first-order autonomous nonlinear ordinary differential equations (ODEs) is analyzed. The objectives are to gain a basic understanding of the difference in the dynamics of numerics between the scalars and systems of nonlinear autonomous ODEs and to set a baseline global asymptotic solution behavior of these schemes for practical computations in computational fluid dynamics. We show how "numerical" basins of attraction can complement the bifurcation diagrams in gaining more detailed global asymptotic behavior of time discretizations for nonlinear differential equations (DEs). We show how in the presence of spurious asymptotes the basins of the true stable steady states can be segmented by the basins of the spurious stable and unstable asymptotes. One major consequence of this phenomenon which is not commonly known is that this spurious behavior can result in a dramatic distortion and, in most cases, a dramatic shrinkage and segmentation of the basin of attraction of the true solution for finite time steps. Such distortion, shrinkage and segmentation of the numerical basins of attraction will occur regardless of the stability of the spurious asymptotes, and will occur for unconditionally stable implicit linear multistep methods. In other words, for the same (common) steady-state solution the associated basin of attraction of the DE might be very different from the discretized counterparts and the numerical basin of attraction can be very different from numerical method to numerical method. The results can be used as an explanation for possible causes of error, and slow convergence and nonconvergence of steady-state numerical solutions when using the time-dependent approach for nonlinear hyperbolic or parabolic PDEs.

KEY WORDS: Spurious steady-state numerical solutions, spurious asymptotes, global asymptotic behavior, nonlinear ODEs, numerical methods, time discretizations.

* Part of the material appeared in the Proceedings of the 9th GAMM Conference on Numerical Methods in Fluid Mechanics, Lausanne, Switzerland, Sept. 25-27, 1991. Full text appeared as a NAS Applied Research Technical Report RNR-92-008, March 1992, NASA Ames Research Center.

[†] Part of this work was performed as a visiting scientist at the NASA Ames Research Center.

1. INTRODUCTION

The tool that is utilized for the current study belongs to a multidisciplinary field of study in numerical analysis, sometimes referred to as “The Dynamics of Numerics¹”. Here the phrase “to study the dynamics of numerics” (dynamical behavior of a numerical scheme) is restricted to the study of local and global asymptotic behavior and bifurcation phenomena of the nonlinear difference equations resulting from finite discretizations of a nonlinear differential equation (DE) subject to the variation of discretized parameters such as the time step, grid spacing, numerical dissipation coefficient, etc. In this paper, standard terminologies of nonlinear dynamics, chaotic dynamics (Guckenheimer and Holmes, 1983; Hale and Kocak, 1991) and computational fluid dynamics (CFD) are assumed. For an introduction to the dynamics of numerics and its implications for algorithm development in CFD, see Yee *et al.* (1991) and Yee (1991) and references cited therein.

1.1 Background

The phenomenon that a nonlinear DE and its discretized counterpart can have different dynamical behavior (asymptotic behavior) was not uncovered fully until recently. Aside from truncation error and machine round-off error, a more fundamental distinction between the DE (continuum) and its discretized counterparts for genuinely nonlinear behavior is extra solutions in the form of spurious stable and unstable asymptotes that can be created by the numerical method. Here we use the term “discretized counterparts” to mean the finite difference equations (or discrete maps) resulting from finite discretizations of the underlying DE. Also we use the term “spurious asymptotic numerical solutions” to mean asymptotic solutions that satisfy the discretized counterparts but do not satisfy the underlying ordinary differential equations (ODEs) or partial differential equations (PDEs). Asymptotic solutions here include steady-state solutions (fixed points of period one for the discretized equations), periodic solutions, limit cycles, chaos and strange attractors. See Section III and Guckenheimer and Holmes (1983), Hale and Kocak (1991) and Yee *et al.* (1991) for definitions.

Iserles (1988) showed that while linear multistep methods (LMMs) for solving ODEs possess only the fixed points (fixed points of period one) of the original DEs, popular Runge-Kutta methods may exhibit additional, spurious fixed points. It has been demonstrated by the authors and collaborators (Yee *et al.*, 1991; Yee, 1991; Sweby *et al.*, 1990; Griffiths *et al.*, 1992; Yee and Sweby, 1993a, 1993b) for nonlinear ODEs, and Lafon and Yee (1991, 1992) for nonlinear reaction-convection model equations that such spurious fixed points as well as spurious fixed points of higher periods may be stable below the linearized stability limit of the scheme, depending on the initial data. Iserles *et al.* (1990), Hairer *et al.* (1989) and Humphries (1991) further advanced some theoretical understanding of the dynamics of numerics for initial value problems of ODEs. Iserles *et al.* and Hairer *et al.* classified and gave guidelines and theory on the types of Runge-Kutta methods that do not exhibit spurious period one or period two fixed points. Humphries (1991) showed that under appropriate assumptions if stable

¹ Named after the First IMA Conference on Dynamics of Numerics and Numerics of Dynamics, University of Bristol, England, July 31–August 2, 1990.

spurious fixed points exist as the time-step approaches zero, then they must either approach a true fixed point or become unbounded. However, convergence in practical calculations involves a finite time step Δt as the number of integrations $n \rightarrow \infty$ rather than $\Delta t \rightarrow 0$, as $n \rightarrow \infty$. There appear to be missing links between theoretical development and practical scientific computation. Our aim is to provide some of these missing links that were not addressed in Iserles (1988), Iserles *et al.* (1990), Hairer *et al.* (1989), Humphries (1991) and our earlier work. In particular, we want to show in more detail the global asymptotic behavior of time discretizations when finite but not extremely small Δt is used. Other aspects that were not addressed in Iserles (1988) for different iteration procedures in solving the resulting nonlinear algebraic equations are reported in greater depth in our companion papers (Yee and Sweby, 1993a, 1993b).

1.2 Relevance and Motivations

Although the understanding of the dynamics of numerics of systems of nonlinear ODEs and PDEs is important in its own right and has applications in the various nonlinear scientific fields, our main emphasis is CFD applications. Time-marching types of methods (time-dependent approach) are commonly used in CFD because the steady PDEs of higher than one dimension are usually of the mixed type. When a time-dependent approach is used to obtain steady-state numerical solutions of a fluid flow or a steady PDE, a boundary value problem (BVP) is transformed into an initial-boundary value problem (IBVP) with unknown initial data. If the steady PDE is strongly nonlinear and/or contains stiff nonlinear source terms, phenomena such as slow convergence, nonconvergence or spurious steady-state numerical solutions and limit cycles commonly occur even though the time step is well below the linearized stability limit and the initial data are physically relevant. One of our goals is to search for logical explanations for these phenomena via the study of the dynamics of numerics. Here the term “time-dependent approach” is used loosely to include some of the iteration procedures (due to implicit time discretizations), relaxation procedures, and preconditioners for convergence acceleration strategies used to numerically solve steady PDEs. This is due to the fact that most of these procedures can be viewed as approximations of time-dependent PDEs (but not necessarily the original PDE that was under consideration). If one is not careful, numerical solutions other than the desired one of the underlying PDE can be obtained (in addition to spurious asymptotes due to the numerics).

One consequence of the existence of stable and unstable spurious asymptotes below or above the linearized stability limit of the numerical schemes is that these spurious features may greatly affect the dynamical behavior of the numerical solution in practice due to the use of a finite time step. As discussed in details in later sections and also in Yee *et al.* (1991), Yee and Sweby (1993a,b), Lafon and Yee (1992), Sweby and Yee (1991), Yee *et al.* (1992), it is possible that for the same steady-state solution, the associated basin of attraction of the underlying DEs (which initial conditions lead to which asymptotic states) might be very different from that of the basin of attraction of the discretized counterparts due to the existence of spurious stable and unstable asymptotic numerical solutions. In other words, there is a separate dependence on initial data for the individual DEs and their discretized counterparts. Here the basin of attraction is a domain of a set of initial conditions whose solution curves (trajectories)

all approach the same asymptotic state. Also we use the term “exact” and “numerical” basins of attraction to distinguish “basins of attraction of the underlying DEs” and “basins of attraction of the discretized counterparts”.

In view of the spurious dynamics, it is possible that numerical computations may converge to an incorrect steady state or other asymptote which appears to be physically reasonable. One major implication is that what is expected to be physical initial data associated with the underlying steady state of the DE might lead to a wrong steady state, a spurious asymptote, or a divergence or nonconvergence of the numerical solution. In addition, the existence of spurious limit cycles may result in the type of nonconvergence of steady-state numerical solutions observed in time-dependent approaches to the steady states. It is our belief that the understanding of the symbiotic relationship between the strong dependence on initial data and permissibility of spurious stable and unstable asymptotic numerical solutions at the fundamental level can guide the tuning of the numerical parameters and the proper and/or efficient usage of numerical algorithms in a more systematic fashion. It can also explain why certain schemes behave nonlinearly in one way but not another. Here strong dependence on initial data means that for a finite time step Δt that is not sufficiently small, the asymptotic numerical solutions and the associated numerical basins of attraction depend continuously on the initial data. Unlike nonlinear problems, the associated numerical basins of attraction of linear problems are independent of Δt as long as Δt is below a certain upper bound.

Nonunique Steady-State Solutions of Nonlinear DEs vs. Spurious Asymptotes: The phenomenon of generating spurious steady-state numerical solutions (or other spurious asymptotes) by certain numerical schemes is often *confused* with the nonuniqueness (or *multiple steady states*) of the DE. In fact, the existence of nonunique steady-state solutions of the continuum can complicate the numerics tremendously (e.g., the basins of attraction) and is *independent* of the occurrence of spurious asymptotes of the associated scheme. But, of course, a solid background in the theory of nonlinear ODEs and PDEs and their dynamical behavior is a prerequisite in the study of the dynamics of numerics for nonlinear PDEs. See Yee *et al.*, 1991 for a discussion. It is noted that the approach and primary goal of our work is quite different from the work of e.g., Beam and Bailey (1988) and Jameson (1991). The main goal of Beam and Bailey (1988) and Jameson (1991) was to study the nonunique steady-state solutions admitted by the PDE as the physical parameter is varied. Our primary interest is to establish some working tools and guidelines to help delineate the true physics from numerical artifacts via the dynamics of numerics approach. The knowledge gained from our series of studies (Yee *et al.*, 1991; Lafon and Yee, 1991; Lafon and Yee, 1992) hopefully can shed some light on the controversy about the existence of multiple steady-state solutions through numerical experiments for certain flow types of the Euler and/or Navier Stokes equations.

1.3 Objectives and Outline

The primary goal of the series of papers (present and the companion papers Yee *et al.*, 1991; Yee and Sweby, 1993a, b; Lafon and Yee, 1991; Lafon and Yee, 1992) is to lay the foundation for the utilization of the dynamics of numerics in algorithm development for computational sciences in general and CFD in particular. This is part II of this series of papers on the same topic. Part I (Yee *et al.*, 1991) concentrated on the dynamical behavior

of time discretizations for scalar nonlinear ODEs. The intent of part I was to serve as an introduction to motivate this concept to researchers in the field of CFD and to present new results for the dynamics of numerics for first-order scalar autonomous ODEs.

The present paper, the second of this series, is devoted to the study of the dynamics of numerics for 2×2 systems of ODEs. Here we show how “numerical” basins of attraction can complement the bifurcation diagrams in gaining more detailed global asymptotic behavior of numerical methods for nonlinear DEs. We show how in the presence of spurious asymptotes the basins of the true stable steady states can be segmented by the basin of the spurious stable and unstable asymptotes. One major consequence of this phenomenon which is not commonly known is that this spurious behavior can result in a dramatic distortion and, in most cases, a dramatic shrinkage and segmentation of the basin of attraction of the true solution for finite time steps. Such distortion, shrinkage and segmentation of the numerical basins of attraction will occur regardless of the stability of the spurious asymptotes, and will occur for unconditionally stable implicit linear multistep methods. In other words, for the same steady-state solution, the associated basin of the DE might be very different from its discretized counterparts. The basins can also be very different from numerical method to numerical method. The present study reveals for the first time the detail interlocking relationship of numerical basins of attraction and the causes of error, and slow convergence and nonconvergence of steady-state numerical solutions when using the time-dependent approach.

The article of Lafon and Yee (1991), the third of this series, was devoted to the study of the dynamics of numerics of commonly used numerical schemes in CFD for a model reaction-convection equation. The article of Lafon and Yee (1992), the fourth of this series, was devoted to a more detailed study of the effect of numerical treatment of nonlinear source terms on nonlinear stability of steady-state numerical solution for the same model nonlinear reaction-convection BVP. In our companion papers (Sweby *et al.*, 1990; Griffiths *et al.*, 1991a, 1992b), a theoretical bifurcation analysis of a class of explicit Runge-Kutta methods and spurious discrete travelling wave phenomenon were presented. In yet another companion paper, Yee and Sweby (1993a), the global asymptotic nonlinear behavior of three standard iterative procedures in solving nonlinear systems of algebraic equations arising from four implicit LMMs is analyzed numerically.

1.4 Outline

The outline of this paper is as follows. Section II discusses the connection of the dynamics of numerics for systems of ODEs and numerical approximations of time-dependent PDEs. Section III reviews background material for nonlinear ODEs and their numerical methods. Section IV describes four 2×2 systems of nonlinear first-order autonomous model ODEs. Section V describes the 11 time discretizations and the associated bifurcation diagrams for the four model ODEs. Section VI discusses the combined basins of attraction and bifurcation diagrams for the underlying schemes. Comparison between a linearized implicit Euler and Newton method is briefly discussed in Section 6.5. The paper ends with some concluding remarks in Section VII.

2. THE DYNAMICS OF NUMERICS OF SYSTEMS OF ODEs AND NUMERICAL APPROXIMATIONS OF TIME-DEPENDENT PDEs

For finite discretizations of PDEs, spurious asymptotes and especially spatially-varying spurious steady states can be independently introduced by time and spatial discretizations (Yee *et al.*, 1991; Lafon and Yee, 1991; Lafon and Yee, 1992). The interaction between temporal and spatial dynamical behavior is more complicated when one is dealing with the nonseparable temporal and spatial finite-difference discretizations such as the Lax-Wendroff type. The analysis and the different features of the numerics due to temporal and spatial discretizations can become more apparent by separable temporal and spatial finite difference methods (FDM). A standard method for obtaining such a FDM is the method of lines (MOL) procedure where the time-dependent PDE is reduced to a system of ODEs (by replacing the spatial derivatives by finite difference approximations). The resulting approximation is called semi-discrete, since the time variable is left continuous. The semi-discrete system in turn can be solved by the desired time discretizations. Similar semi-discrete systems can be obtained by finite element methods except in this case an additional mass matrix is involved. Besides the MOL approach, coupled nonlinear ODEs can arise in many other ways when analyzing nonlinear PDEs. See for example Globus *et al.* (1991), Hung *et al.* (1991), Foias *et al.* (1985), Temam (1989), Kwak (1991), Schechter and Shearer (1990), and Shearer *et al.* (1987). Among these possibilities, the idea of inertial manifold (IM) and approximate inertial manifold (AIM) for incompressible Navier-Stokes (Foias *et al.*, 1985; Temam, 1989; Kwak, 1991), the relationship between shock waves, heteroclinic orbits of systems of ODEs (Schechter and Shearer, 1990; Shearer *et al.*, 1987), and flow visualization of numerical data (Globus *et al.*, 1991; Hung, 1991) are touched upon here.

2.1 *Asymptotic Analysis of the Method of Lines Approach*

When the ODEs are obtained from a semi-discrete approximations of PDEs, the resulting system of ODEs contains additional system parameters and discretized parameters as opposed to physical problems governed by ODEs. Depending on the number of grid points “ J ” used, the dimensions of the resulting system of semi-discrete approximations of ODEs can be very large. Also, depending on the differencing scheme the resulting discretized counterparts of a PDE can be nonlinear in Δt , the grid spacing Δx and the numerical dissipation parameters, even though the DEs consist of only one parameter or none. One major consideration is that one might be able to choose a “safe” numerical method to solve the resulting system of ODEs to avoid spurious stable steady states due to time discretizations. However, spurious steady states and especially spatially varying steady states introduced by spatial discretizations in nonlinear hyperbolic and parabolic PDEs for CFD applications appear to be more difficult to avoid. In the case of the MOL approach, if spurious steady states due to spatial discretizations exist, the resulting ODE system has already inherited this spurious feature as part of the exact solutions of the semi-discrete case. We remark that spurious stable and unstable asymptotes other than the steady states due to time discretizations are also more difficult to avoid than spurious steady states. See Sections V and VI for some illustrations. Taking for example the nonlinear ODE models that are

considered, it is relatively easy to avoid spurious steady states due to time discretizations since, if a numerical steady state U^* for the ODE $dU/dt = S(U)$ is spurious, then $S(U^*) \neq 0$. This is not the case for spurious asymptotes such as limit cycles.

In addition to the aforementioned considerations, it is well known from the theory of nonlinear dynamics for ODEs that much of the established theory and known behavior of nonlinear dynamics are restricted to lower dimensional first-order ODEs (or for problems that exhibit lower dimensional dynamical behavior). Moreover, if higher than two-time level numerical methods are used, the dynamics of these discretized counterparts usually are richer in structure and more complicated to analyze than their two-time level cousins. Therefore, in order to gain a first hand understanding of the subject we restrict our study to 2×2 systems of first-order autonomous ODEs and two-time level numerical methods with a fixed time step, even though the current study is far removed from the realistic setting. Studies of 3×3 systems and general $J \times J$ systems are in progress.

Due to the complexity of the subject matter, this paper concerns fixed time step (and fixed grid spacing) time-marching methods only. The fixed or local variable time step control method study can also shed some light on identifying whether certain flow patterns are steady or unsteady. See Yee *et al.* (1990) for some examples. Proper regulation of a variable time step to prevent the occurrence of spurious steady-state numerical solutions will be a subject of future research. In order to isolate the different causes and cures of slow convergence and nonconvergence of time-marching methods, our study concerns nonlinearity and stiffness that are introduced by DEs containing smooth solutions. Nonlinearity and stiffness that are introduced by the scheme, the coupling effect in the presence of a source term (terms) in coupled system of PDEs, the highly stretched nonuniform structured and unstructured grids, the discontinuities in grid interfaces and/or the discontinuities inherent in the solutions, and external flows that need special boundary condition treatment with a truncated finite computation domain are added factors and require additional treatment or different analysis. These are not considered at the moment. Generalization of our study to include grid adaption as one of the sources of nonlinearity and/or stiffness introduced by the numerics is reported in Sweby and Yee (1964) and Budd *et al.* (1994).

2.2 Inertial Manifold (IM) and Approximate Inertial Manifold (AIM)

The concept of IMs was introduced by Foias *et al.* (1985). See Foias *et al.* (1985), Temam (1989) and Kwak (1991) for details of the subject. The key idea of IMs and AIMs is to establish theories to aid in better understanding of nonlinear phenomena and turbulence via the study of the interaction of short and long wavelengths of dissipative systems. Basically, an IM is a finite-dimensional submanifold that contains all the attractors and invariant sets of an infinite-dimensional dynamical system described by some dissipative PDEs. It establishes the criterion for the reduction of long-term dynamics of certain infinite-dimensional problems to a finite system of ODEs. An attractive feature is that the reduction introduces no error in the problem. That is, the IM contains all pertinent information about the long-term dynamics of the original system. One of the main objectives of AIMs is to handle cases where the IMs are not known to exist. AIMs also can help in finding good algorithms for dealing with

the IMs that are known to exist. AIMs may also help reduce finite but extremely large systems of ODEs to lower-dimensional problems. In a nut shell, the derivation of IMs and AIMs is based on the decomposition of the unknown function into large-scale and small scale components. In the case of fluid dynamics, those structures can be identified as large and small eddies. Thus an IM or AIM corresponds to an exact or approximate interaction law between the short and long wavelengths. Kwak (1991) showed that the long-term dynamics of some two-dimensional incompressible Navier-Stokes equations can be completely described by a finite system of ODEs. Kwak does so by finding a nonlinear change of variable that embeds the incompressible Navier-Stokes equations in a system of reaction-diffusion equations that possess an IM. All of the theories of IMs and AIMs are very involved and interested readers are encouraged to read Foias *et al.* (1985), Temam (1989) and Kwak (1991) and the references cited therein.

2.3 Relationship Between Shock Waves and Heteroclinic Orbits of Systems of ODEs

Another example of the importance of understanding the “dynamics” and the “dynamics of numerics” of systems of ODEs is related to the study of shocks using equilibrium bifurcation diagrams of associated vector fields. This was introduced by Shearer *et al.* (1987). The authors find of great interest how one can reduce the study of admissible shock wave solutions of a 2×2 hyperbolic conservation laws to the study of heteroclinic orbits of a system of nonlinear ODEs. Further development in this area can help in constructing suitable approximate Riemann solvers in numerical computations. Schecter and Shearer (1990) studied undercompressive shocks for nonstrictly hyperbolic conservation laws by adding information to the equilibrium bifurcation diagrams (introduced by Shearer *et al.*) about heteroclinic orbits of the vector fields. The augmented equilibrium bifurcation diagrams are then used in the construction of solutions of Riemann problems.

2.4 Dynamics of Numerics and Flow Visualizations of Numerical Data

The use of flow visualization of numerical data (numerical solutions of finite discretizations of e.g., fluid flow problems) in an attempt to understand the true flow physics has become increasingly popular in the last decade. See, Globus *et al.* (1991) and Hung *et al.* (1991) and references cited therein. Many of the techniques rely on the extraction of the boundary surfaces by analyzing a set of appropriate vector fields. Approximations are then performed based on this set of vector fields. The study of the topological features of certain flow physics based on the numerical data is then related to the study of fixed points of the associated systems of ODEs. Fluid problems with known flow physics can be used to reveal how well the associated vector fields of the numerical data can mimic the true physics. It can also help to delineate spurious flow patterns that are solely due to the numerics. At the present time we are entering into the regime where CFD is extensively used to aid the understanding of complicated flow physics that is not amenable to analysis otherwise. In the situation where the numerical data indicate flow structures which are not easily understood, a good understanding of the spurious dynamics that can be introduced by the numerics is needed.

3. PRELIMINARIES

Consider a 2×2 system of first-order autonomous nonlinear ODEs of the form

$$\frac{dU}{dt} = S(U), \quad (3.1)$$

where U and S are vector functions of dimension 2, and $S(U)$ is nonlinear in U . A fixed point U_E of an autonomous system (3.1) is a constant solution of (3.1); that is

$$S(U_E) = 0, \quad (3.2)$$

where the subscript “E” stands for “exact” and U_E denotes the fixed points of the ODE as opposed to the additional fixed points of the discretized counterparts (spurious fixed points) due to the numerical methods which we will encounter later.

Let the eigenvalues of $J(U_E) = (\partial S / \partial U)|_{U_E}$ (the Jacobian matrix of $S(U)$ evaluated at U_E) be λ_1 and λ_2 . Here $J(U_E)$ is assumed to be nonzero. The fixed point U_E is hyperbolic if $\text{Re}(\lambda_i) \neq 0$, $i = 1, 2$. If both λ_i are real, U_E is a saddle if $\lambda_1 \lambda_2 < 0$ and a node if $\lambda_1 \lambda_2 > 0$. If exactly one $\lambda_i = 0$, then U_E is semihyperbolic. If the eigenvalues are complex, then U_E is a spiral. The “tightness” of the spiral is governed by the magnitude of the imaginary part of the eigenvalues. If the eigenvalues both have a zero real part, then U_E is non-hyperbolic. Such a fixed point is called a center. Under this situation, more analysis is needed to uncover the real behavior of (3.1) around a non-hyperbolic fixed point. The fixed point U_E is stable if both λ_1 and λ_2 have negative real parts. U_E is unstable if a λ_i has a positive real part. In the non-hyperbolic case the fixed point is neutral.

If due to a variation of a parameter of the ODE a fixed point becomes unstable, then, if at the point of instability the eigenvalues are distinct and real, the resulting bifurcation will be to another fixed point. Such bifurcation is called a steady bifurcation. If, however, the eigenvalues are complex, then the bifurcation will be of a Hopf type. This is a slightly simplified classification, since our main concern in this work is not on the variation of the ODE parameter. Detailed background information can be found in (Guckenheimer and Holmes, 1983; Hale and Kocak, 1991).

Consider a nonlinear discrete map from a finite discretization of (3.1)

$$U^{n+1} = U^n + D(U^n, r), \quad (3.3)$$

where $r = \Delta t$ and $D(U^n, r)$ is linear or nonlinear in r depending on the numerical method. A fixed point U_D of (3.3) is defined by $U^{n+1} = U^n$, or

$$U_D = U_D + D(U_D, r) \quad (3.4)$$

or $D(U_D, r) = 0$. A fixed point U_D of period $p > 0$ of (3.3) is defined by $U^{n+p} = U^n$ with $U^{n+k} \neq U^n$ of $k < p$. In the context of discrete systems, the term “fixed point” without indicating the period means “fixed point of period 1” or the steady-state solution of (3.3). Here we use the term asymptote to mean a fixed point of any period, a limit cycle (in the discrete sense – invariant set), chaos, or a strange attractor.

The type of finite discretization of (3.1) represented in (3.3) assumed the use of two-time level schemes. Otherwise the vector dimension of (3.3) would be $2(k-1)$ instead of 2 where k is the number of the time level of the scheme. Here the vector function D is assumed to be consistent with the ODE (3.1) in the sense that fixed points of the ODE are fixed points of the scheme; however, the reverse need not hold. It is this feature accompanied by other added dynamics, that the discretized counterparts of the underlying ODE possess a much richer dynamical behavior than the original ODE. Thus the fixed points U_D of $D(U_D, r) = 0$ may be true fixed points U_E of (3.1) or spurious fixed points U_S . The spurious fixed points U_S are not roots of $S(U) = 0$. That is $S(U_S) \neq 0$. Spurious asymptotes are asymptotic numerical solutions of (3.3) but not (3.1).

Letting $U^n = U_D + \delta^n$, then a perturbation analysis on (3.3) yields

$$\delta^{n+1} = \left(I + \frac{\partial D(U_D, r)}{\partial U} \right)^{n+1} \delta^0. \quad (3.5)$$

Assuming $\partial D(U_D, r)/\partial U \neq 0$, then the fixed point U_D is stable if the eigenvalues of $J_D = I + \partial D(U_D, r)/\partial U$ lie inside the unit circle. If both eigenvalues are real and both lie inside (outside) the unit circle, then the fixed point is a stable (unstable) node. If one is inside the unit circle and the other outside, then the fixed point is a saddle. If both eigenvalues are complex, then the fixed point is a spiral. If the eigenvalues lie on the unit circle, then the fixed point of (3.3) is indeterminate and additional analysis is required to determine the true behavior of (3.3) around this type of fixed point. For a more refined definition and the difference in fixed point definition between ODEs and discrete maps, see Panov *et al.* (1956), Perron (1929) and Hsu (1987) and references cited therein. The reader is referred to Guckenheimer and Holmes (1983), Hale and Kocak (1991), Langford and Iooss (1980), and Werner (1980) for full details on the subject of bifurcation theory.

An important feature which can arise (for both systems of ODEs (3.1) and their discretizations) as the result of a Hopf bifurcation is a limit cycle where the trajectory traverses a closed curve in phase space. In all but a few simple cases such limit cycles are beyond analysis.

4. MODEL 2×2 SYSTEMS OF NONLINEAR FIRST-ORDER AUTONOMOUS ODEs

Four 2×2 systems of nonlinear first-order autonomous model ODEs are considered. The systems considered with $U^T = (u, v)$ or $z = u + iv$ are a

1. Dissipative complex model:

$$\frac{dz}{dt} = z(i + \varepsilon - |z|^2) \quad (4.1)$$

2. Damped Pendulum model:

$$\frac{du}{dt} = v \quad (4.2a)$$

$$\frac{dv}{dt} = -\varepsilon v - \sin(u) \quad (4.2b)$$

3. Predator-Prey model:

$$\frac{du}{dt} = -3u + 4u^2 - 0.5uv - u^3 \quad (4.3a)$$

$$\frac{dv}{dt} = -2.1v + uv \quad (4.3b)$$

4. Perturbed Hamiltonian System model:

$$\frac{du}{dt} = \varepsilon(1 - 3u) + \frac{3}{4}[1 - 2u + u^2 - 2v(1 - u)] \quad (4.4a)$$

$$\frac{dv}{dt} = \varepsilon(1 - 3v) - \frac{3}{4}[1 - 2v + v^2 - 2v(1 - v)] \quad (4.4b)$$

Here ε is the system parameter for (4.1), (4.2) and (4.4).

The perturbed Hamiltonian model can be related to the numerical solution of the viscous Burgers' equation with no source term

$$\frac{\partial u}{\partial t} + \frac{1}{2} \frac{\partial(u^2)}{\partial x} = \beta \frac{\partial^2 u}{\partial x^2} \quad \beta > 0. \quad (4.5)$$

Let $u_j(t)$ represent an approximation to $u(x_j, t)$ of (4.5) where $x_j = j\Delta x$, $j = 1, \dots, J$, with Δx the uniform grid spacing. Consider the three-point central difference in space with periodic condition $u_{J+1} = u_1$, and assume $\sum_{j=1}^J u_j = \text{constant}$, which implies that $\sum_{j=1}^J du_j/dt = 0$. If we take $J = 3$ and $\Delta x = 1/3$ then, with $\varepsilon = 9\beta$, this system can be reduced to a 2×2 system of first-order nonlinear autonomous ODEs (4.4) with $U^T = (u_1, u_2) = (u, v)$. In this case, the nonlinear convection term is contributing to the nonlinearity of the ODE system (4.4).

These four equations were selected to bring out the dynamics of numerics for four different types of solution behavior of the ODEs. The dissipative complex system (4.1) possesses either a unique stable fixed point or limit cycle with an unstable fixed point depending on the value of ε . This is the rare situation where the analytical expression of a limit cycle can be found. The purpose of choosing (4.1) is to illustrate the numerical accuracy of computing a limit cycle and the spurious dynamics associated with this type of asymptote. The damped pendulum (4.2), arising from modelling of a physical process, exhibits a periodic structure of an infinite number of fixed points. The predator-prey model (4.3), arising from modelling of biological process, exhibits multiple stable fixed points without a periodic pattern as model (4.2). The perturbed Hamiltonian model (4.4), which arises as a gross simplification of finite discretization of

the viscous Burgers' equation, exhibits an unique stable fixed point. Following the classification of fixed points of (3.1) in Section III, one can easily obtain the following:

Fixed Point of (4.1): The dissipative complex model has a unique fixed point at $(u, v) = (0, 0)$ for $\varepsilon \leq 0$. The fixed point is a stable spiral if $\varepsilon < 0$. It is a center if $\varepsilon = 0$. For $\varepsilon > 0$, the fixed point $(0, 0)$ becomes unstable with the birth of a stable limit cycle with radius equal to $\sqrt{\varepsilon}$ centered at $(0, 0)$. Figure 4.1 shows the phase portrait ($u-v$ plane) of system (4.1) for $\varepsilon = -1$ and $\varepsilon = 1$ respectively. Here the entire (u, v) plane belongs to the basins of attraction of the stable fixed point $(0, 0)$ if $\varepsilon < 0$. On the other hand, if $\varepsilon > 0$, the entire (u, v) plane except the unstable fixed point $(0, 0)$ belongs to the basin of attraction of the stable limit cycle centered at $(0, 0)$.

Fixed Points of (4.2): The damped pendulum (4.2) has an infinite number of fixed points, namely $(k\pi, 0)$ for integer k . If k is odd, the eigenvalues of the Jacobian $J(U_E)$ are of opposite sign and these fixed points are saddles. If k is even, however, two cases must be considered, depending on the value of ε . If $\varepsilon < 2$ and positive, the eigenvalues are complex with negative real part and the fixed points are stable spirals. If $\varepsilon \geq 2$, the eigenvalues are real and negative and the fixed points are nodes. If $\varepsilon = 0$, the spirals become centers. Figure 4.2 shows the phase portrait and their corresponding basins of attraction for system (4.2). The different shades of grey regions represent the various basins of attraction of the respective stable fixed points for $\varepsilon = 0.5$ and $\varepsilon = 2.5$.

Fixed Points of (4.3): The fixed points of the predator-prey equation are less regular than those for the damped pendulum equation. System (4.3) has four fixed points $(0, 0)$, $(0, 1)$, $(3, 0)$ and $(2.1, 1.98)$. By looking at the eigenvalues of the Jacobian of S , one finds that $(0, 0)$ is a stable node, $(2.1, 1.98)$ is a stable spiral, and $(1, 0)$ and $(3, 0)$ are saddles. Figure 4.3 shows the phase portrait and their corresponding basins of attraction for system (4.3). The different shades of grey regions represent the various basins of attraction of the respective stable fixed points. The white region represents the basin of

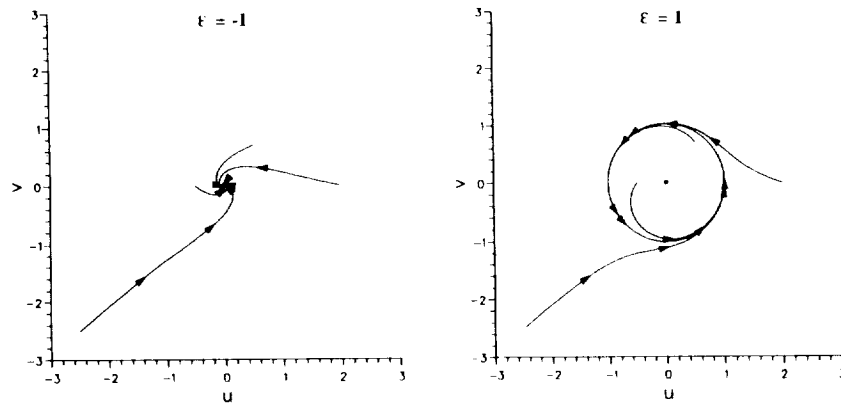


Figure 4.1 Phase Portraits and basins of Attraction Dissipative Complex Equation.

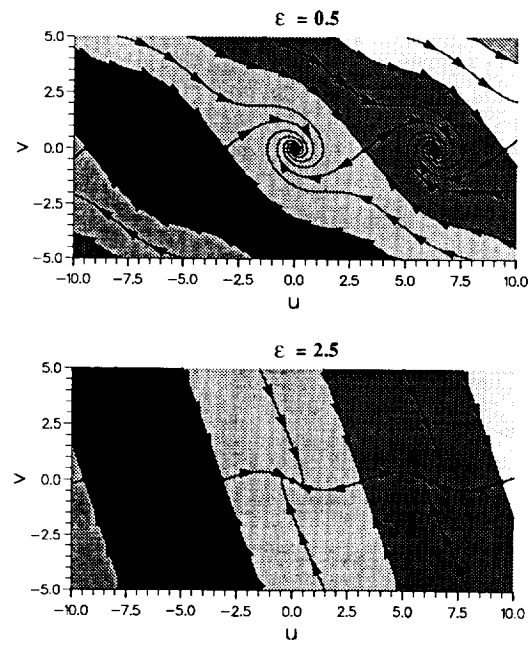


Figure 4.2 Phase Portraits and Basins of Attraction Damped Pendulum Equation.

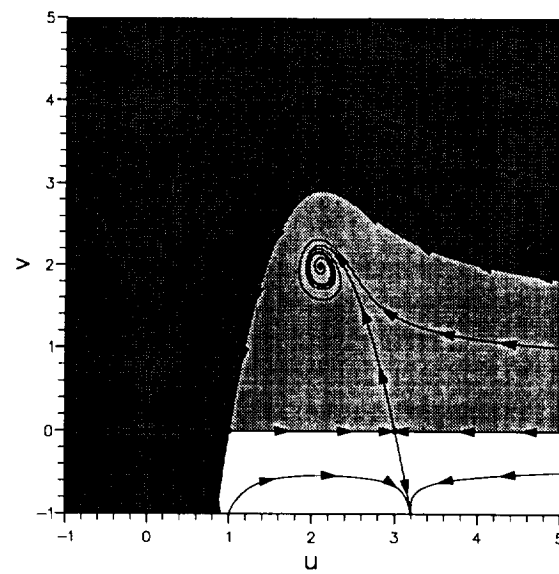


Figure 4.3 Phase Portraits and Basins of Attraction Predator-Prey Equation.

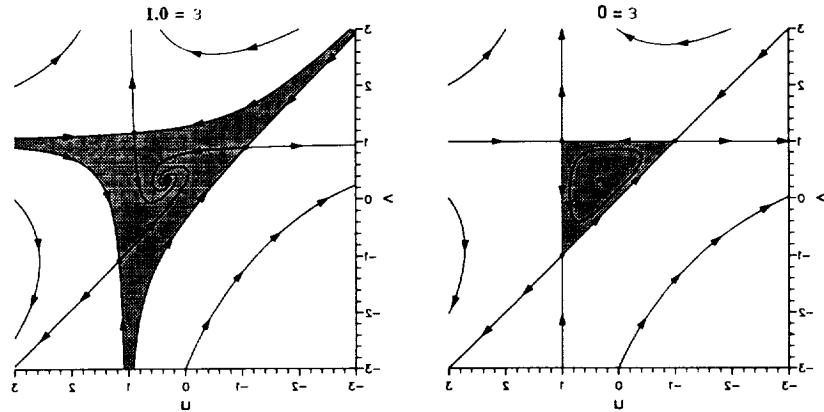


Figure 4.4 Phase Portraits and Basins of Attraction Viscous Burger's Equation (Central Difference in Space).

divergent solutions. Note that the trajectories near the unstable separatrices actually do not merge with the unstable branch of separatrices, but only appear to merge due to the thick drawings of the solution trajectories.

Fixed Points of (4.4): The perturbed Hamiltonian has four steady-state solutions of which three are saddles and one is a stable spiral at $(1/3, 1/3)$ for $\varepsilon \neq 0$. For $\varepsilon = 0$ the stable spiral becomes a center. Figure 4.4 shows the phase portrait and their corresponding basins of attraction for system (4.4). The shaded region represents the basins of attraction for the fixed point $(1/3, 1/3)$ for $\varepsilon = 0$ and $\varepsilon = 0.01$. The white region represents the basin of divergent solutions. From here on we refer to (4.4) also as a viscous Burgers' equation with central difference in space.

5. NUMERICAL METHODS AND BIFURCATION DIAGRAMS

This section describes the 11 time discretizations and their corresponding bifurcation diagrams for the four model ODEs (4.1)–(4.4). The 11 numerical methods are listed in Section 5.1. Section 5.2 discusses the stability of selected fixed points of the discretized counterparts of the model ODEs as functions of system parameters. Section 5.3 discusses the bifurcation diagrams as a function of the discretized parameter Δt with the system parameter held fixed.

5.1 Numerical Methods

The 9 explicit and two implicit methods considered are the explicit Euler, two second-order Runge-Kutta, namely, the modified Euler (R-K 2) and the improved Euler (R-K 2), two third-order Runge-Kutta (R-K 3), a fourth-order Runge-Kutta (R-K 4), the two and three-step predictor-corrector (Lambert, 1973), and noniterative linearized forms of the implicit Euler and the trapezoidal methods.

(1) **Explicit Euler (1st-order; R-K 1):**

$$U^{n+1} = U^n + rS^n; \quad S^n = S(U^n), \quad (5.1)$$

(2) **Modified Euler (R-K 2):**

$$U^{n+1} = U^n + rS\left(U^n + \frac{r}{2}S^n\right), \quad (5.2)$$

(3) **Improved Euler (R-K 2):**

$$U^{n+1} = U^n + \frac{r}{2}[S^n + S(U^n + rS^n)], \quad (5.3)$$

(4) **Heun (R-K 3):**

$$U^{n+1} = U^n + \frac{r}{4}(k_1 + 3k_3) \quad (5.4)$$

$$k_2 = S^n$$

$$k_2 = S\left(U^n + \frac{r}{3}k_1\right)$$

$$k_3 = S\left(U^n + \frac{2r}{3}k_2\right),$$

(5) **Kutta (R-K 3):**

$$U^{n+1} = U^n + \frac{r}{6}(k_1 + 4k_2 + k_3) \quad (5.5)$$

$$k_1 = S^n$$

$$k_2 = S\left(U^n + \frac{r}{2}k_1\right)$$

$$k_3 = S(U^n - rk_1 + 2rk_2),$$

(6) **R-K 4:**

$$U^{n+1} = U^n + \frac{r}{6}(k_1 + 2k_2 + 2k_3 + k_4) \quad (5.6)$$

$$k_1 = S^n$$

$$k_2 = S\left(U^n + \frac{r}{2}k_1\right)$$

$$k_3 = S\left(U^n + \frac{r}{2}k_2\right)$$

$$k_4 = S(U^n + rk_3),$$

(7, 8) **Predictor-corrector for m = 2, 3 (PC2, PC3):**

$$U^{(0)} = U^n + rS^n$$

$$U^{(k+1)} = U^n + \frac{r}{2}[S^n + S^{(k)}], \quad k = 0, 1, \dots, m-1$$

$$U^{n+1} = U^n + \frac{r}{2}[S^n + S^{(m-1)}], \quad (5.7)$$

(9) **Adam-Bashforth (2nd-order):**

$$U^{n+1} = U^n + \frac{r}{2}[3S(U^n) - S(U^{n-1})], \quad (5.8)$$

(10) **Linearized Implicit Euler:**

$$U^{n+1} = U^n + r(I - rJ^n)^{-1}S^n \quad (5.9)$$

$$J^n = \left(\frac{\partial S}{\partial U}\right)^n \quad \text{and} \quad \det(I - rJ^n) \neq 0,$$

(11) **Linearized Trapezoidal:**

$$U^{n+1} = U^n + r\left(I - \frac{r}{2}J^n\right)^{-1}S^n \quad (5.10)$$

$$J^n = \left(\frac{\partial S}{\partial U}\right)^n \quad \text{and} \quad \det\left(I - \frac{r}{2}J^n\right) \neq 0,$$

where the numeric identifier after the “**R-K**” indicates the order of accuracy of the scheme and $r = \Delta t$ and $\det(\)$ means the determinant of the quantity inside the (). Schemes (10) and (11) are unconditionally stable methods. See Beam and Warming (1976) and Yee (1989) for the versatility of the linearized implicit Euler and linearized trapezoidal methods in CFD applications. A comparison between Newton method in solving the steady part of the ODEs and the linearized implicit method (5.9) for model (4.4) is included in Section 6.5. Studies on Newton method in solving the steady state part of the PDE and some iteration procedures in solving the nonlinear algebraic

equation resulting from four implicit LMMs are reported in a separate paper (Yee and Sweby 1933a). Although the explicit Euler can be considered as an R-K 1, it is also a LMM. All of the R-K methods (higher than first order) and the predictor-corrector methods are nonlinear in the parameter space r , and all LMMs are linear in r . As discussed in Yee *et al.* (1991), a necessary condition for a scheme to produce spurious fixed points of period one is the introduction of nonlinearity in the parameter space r . It can be shown later that this property plays a major role on the shapes and sizes of the associated numerical basins of attraction of the scheme. For simplicity in referencing, hereafter we use “implicit Euler” and “trapezoidal” to mean the linearized forms (5.9) and (5.10), respectively, unless otherwise stated.

5.2 Stability of Fixed Points of Numerical Methods as a Function of System Parameters

In our later study, we assume a fixed system parameter so that only the discretized parameter comes into play. However, in order to get a feel for the numerical stability of these schemes around selected stable fixed points U_E as a function of the system parameter ε , Figures 5.1–5.3 show the stability regions of the schemes as a function of the

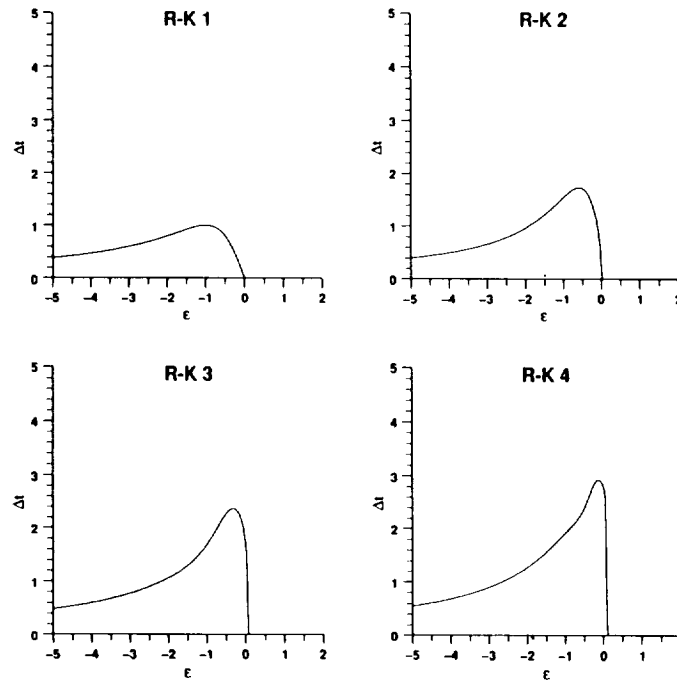


Figure 5.1 Stability Regions vs. System Parameters Dissipative Complex Equation.

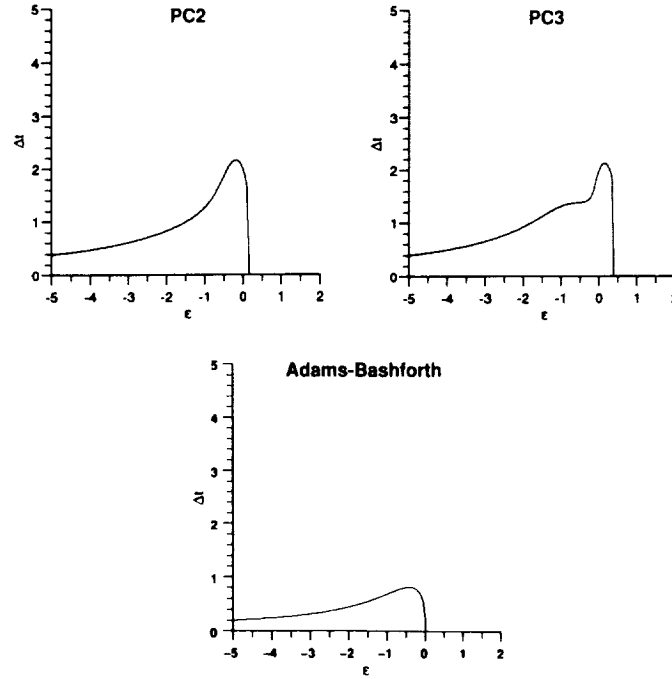


Figure 5.1 (Continued)

system parameter ϵ around a selected fixed point for each of the models. The linearized stability regions for the R-K methods of the same order behave in exactly the same manner, and the linearized stability regions around stable U_E of the linearized implicit methods are not interesting, since they have the same regions of stability as the ODEs.

The stability diagrams presented were obtained by numerically solving the absolute stability polynomials for the various methods, in most cases using Newton iteration. For the Runge-Kutta schemes (of order $p \leq 4$) the stability (Griffiths *et al.*, 1992; Lambert, 1973) condition is that

$$\left| 1 + \lambda r + \cdots + \frac{\lambda^p r^p}{p!} \right| < 1, \quad (5.11)$$

where λ are the eigenvalues of the Jacobian of $S(U)$. For the Predictor-Corrector of steps $p = 2, 3$ the stability condition is that

$$\left| 1 + \lambda r + \cdots + \frac{\lambda^p r^p}{2^p} \right| < 1, \quad (5.11)$$

and for the Adams-Bashforth method the roots μ of

$$\mu^2 - \left(1 + \frac{3\lambda r}{2}\right)\mu + \frac{\mu}{2} = 0 \quad (5.13)$$

satisfy $|\mu| < 1$. Note that all of these expressions only hold for the U_E fixed points of the system.

In all cases the boundary of the stability region is when unit modulus is attained. The linearized implicit Euler and trapezoidal methods are unconditionally stable for the stable exact fixed points U_E of the ODE systems we are considering.

These stability regions can be used to isolate the key regions of the ε parameter to be considered for the study of dynamics of numerics later. Due to the enormous number of possibilities, detailed study can only concentrate on one to two representative system parameters. Even with such a restriction, as can be seen later, computing the corresponding bifurcation diagrams and basins of attraction is very CPU intensive. Fortunately the computation can be made highly parallel. Figures 5.1–5.3 also can serve as a spot check on the numerical results presented in the next section.

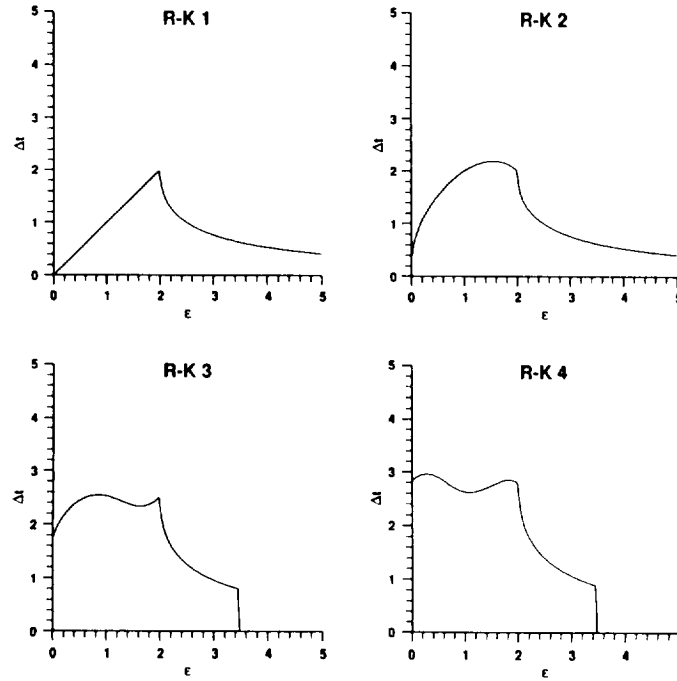


Figure 5.2 Stability Regions vs. System Parameters Damped Pendulum Equation.

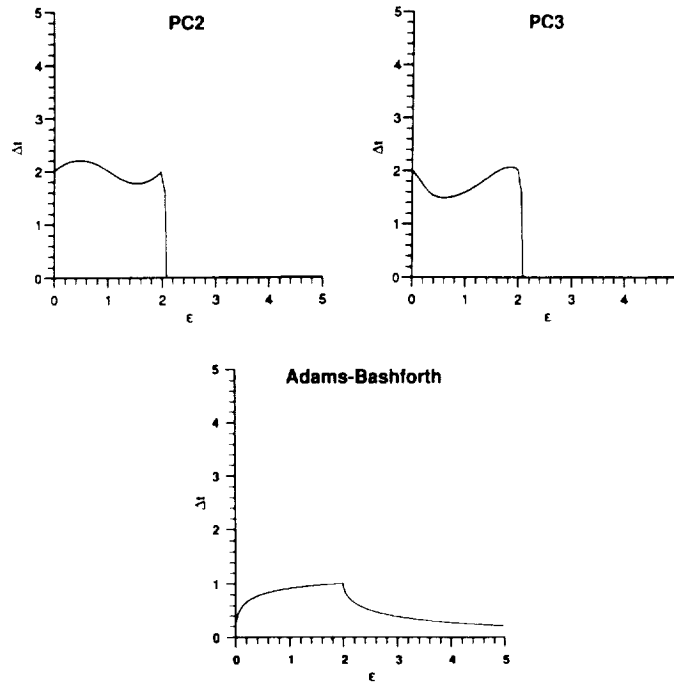


Figure 5.2 (Continued)

5.3 Bifurcation Diagrams

In this section, we show the bifurcation diagrams of selected R-K methods. It illustrates some of the many ways in which the dynamics of a numerical discretization of 2×2 first-order autonomous nonlinear system of ODEs can differ from the system itself. Note that there is no limit cycle or higher dimensional tori counterpart for the scalar first-order autonomous ODEs. Spurious limit cycles and higher dimensional tori can only be introduced by the numerics when solving nonlinear ODEs other than scalar first-order autonomous ODEs (if 2-time level schemes are used) and/or by using a scheme with higher than two-time level for the scalar first-order autonomous ODEs. In Section VI, we showed how numerical basins of attraction can complement the bifurcation diagrams in gaining more detailed global asymptotic behavior of numerical schemes. We purposely present our results in this order (not showing the basins of attraction) in order to bring out the importance of basins of attraction for the time-dependent approach in obtaining steady-state numerical solutions.

Even though the analytical solutions of these models are known, depending on the scheme, the dynamics of their discretized counterparts might be very difficult to analyze. In particular, some analytical linearized analysis (without numerical computations) of fixed points of periods one and two is possible for the predator-prey and the damped pendulum case. However, analytical analysis for the dissipative complex

model and the perturbed Hamiltonian is not practical. For a detailed analysis of these selected cases, readers are referred to Sweby and Yee (1991). *For the majority of the cases where rigorous analysis is impractical we study the dynamics of numerics using numerical experiments.*

Note that some global solution behavior of fixed points of the nonlinear discretized equations (5.1)–(5.10) for (4.1)–(4.4) can be obtained by the pseudo arclength continuation method devised by Keller (1977), a standard numerical method for obtaining bifurcation curves in bifurcation analysis. A major shortcoming of the pseudo arclength continuation method is that for problems with complicated bifurcation patterns, it cannot provide the complete bifurcation diagram without known start up solutions for each of the main bifurcation branches before one can continue the solution along a specific main branch. *For spurious asymptotes it is usually not easy to locate even just one solution on each of these branches.*

The nature of our calculations requires thousands of iterations of the same equation with different ranges of initial data on a preselected (u, v) domain and range of the discretized parameter space Δt . Since the NASA Ames CM-2 allows vast numbers (typically 65,536) of calculations to be performed in parallel, our problem is perfect for computation on the CM-2.

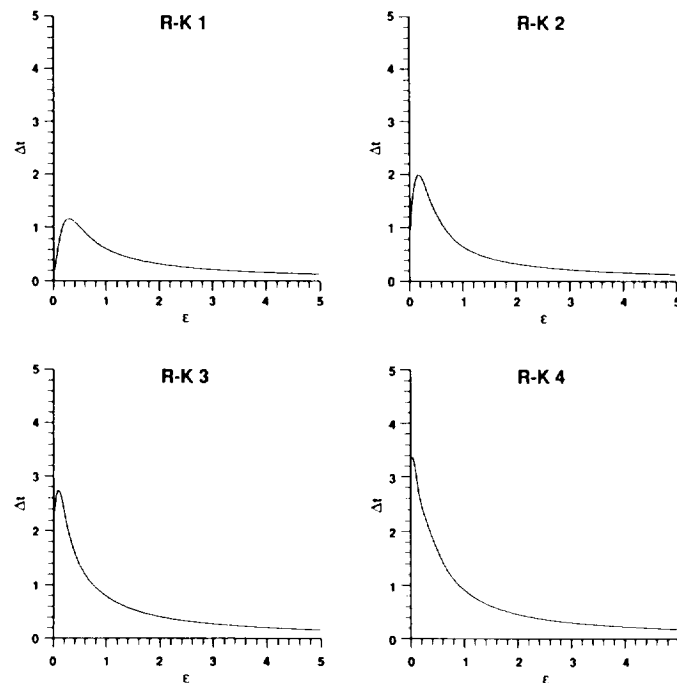


Figure 5.3 Stability Regions vs. System Parameters Viscous Burgers' Equation (Central Difference in Space).

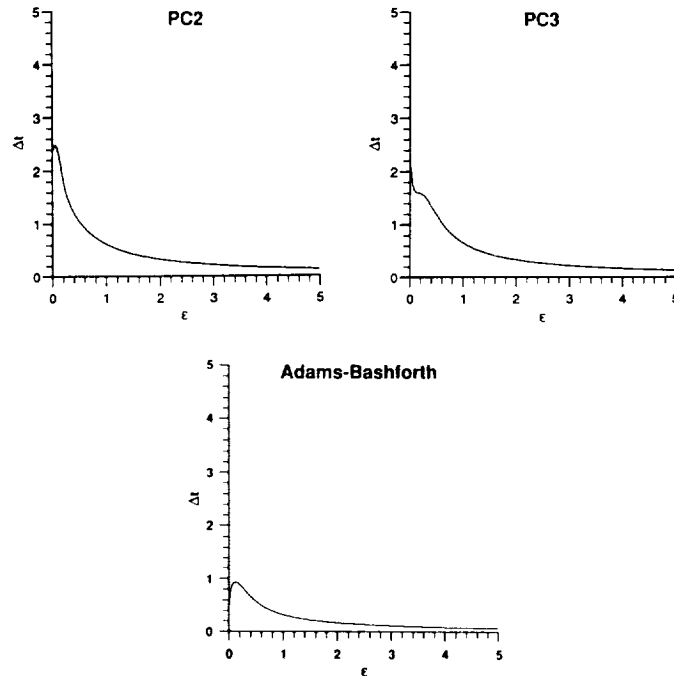


Figure 5.3 (Continued)

To obtain a “full” bifurcation diagram, the domain of initial data and the range of the Δt parameter are typically divided into 512 equal increments. For each initial datum and Δt , the discretized equations are preiterated 3,000–5,000 (more or less depending on the ODE and scheme) before the next 4,000–6,000 iterations are plotted. The preiterations are necessary in order for the trajectories to settle to their asymptotic value. The high number of iterations plotted (overlay on the same plot) is to detect periodic orbits or invariant sets. Since the results are a three dimensional graph $((\Delta t, u, v))$, we have taken slices in a given constant v - and u -plane in order to enhance viewing the decrease CPU computations. Note that with this method of computing the bifurcation diagrams, only the stable branches are plotted. Some of the bifurcation diagrams in a $v = \text{constant}$ plane for the four model ODEs and for the modified Euler, improved Euler, Kutta and R-K 4 methods are shown in Figures 5.4–5.8. Figure 5.4 shows a typical example of spurious stable fixed points (branches 3 and 4 on the diagram) occurring below the linearized stability by the modified Euler method. It also shows the existence of spurious asymptotes such as limit cycles, higher order periodic solutions and possibly numerical chaos (chaos introduced by numerics). See later sections and subsections for further details. Selected bifurcation diagrams for the rest of the numerical methods are illustrated in Section IV with basins of attraction superimposed (see Figures 6.3–6.5, 6.13, 6.14, and 6.19–6.20). See also the original NASA internal report RNR-92-008, March 1992 for additional illustrations. Due to the

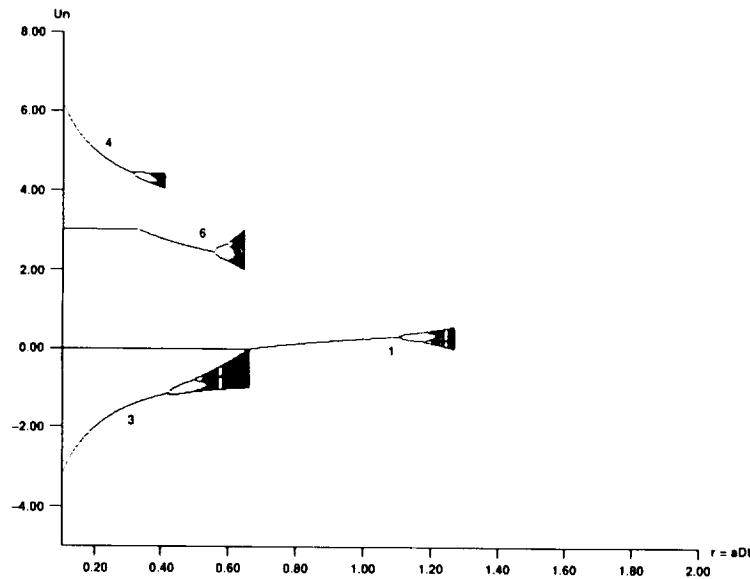


Figure 5.4 Bifurcation Diagram Predator-Prey Equation Modified Euler.

plotting package, the labels (u_n, v_n) on all of the figures are (u^n, v^n) . In the plots, $r = \Delta t$ unless stated.

The term “full bifurcation” as defined in Yee *et al.* (1991) is used to mean bifurcation diagrams that cover the essential lower-order periods in such a way as to closely resolve the “true” bifurcation diagram of the underlying discrete map for a selected range of initial data domains. This is necessary since solutions with different initial conditions will converge to different asymptotic limits. All of the computations shown are “full” bifurcation diagrams.

The following summarizes the spurious dynamical behavior of the 11 numerical methods based on selected domains of initial data and ranges of the discretized parameter r . Numerical results agree with the analytical linearized analysis reported in Sweby and Yee (1991).

Bifurcation Diagrams of Numerical Methods for Model (4.1): For $\varepsilon = 0$, (4.1) is nondissipative (or a Hamiltonian system), and all of the 11 numerical methods which are non-symplectic converge quite slowly to the fixed point $(0,0)$. We conjecture that symplectic schemes (Sanz-Serna, 1990) would be more appropriate for $\varepsilon = 0$. For sufficiently small negative (positive) ε , all of the studied schemes converge extremely slowly to the stable spiral (limit cycle). This is a typical example of slow convergence of the numerical solution due to the stiffness of the system parameter. While the bifurcation diagrams for $\varepsilon \leq 0$ for the various numerical methods are not too interesting, the bifurcation diagrams for $\varepsilon > 0$ are very instructive. Figure 5.5 shows the bifurcation diagrams for the four R-K methods for $\varepsilon = 1$.

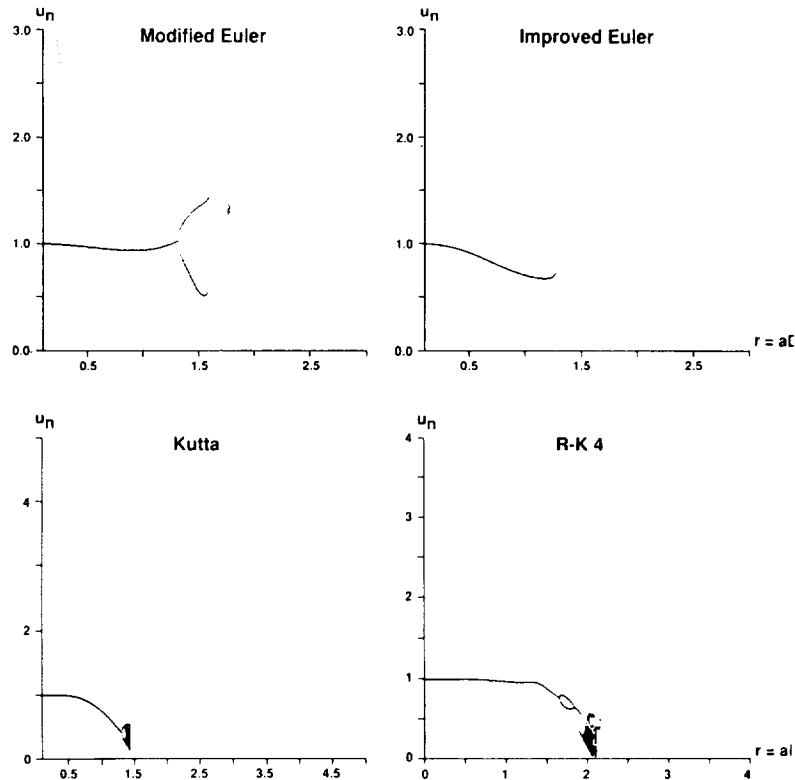


Figure 5.5 Bifurcation Diagrams Dissipative Complex Equation, $\varepsilon = 1$, $\nu = 0.0$.

Note also that R-K 4 method gives the most overall accurate numerical approximations of the true limit cycle with radius $\sqrt{\varepsilon}$ centered at $(0,0)$. The Adam-Bashforth, PC2, PC3, implicit Euler and trapezoidal methods give the least accurate numerical approximation of the limit cycle for r closer to the linearized stability. The R-K 4 and Heun methods produced spurious higher-order limit cycles (invariant set of multiple circles on the diagrams). See Section IV and Figures 6.6 and 6.8 for more details. These diagrams illustrate the unreliability of trying to compute a true limit cycle with any sizable r . This should not be surprising since the scheme only gives an $O(r^p)$ approximation to the solution trajectories. In addition, since the limit cycle is not a fixed point, we would expect inaccuracies to be introduced. However, inaccuracies are not easy to detect in practice, especially when a numerical solution produces the qualitative features expected. See Section VI and Figures 6.3–6.9 for additional details. All of the studied explicit methods produce spurious asymptotes.

For $\varepsilon > 0$, the trapezoidal method produces no spurious steady states. However, the implicit Euler method in addition to maintaining an unconditionally stable feature of the exact limit cycle, also turns the unstable fixed point $U_E = (0,0)$ of the ODE (4.1) into a stable fixed point for $r \geq 1$. See Figures 6.5, 6.8 and 6.9 for additional details.

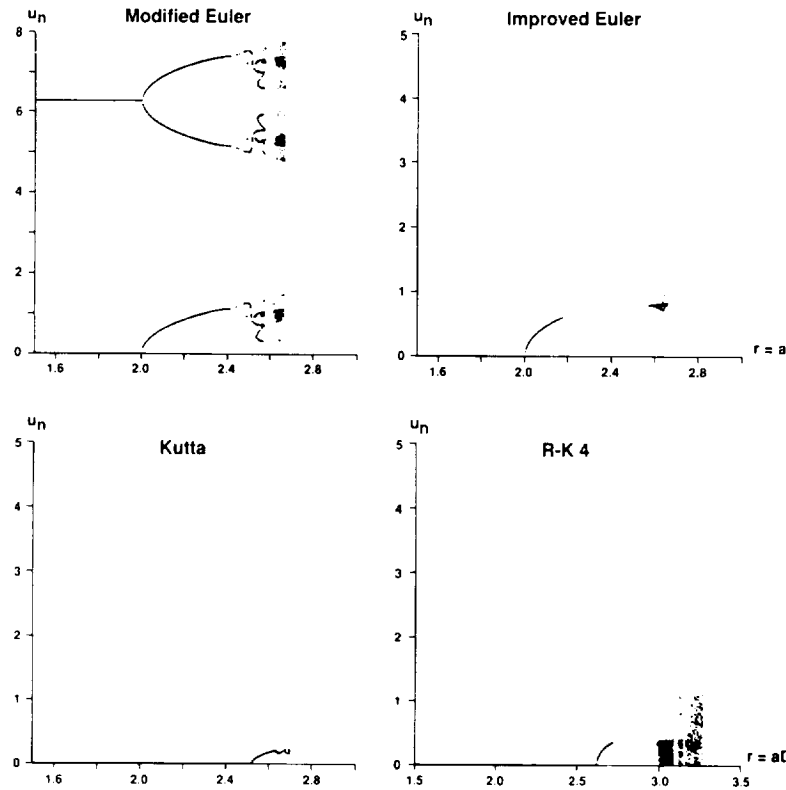


Figure 5.6 Bifurcation Diagrams Damped Pendulum Equation, $\varepsilon = 1$, $\nu = 0.0$.

Bifurcation Diagrams of Numerical Methods for Model (4.2): All of the studied explicit and implicit methods produce spurious asymptotes. In particular, some of the explicit methods (even explicit Euler) produce spurious limit cycles for certain ε values. For certain ranges of r and ε values the implicit Euler and trapezoidal methods turn the saddle points of (4.2) into an unstable fixed point of different type (see Figure 6.12). For the modified Euler method, spurious steady states occur below the linearized stability limit of the scheme. See Section VI and Figures 6.10–6.12 for additional details.

Bifurcation Diagrams of Numerical Methods for Model (4.3): Again, all of the studied explicit and implicit methods generate spurious asymptotes. Also, some of the explicit methods produce spurious limit cycles. For certain ranges of the r , the trapezoidal method turns the saddle points (exact fixed points of (4.3)) into unstable fixed points of different types, and the implicit Euler method turns the saddle points into stable fixed points of different type. The numerical results coincide with analytical analysis by examining the eigenvalues of the Jacobian of the resulting discrete map. Transcritical bifurcations introduced by the R-K 4 method resulted in the production of spurious steady state below (and very near) the linearized stability limit of the scheme. See, Section VI and Figures 6.13–6.18 for additional details.

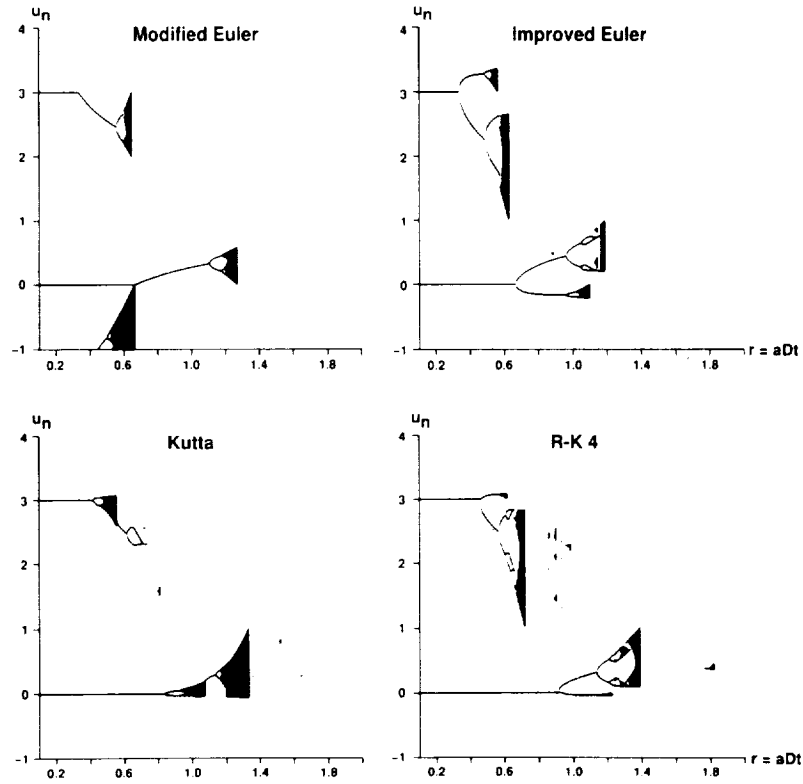


Figure 5.7 Bifurcation Diagrams Predator-Prey Equation, $v = 0.0$.

More than one spurious fixed point below the linearized stability of the scheme was introduced by the modified Euler method (see Fig. 5.4). From the form of the modified Euler scheme it is easily seen that as well as the exact fixed points U_E of the ODEs, any other value U_S satisfying

$$U_S + \frac{r}{2} S(U_S) = U_E \quad (5.14)$$

will also be a fixed point of the scheme. As mentioned earlier, we refer to these additional fixed points as spurious fixed points. Note that the U_E on the right-hand side of (5.14) encompasses both stable and unstable fixed points of the ODE and so, for the predator-prey equations (since S contains cubic terms in U), there are up to twelve (real) spurious steady states, three for each exact fixed point U_E . In fact there are six such spurious steady states which lie in the $v = 0$ plane. All of them occur below the linearized stability limits of the exact fixed points, although not all are stable there. Four (stable ones) of the six are shown in the bifurcation diagram of Figure 5.4, numbered 1, 3, 4, 6 of the bifurcation branch. The other two are unstable. Note also that the branch numbered 6 is in fact not stable but represents the stable eigen-direction (separatrix) in the $v = 0$ plane of a saddle point.

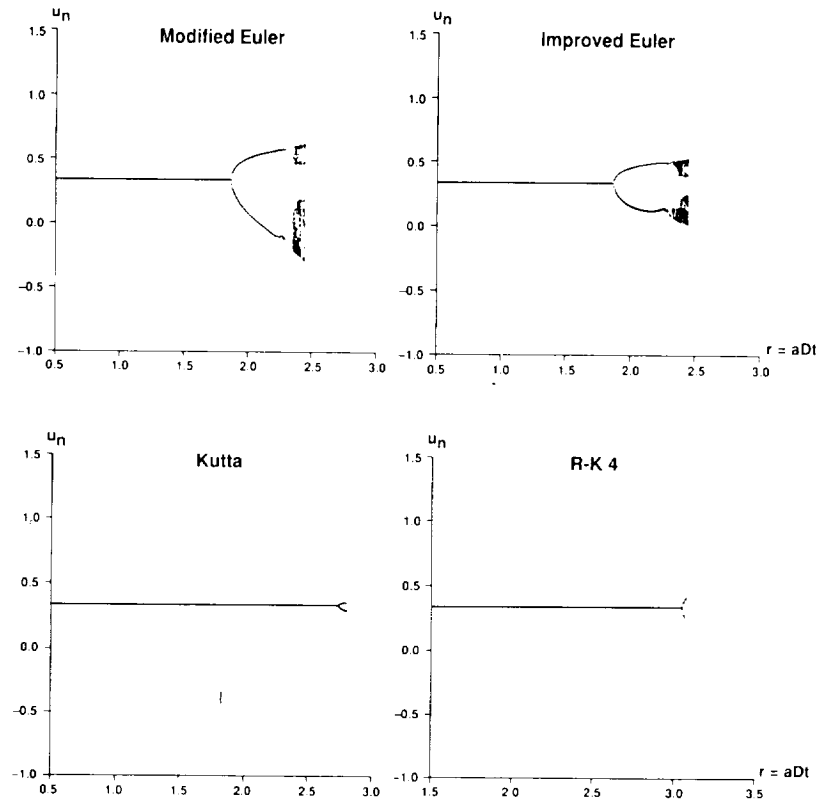


Figure 5.8 Bifurcation Diagrams Viscous Burgers' Equation, $\varepsilon = 0.1$, $r = 0.333$ (Central Difference in Space).

Bifurcation Diagrams of Numerical Methods for Model (4.4): For $\varepsilon = 0$, the ODE (4.4) is nondissipative and thus for small r , slow convergence was experienced. For r beyond the linearized limit and with $\varepsilon = 0$ all of the explicit methods produce spurious limit cycles. For $\varepsilon > 0$ (and not too large) all of the studied 11 explicit and implicit methods produce spurious asymptotes. Also, all of the explicit methods produce spurious limit cycles. For $\varepsilon = 0.1$, the Kutta and Heun methods introduce spurious asymptotes (higher than period one) that are below the linearized stability limit of the scheme. See Figures 6.19–6.25 for additional details.

6. BASINS OF ATTRACTION AND BIFURCATION DIAGRAM

This section illustrates how basins of attraction can complement the bifurcation diagrams in gaining more detailed global asymptotic behavior of time discretizations

for nonlinear DEs. Two different representations of the numerical basins of attraction were computed on the NASA Ames CM-2. One representation is bifurcation diagrams as a function of Δt with numerical basins of attraction superimposed on a constant v - or u -plane. The other representation is the numerical basins of attraction with stable asymptotes superimposed on the phase plane (u, v) . Before discussing numerical results for each of the model ODEs, the next subsection gives some preliminaries on how to compute and on how to interpret the basins of attraction diagrams for the CM-2.

6.1 Introduction

To obtain a bifurcation diagram with numerical basins of attraction superimposed on the CM-2, the preselected domain of initial data on a constant v - or u -plane and the preselected range of the Δt parameter are divided into 512 equal increments. Again, for the bifurcation part of the computations, with each initial datum and Δt , the discretized equations are preiterated 3,000–5,000 steps before the next 5,000 iterations (more or less depending on the problem and scheme) are plotted. The bifurcation curves appear on the figures as white curve, white dot and white dense dots. While computing the bifurcation diagrams it is possible to overlay basins of attraction for each value of Δt used. For the numerical basins of attraction part of the computation with each value of Δt used, we keep track of where each initial datum asymptotically approaches and color code them (appearing as a vertical strip) according to the individual asymptotes. While efforts were made to match color coding of adjacent strips on the bifurcation diagram, it was not always practical or possible. Care must therefore be taken when interpreting these overlays.

For the basins of attraction on the phase plane (u, v) with selected values of Δt and the stable asymptotes superimposed, the (u, v) domain is divided into 512×512 points of initial datum. With each initial datum and the selected Δt , we preiterate the respective discretized equation 3,000–5,000 steps and plot the next 5,000 steps to produce the asymptotes. Again, for the basins of attraction part of the computations, for each value of Δt used, we keep track of where each initial datum asymptotically approaches and color code them according to the individual asymptotes. All of the selected time steps Δt shown are based on the bifurcation diagram with the basins of attraction superimposed. The chosen time steps were selected to illustrate special features of the different bifurcation phenomena on the (u, v) plane. Details of the techniques used for detection of asymptotes and basins of attraction are given in the appendix of Sweby and Yee (1991). Note that in all of the plots, if color printing is not available, the different shades of grey represent different colors.

As a preliminary, and before discussing our major results, we discuss the numerical basins of attraction associated with modified Euler, improved Euler, Kutta and R-K 4 methods for the two scalar first-order autonomous nonlinear ODEs studied in part I of our companion paper (Yee *et al.*, 1991). The two scalar ODEs are:

$$\frac{du}{dt} = au(1 - u) \quad (6.1)$$

and

$$\frac{du}{dt} = au(1-u)(0.5-u). \quad (6.2)$$

The fixed points for (6.1) with $a > 0$ are $u = 0$ (unstable) and $u = 1$ (stable), and no additional higher order periodic fixed points or asymptotes exist. The basin of attraction for the stable fixed point $u = 1$ is the entire positive plane for all values of $a > 0$.

The fixed points for (6.2) with $a > 0$ are $u = 0$ (unstable), $u = 1$ (unstable) and $u = 0.5$ (stable) and no additional higher-order periodic solutions or asymptotes exist. The basin of attraction for the stable fixed point $u = 0.5$ is $0 < u < 1$ for all $a > 0$. The white curve, white dots and white dense dots of Figures 6.1 and 6.2 show the bifurcation diagrams for four of the R-K methods for (6.1) and (6.2). For more details of the dynamics of numerics for systems (6.1) and (6.2), see Yee *et al.* (1991). Intuitively, in the presence of spurious asymptotes the basins of the true stable steady states can be separated by the numerical basins of attraction of the stable and unstable spurious asymptotes.

Take, for example, the ODE (6.1) where the entire domain u is divided into two basins of attraction for the ODE independent of any real a . Now if one numerically integrates the ODE, depending on the scheme and r , extra stable and unstable fixed points of any order can be introduced by the scheme. The bifurcation part of Figures 6.1 and 6.2, cannot distinguish the types of bifurcation and the periodicity of the spurious fixed points of any order. With the numerical basins of attraction and their respective bifurcation diagrams superimposed on the same plot, the type of bifurcation and to which initial data asymptote to which stable asymptotes become apparent. Note that for Figures 6.1 and 6.2 $r = a\Delta t$.

For example, any initial data residing in the green region in Figure 6.1 for the modified Euler method belong to the numerical basin of attraction of the spurious (stable) branch emanating from $u = 3$ and $r = 1$. Thus, if the initial data is inside the green region, the solution can never converge to the exact steady state using even a small fixed but finite Δt (all below the linearized stability limit of the scheme). Note that the green region extends upward as r decreases below 1. Thus for certain ranges of r values, the domain is divided into four basins (instead of two for the ODE). But of course higher period spurious fixed points exist for other ranges of r and more basins are created within the same u domain.

A similar situation exists for the R-K 4 method (Fig. 6.1), except now the numerical basins of attraction of the spurious fixed points occur very near the linearized stability limit of the scheme, with a small portion occurring below the linearized stability limit. In contrast to the improved Euler method (Fig. 6.1), the green region represents the numerical basins of one of the spurious stable transcritical bifurcation branches of the fixed point. The bifurcation curve directly below it with the corresponding red portion is the basin of the other spurious branch. See Yee *et al.* (1991) or Hale and Kocak (1991) for a discussion of the different types of bifurcations. With this way of color coding the basins of attraction, one can readily see (from the plots) that for ODE (6.1), the modified Euler, improved Euler and R-K 4 methods, experience one steady bifurcation before a period doubling bifurcation occurs (Fig. (6.1)). Using the PC3 method to solve (6.1) (figure not shown; see Yee *et al.*, 1991), more than one consecutive steady bifurcation occurs before period doubling bifurcation. For ODE (6.2), the improved Euler experi-

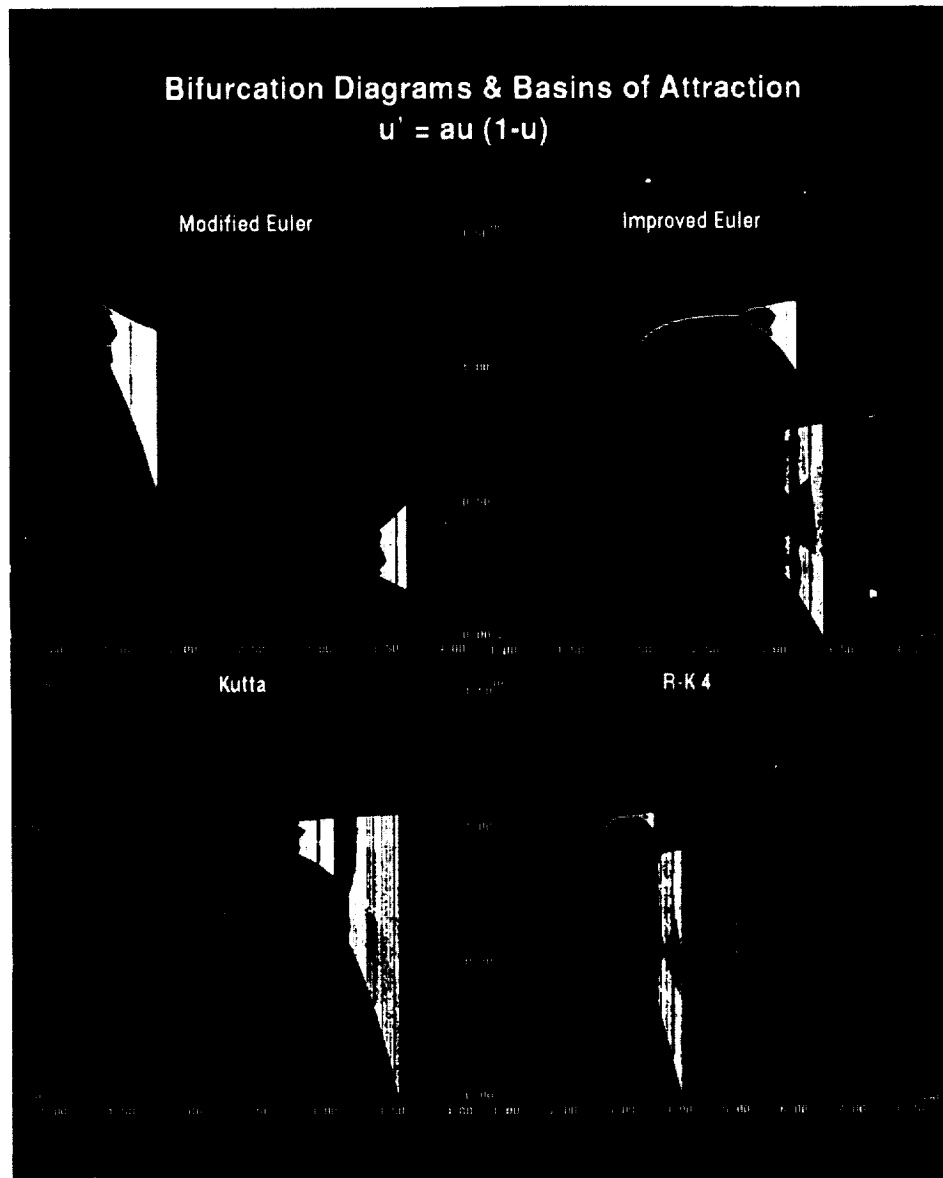


Figure 6.1 (See Color Plate I at the back of this issue.)

ences two consecutive steady bifurcations before a period doubling bifurcation occurs (Fig. (6.2)). Using the PC3 method to solve (6.2) (figure not shown; see Yee *et al.* 1991), four consecutive steady bifurcations occur before period doubling bifurcations. The modified Euler and R-K 4 methods, however, experience only one steady bifurcation before period doubling bifurcations occur.

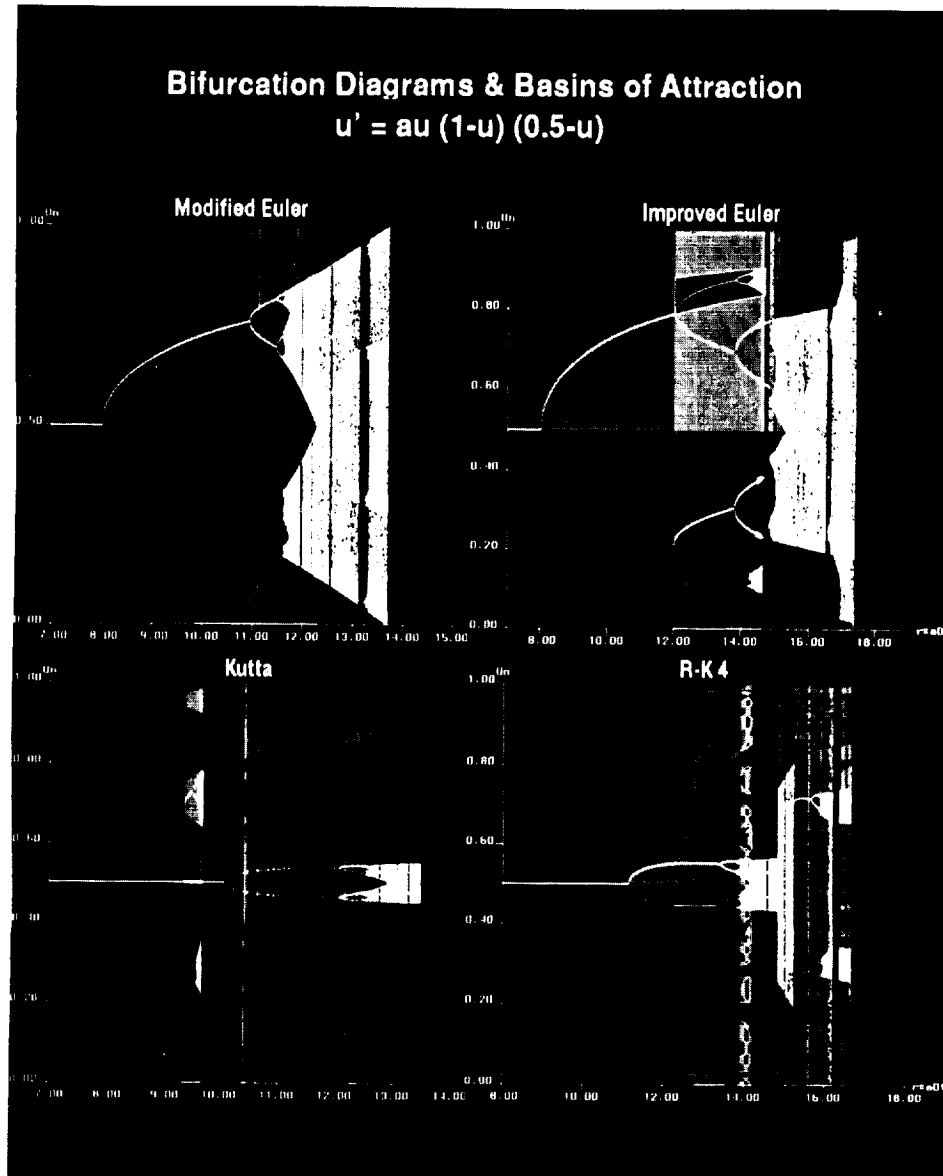


Figure 6.2 (See Color Plate II at the back of this issue.)

The next section presents similar diagrams for the 2×2 systems of model nonlinear ODEs (4.1)–(4.4). In this case, only basins of attraction with bifurcation diagrams superimposed on $v = \text{constant}$ planes are shown. Selected results for both representations of numerical basins of attraction are shown in Figures 6.3–6.5, 6.8–6.25 for the numerical methods. Section 6.6 summarizes similar results presented in Yee and

Sweby (1993a) for iterative procedures in solving nonlinear systems of algebraic equations arising from four implicit LMMs. In the plots $r = \Delta t$. White dots and white curves on the basins of attraction with bifurcation diagrams superimposed represent the bifurcation curves. White dots and white closed curves on the basins of attraction with the numerical asymptotes superimposed represent the stable fixed points, stable periodic solutions or stable limit cycles. The black regions represent divergent solutions.

Note that the streaks on some of plots are either due to the non-settling of the solutions within the prescribed number of preiterations or the existence of small isolated spurious asymptotes. Due to the high cost of computation, no further attempts were made to refine their detailed behavior since our purpose was to show how, in general, the different numerical methods behave in the context of nonlinear dynamics.

6.2 Numerical results for the Dissipative Complex Equation

Figures 6.3–6.5, 6.8, 6.9 show selected results for the two representations of numerical basins of attraction for model (4.1) for $\varepsilon = 1$. The exact solution for (4.1) with $\varepsilon = 1$ is a stable limit cycle with unit radius centered at $(0, 0)$. The basin of attraction for the limit cycle is the entire (u, v) plane except the unstable fixed point $(0, 0)$.

Comparing Figures 6.3–6.5 with Figure 5.5, one can appreciate the added information that the basin of attraction diagrams can provide. As Δt moves closer to the linearized stability limit of the limit cycle, the size (red) of the numerical basins of attraction decreases rapidly. This is due to the existence of spurious unstable asymptotes below as well as above the linearized stability limit. The green region, shown in Figure 6.5 using the implicit Euler method, is the numerical basin of attraction for the stabilized fixed point $(0, 0)$. Note how the implicit Euler method turns an unstable fixed point $(0, 0)$ of the ODE system into a stable one for $\Delta t \geq 1$.

Figures 6.6 and 6.7 show the phase trajectories and Figures 6.8 and 6.9 show the same figures with numerical basins of attraction superimposed for four different Δt by the R-K 4 and implicit Euler methods, respectively. Note how little information Figures 6.6 and 6.7 can provide as compared to Figures 6.8 and 6.9. Note also how rapidly the size of the basin (red) decreases as Δt increases for the R-K 4 method. This phenomenon can relate to practical computations where only a fraction of the allowable linearized stability limit of Δt is safe to use if the initial data is not known. For $\Delta t = 1.75$ and 2, spurious limit cycles of higher order period exist. (The multiple white circles with only one distinct basin of attraction). In this case, the red regions represent the basins of the spurious numerical solutions.

Figure 6.9 illustrates the situation where unconditionally stable LMM schemes can converge to a wrong solution if one picks the initial data inside the green region which are valid physical initial data for the ODE. Thus even though LMM preserved the same number of fixed points as the underlying ODE, these fixed points can change type and stability. This phenomenon is related to the “non-robustness” of implicit methods sometimes experienced in CFD computations. In this type of computation where the initial data are not known, the highest probability of avoiding spurious asymptotes is achieved when a fraction of the allowable linearized stability limit of Δt is employed.

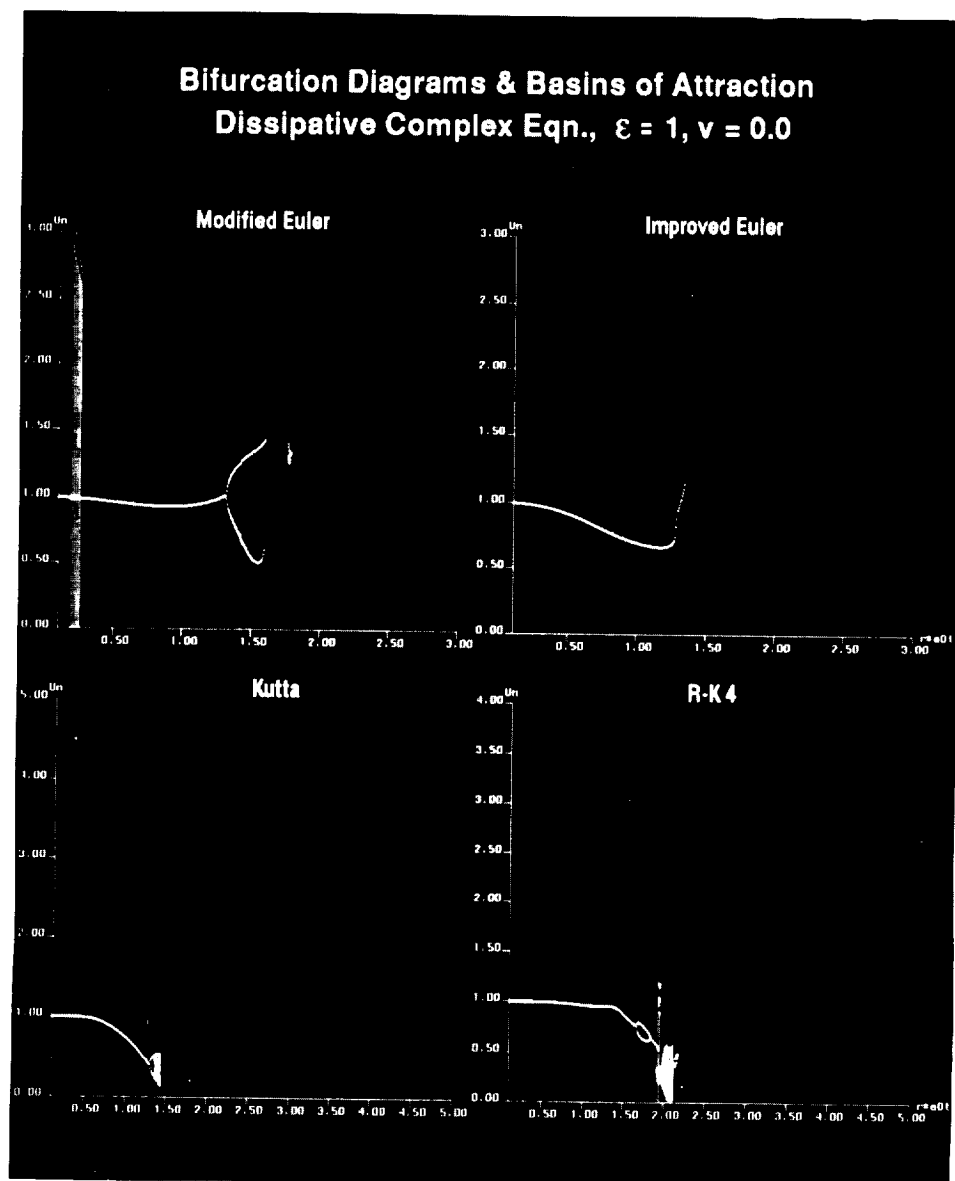


Figure 6.3 (See Color Plate III at the back of this issue.)

6.3 Numerical Results for the Damped Pendulum Equation

Selected results for the studied numerical methods for $\varepsilon = 1$ and $\varepsilon = 1.5$ are shown in Figures 6.10–6.12. Here, for each Δt value the different colors represent different numerical basins of attraction of the respective asymptotes. Observe the striking

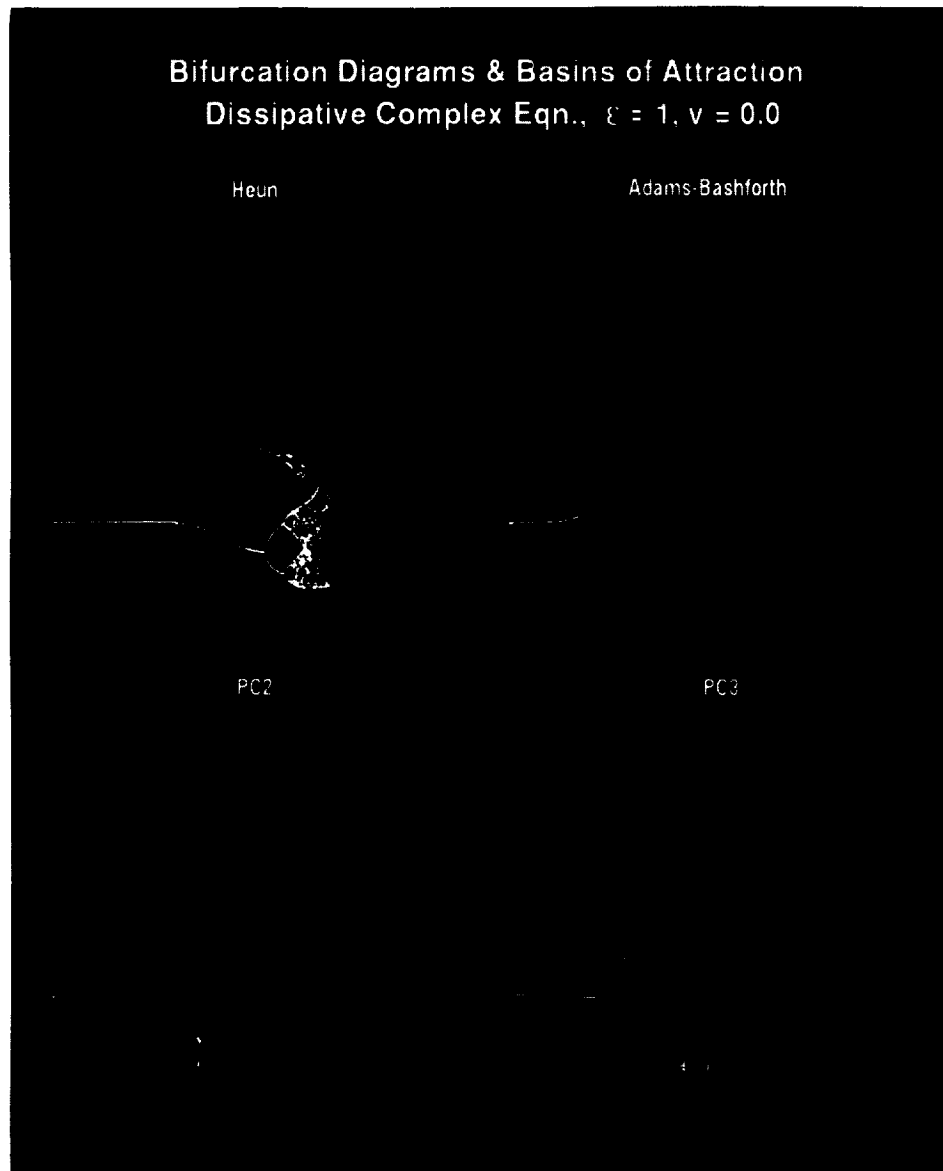


Figure 6.4 (See Color Plate IV at the back of this issue.)

difference in behavior between the explicit and implicit methods. The shapes and sizes of the numerical basins of attraction by the implicit Euler method for $\Delta t = 0.1$ shown in Figure 6.12 appear to be similar to the exact basins of attraction of the DE (4.2). From the different colors of the basins in Figure 6.10 one can readily identify that spurious higher than period one and spurious limit cycles exist for the different Δt values by the

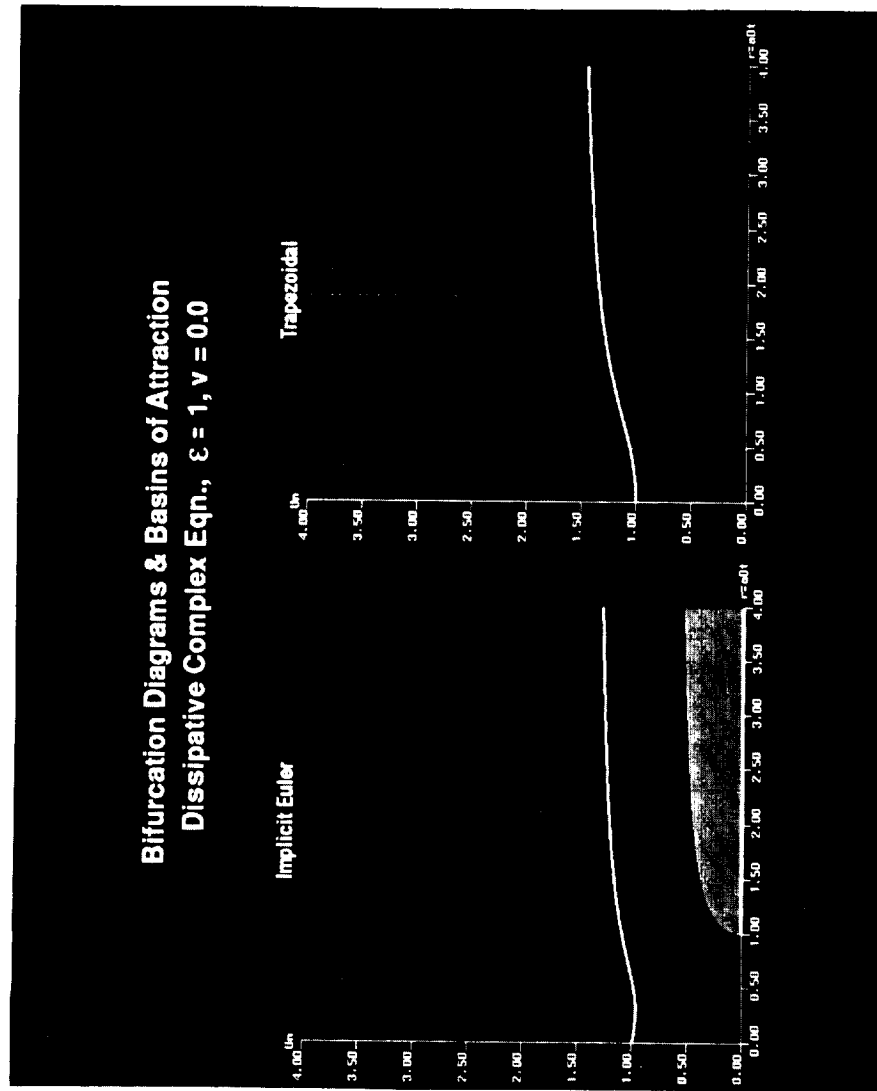


Figure 6.5 (See Color Plate V at the back of this issue.)

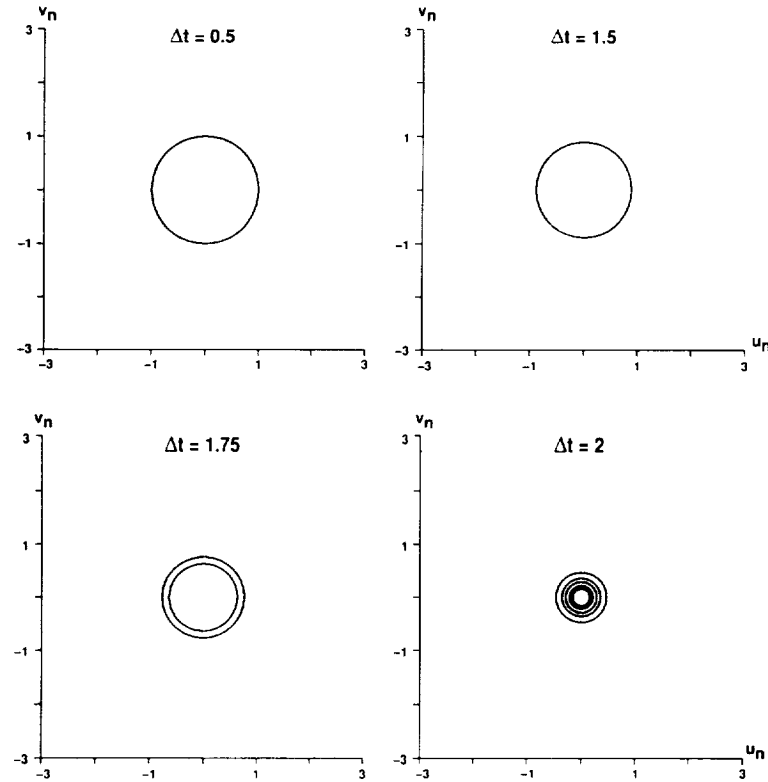


Figure 6.6 Phase Trajectories Dissipative Complex Equation, $\varepsilon = 1$, R-K 4.

explicit Euler method. For $\Delta t = 1.4$, the explicit Euler produces spurious period two fixed points. Figure 6.11 shows the existence of spurious fixed points below the linearized stability limit by the modified Euler method and spurious fixed points of period 4 (the four white dots one each basin) above the linearized stability limit by the R-K 4 method. Figure 6.12 shows the evolution (birth and death) of spurious fixed points of higher-order period for the implicit Euler method. This figure illustrates another situation where unconditionally stable schemes can converge to a wrong solution even though these schemes preserved the same number and type of fixed points as the underlying ODE. In this case it is the birth of spurious stable and unstable asymptotes or even numerical chaos that contributes to the size reduction of the true basins of attraction of the ODE.

6.4 Numerical Results for the Predator-Prey Equation

Selected results for the two representations of numerical basins of attraction are shown in Figures 6.13–6.18. Comparing Figures 6.13, 6.15, 6.16, with Figures 5.4 and 5.7, one can again appreciate the added information that the basin of attraction diagrams can

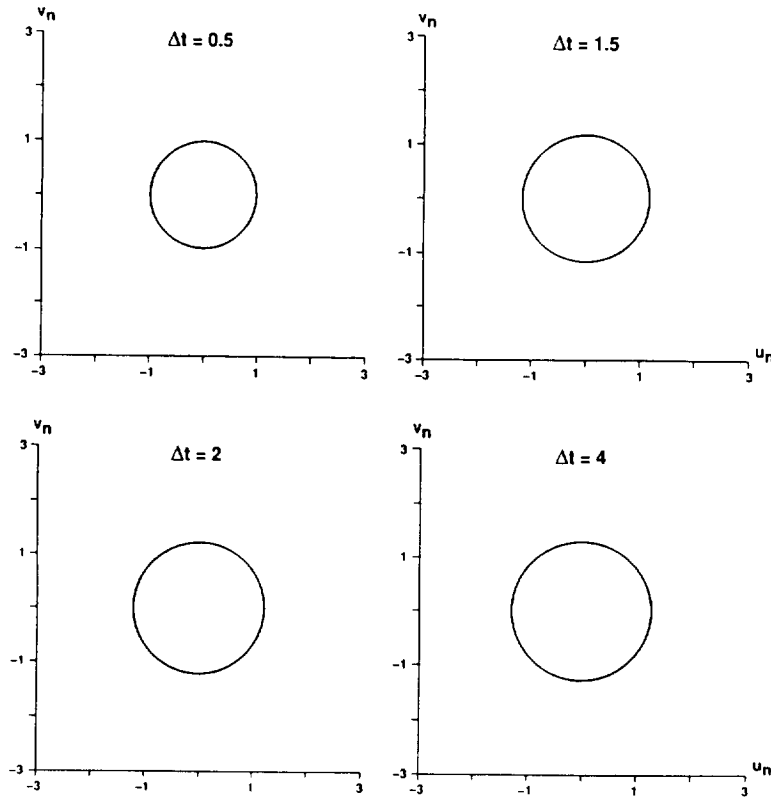


Figure 6.7 Phase Trajectories Dissipative Complex Equation, $\varepsilon = 1$ Linearized Implicit Euler.

provide. Here for all of these figures (except Fig. 6.15 for the last four Δt values), the green regions represent the numerical basins of attraction for the stable spiral $(2.1, 1.98)$ and red regions represent the numerical basins of attraction for the stable node $(0, 0)$.

The numerical basins of attraction in Figure 6.18 with $\Delta t = 0.1$ appear to be the same as the exact basins of attraction of the DE (4.3). The numerical basin of attraction by the implicit Euler for the fixed point $(0, 0)$ with $\Delta t = 0.1$ is larger than the corresponding exact basin of attraction for the DE (4.3). In this case the numerical basin of attraction for the divergent solution (black region) is smaller than the true one. The dramatic difference in shapes and sizes of numerical basins of attraction for the different methods and solution procedure combinations compared with the exact basin of attraction is even more fascinating than for the previous two models.

Take, for example, one of the most interesting cases, the modified Euler method. Figure 6.15 shows how spurious stable fixed points can alter the numerical basins of attraction of the stable node and spiral of the ODE (4.3) for time steps that are below the linearized stability limit of both of these stable fixed points of the ODE (see Figs. 5.4

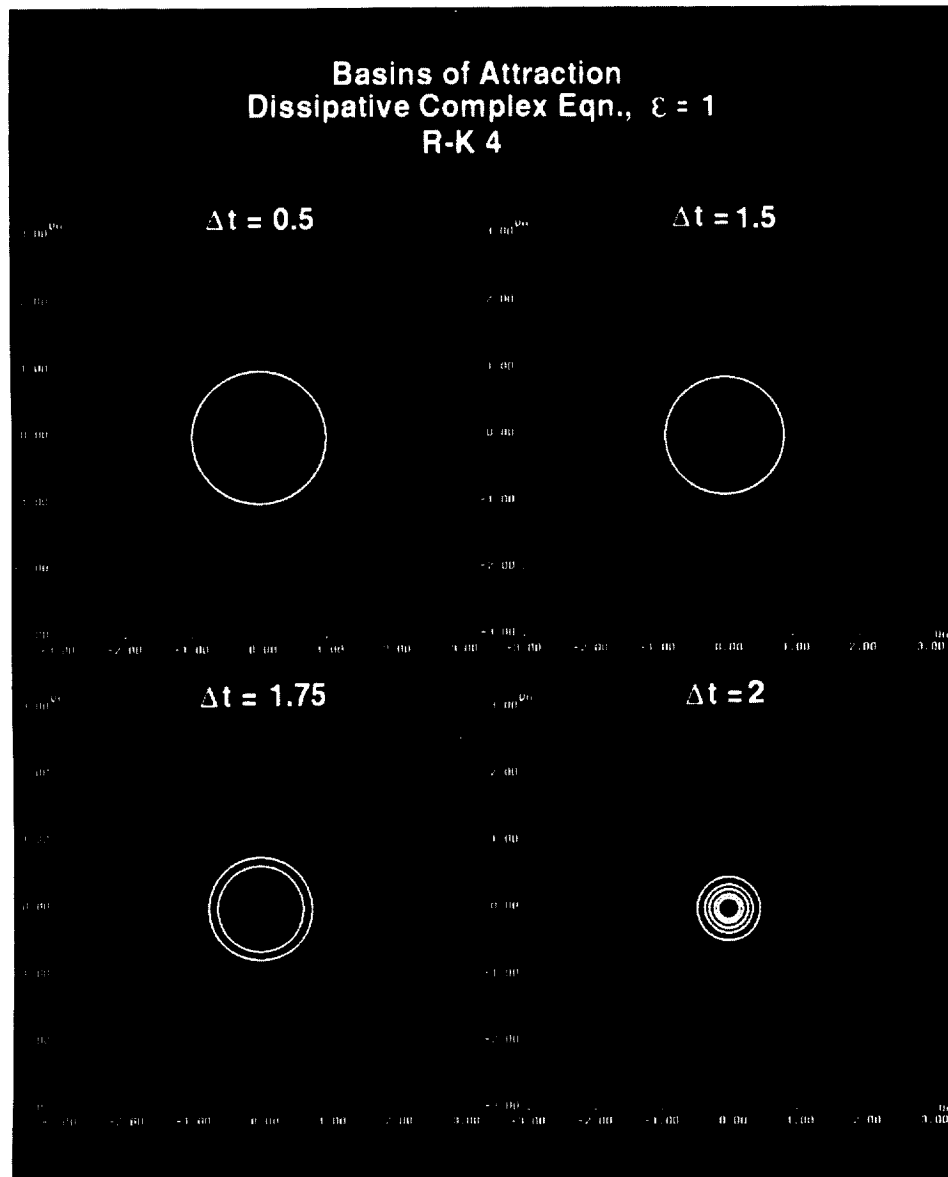


Figure 6.8 (See Color Plate VI at the back of this issue.)

and 6.13). For $\Delta t = 0.8$, the stable node bifurcates into a spurious fixed point. Without performing the bifurcation analysis one would not be able to detect this particular spurious fixed point, since the value of the spurious one is so close to the exact fixed point $U_E = (0, 0)$. For $\Delta t = 0.9524$, there is the birth of a spurious limit cycle (the white close curve). For $\Delta t = 1.2$, spurious higher-order periodic solutions exist. Note that for

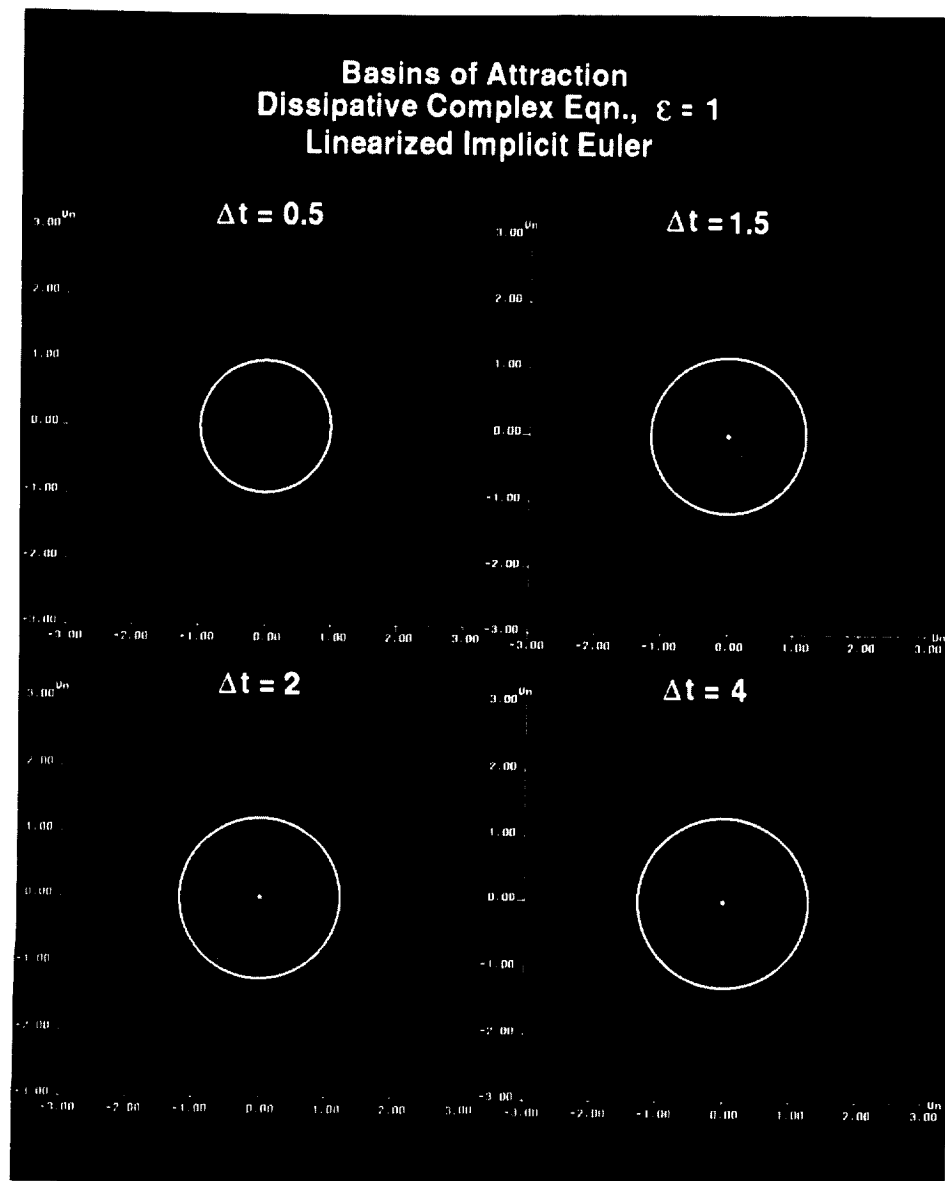


Figure 6.9 (See Color Plate VII at the back of this issue.)

the first four Δt values in Figure 6.15, the fixed points and asymptotic values are colored black instead of white due to the birth of additional numerical basins of attraction that are colored white.

The implicit methods change the two saddle points into stable or unstable fixed points of other types as illustrated in Figures 6.14, 6.17 and 6.18. For the implicit Euler,

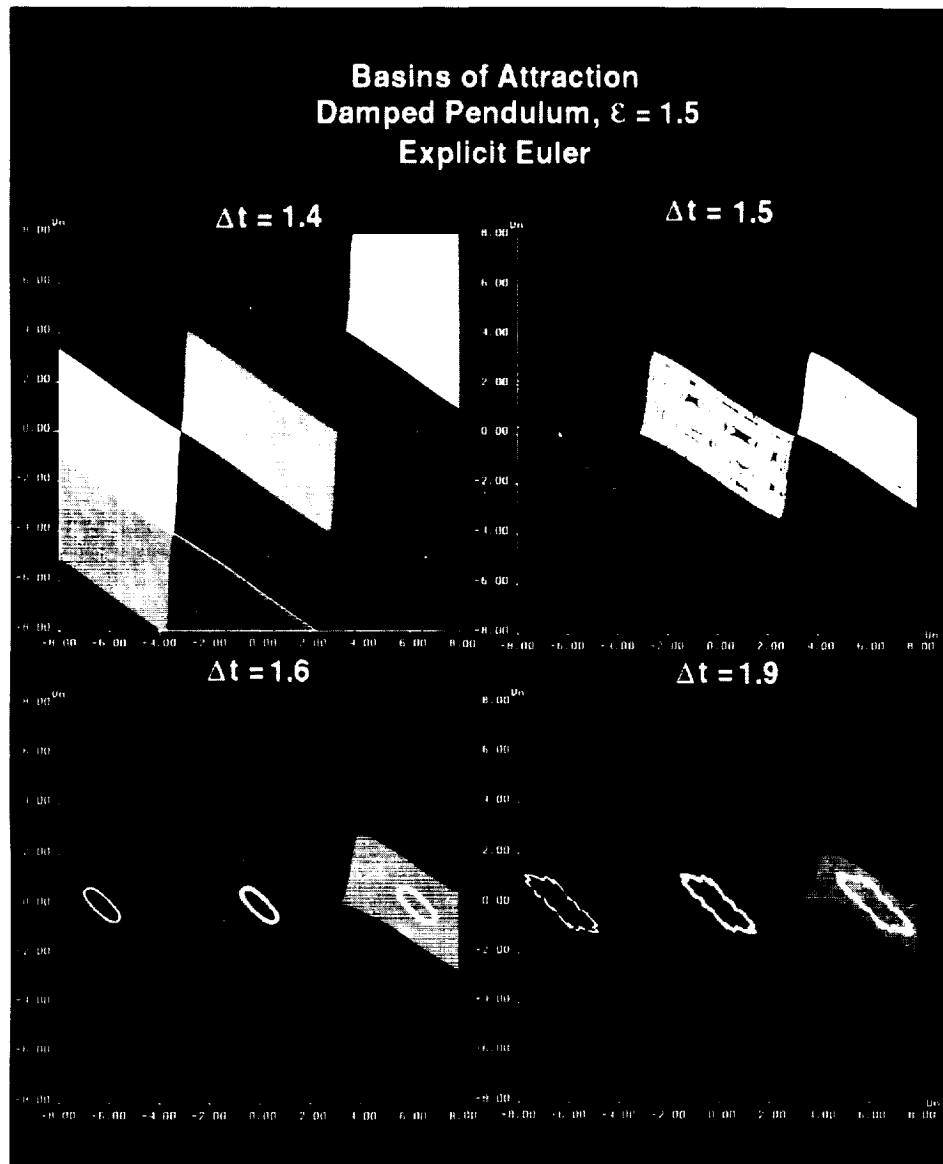


Figure 6.10 (See Color Plate VIII at the back of this issue.)

the two fixed points $(2.1, 1.98)$ and $(0, 0)$ are unconditionally stable and the *stabilized* fixed points $(1, 0)$ and $(3, 0)$ (saddles for the original ODE) are almost unconditionally stable except for small Δt . This is most interesting in the sense that the numerical basins of attraction for the stable exact fixed points U_E of the model (4.3) by the implicit Euler method were permanently altered for Δt near or larger than 3 as illustrated in

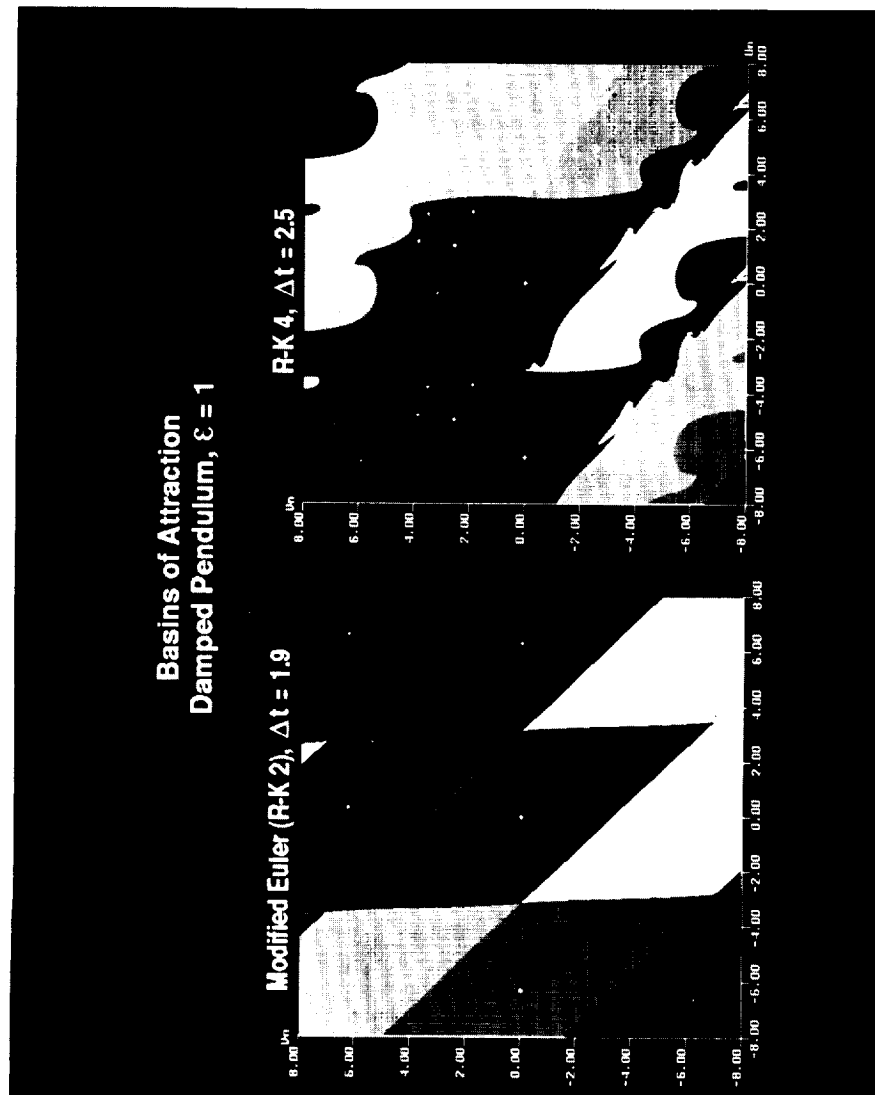


Figure 6.11 (See Color Plate IX at the back of this issue.)

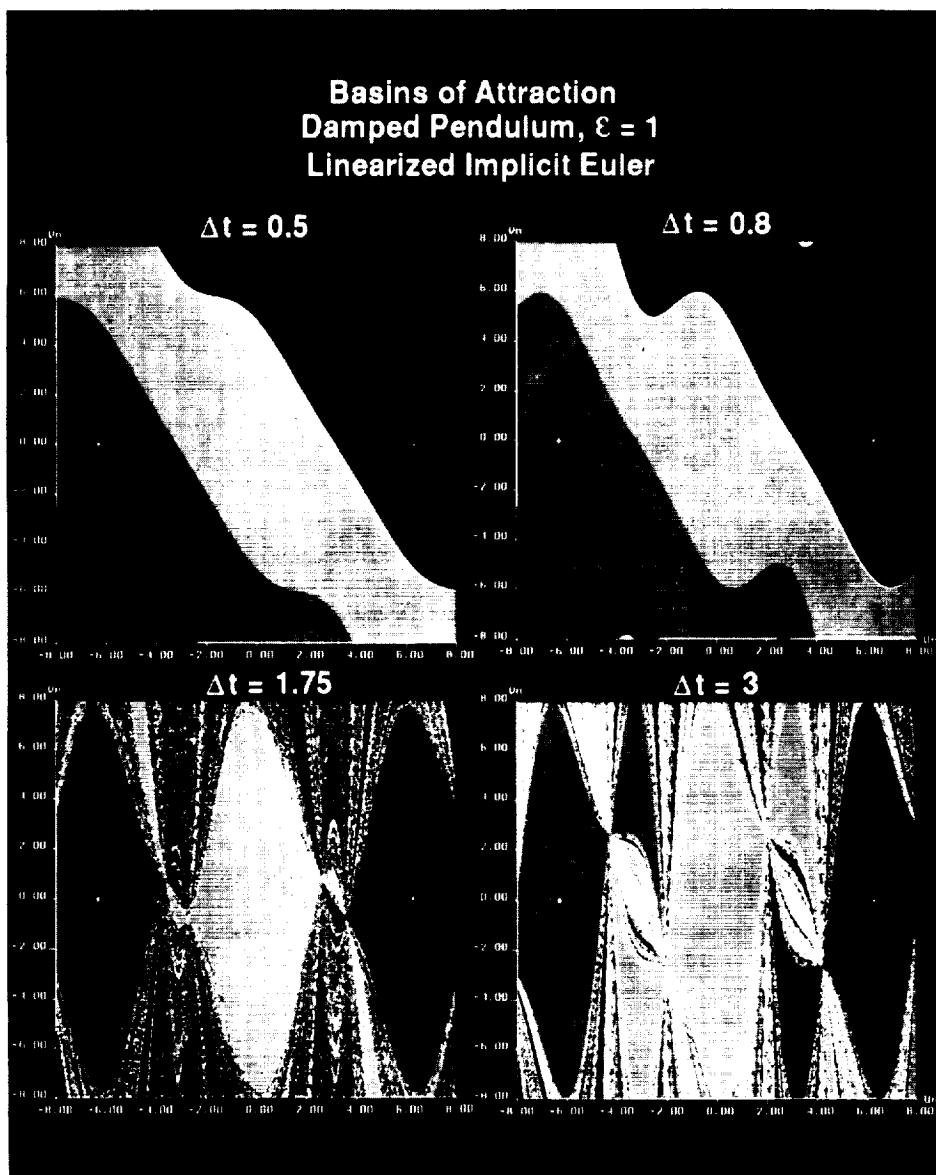


Figure 6.12 (See Color Plate X at the back of this issue.)

Figures 6.14, 6.17. It would be easier to interpret the results in Figure 6.14 if one interchanged the yellow and green colors for $\Delta t \geq 1$. Observe how the newly created numerical basins of attraction by the *stabilized* fixed points $(1, 0)$ and $(3, 0)$ resulted in the segmentation of the numerical basins of attraction of the stable node $(0, 0)$ and stable spiral $(2.1, 1.98)$. Although the trapezoidal method did not turn the two saddle

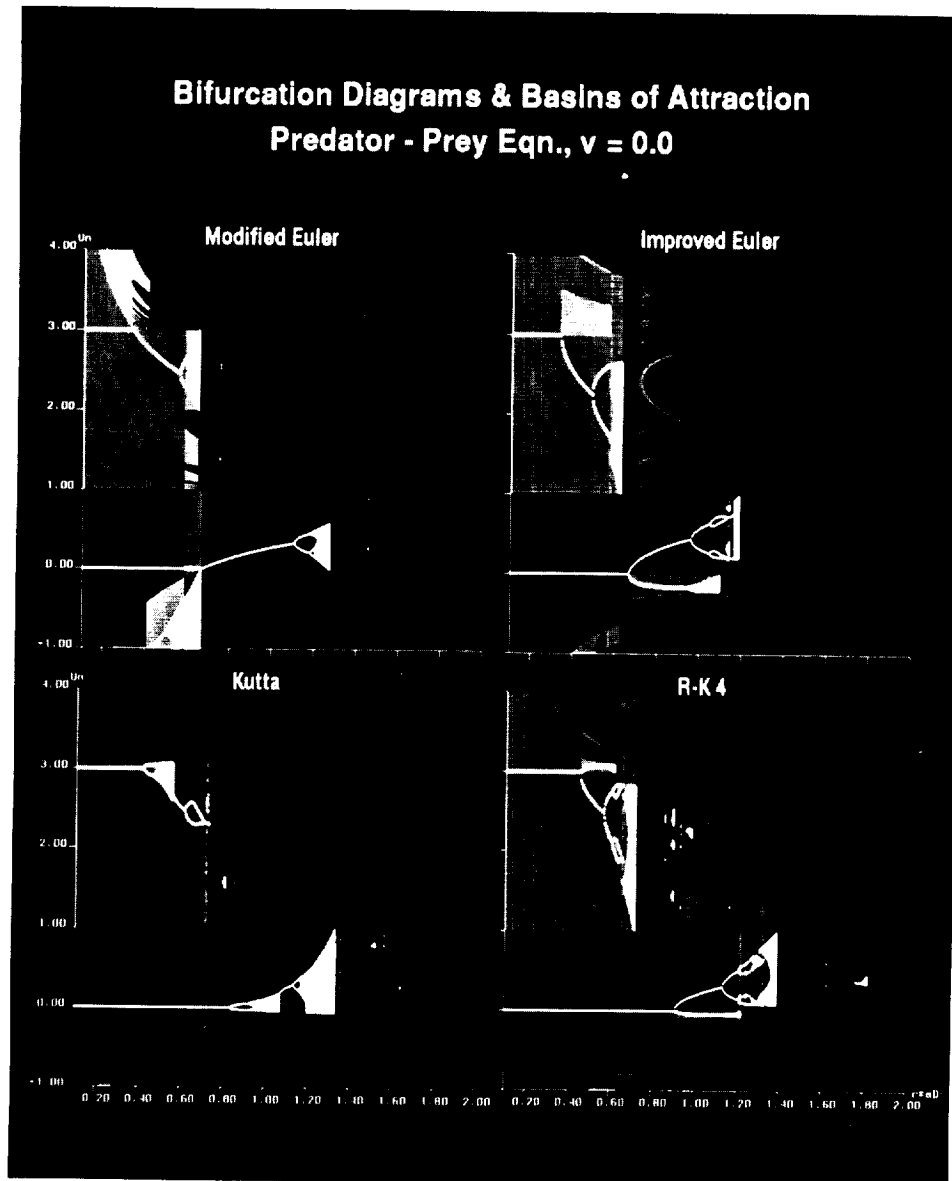


Figure 6.13 (See Color Plate XI at the back of this issue.)

points $(1,0)$ and $(3,0)$ into stable fixed points of different type, they did turn the two saddle points into *unstable* fixed points of different type.

The evolution of the numerical basin of attraction as Δt changes is very traumatic these implicit LMMs. The cause of nonconvergence of these implicit LMMs may due to the fact that their numerical basins of attraction are fragmented. Take for example the

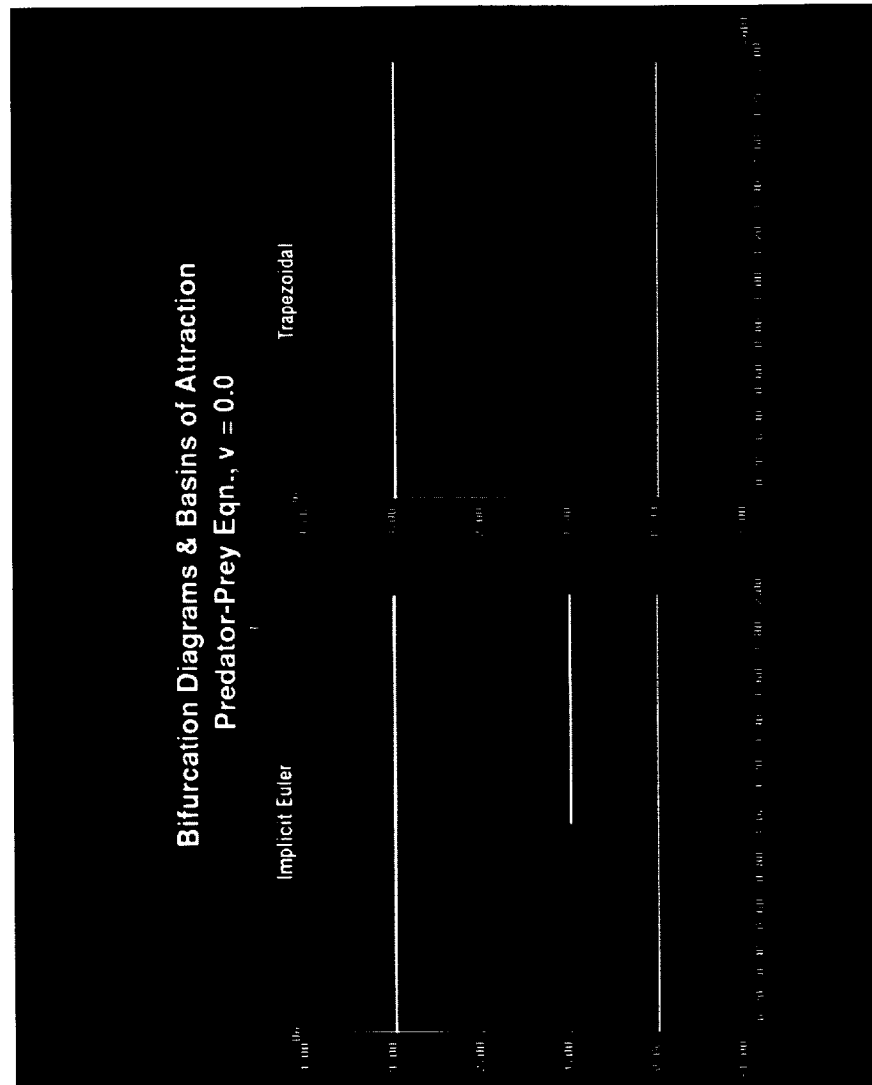


Figure 6.14 (See Color Plate XII at the back of this issue.)

trapezoidal method (Fig. 6.18) where the scheme becomes effectively unstable for large Δt . The size of the numerical basins of attraction for the stable fixed points U_E shrink to almost nonexistence. This phenomenon might be one of the contributing factor to the unpopularity of the trapezoidal method in CFD. The basins are so fragmented and small for large Δt that they are beyond the accuracy of the CM2 to resolve and no

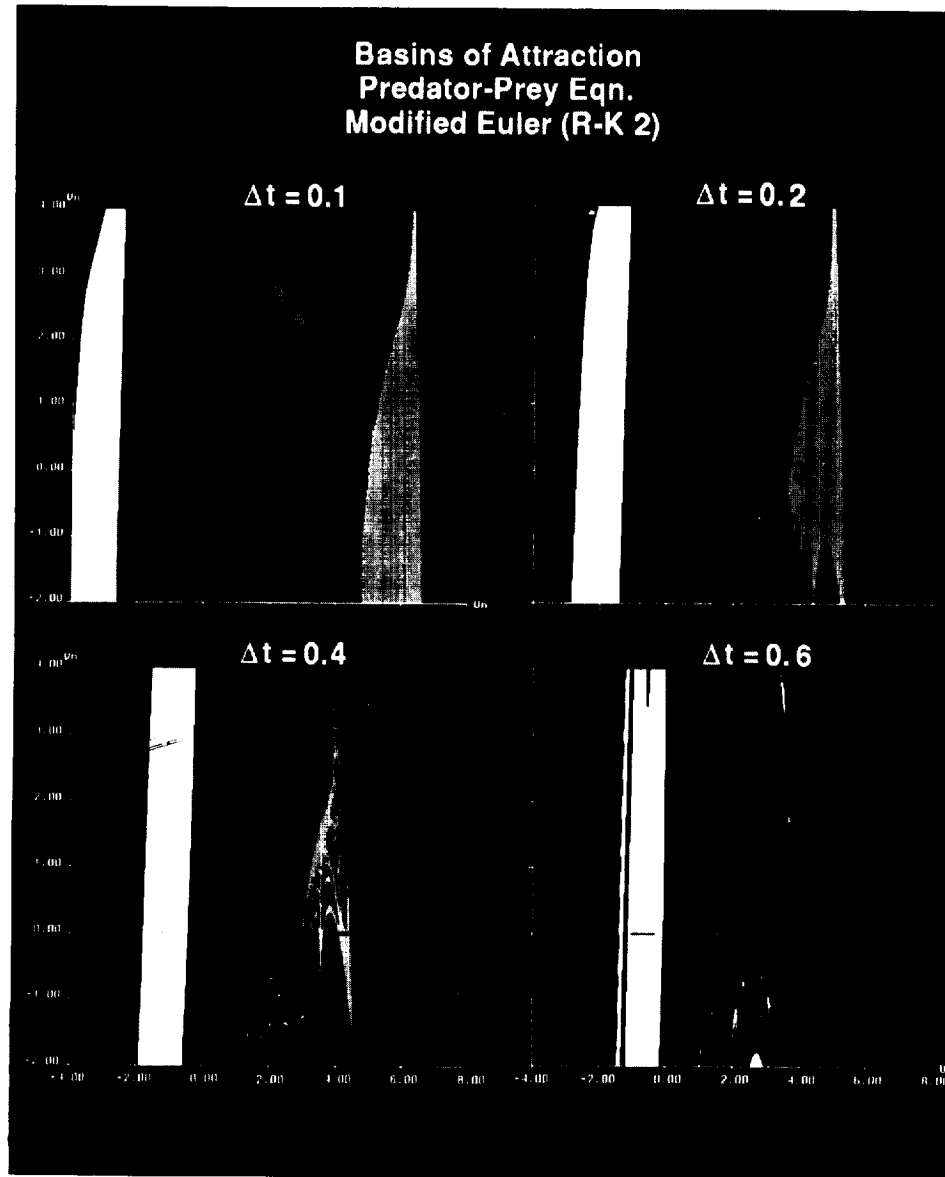


Figure 6.15 (See Color Plate XIII at the back of this issue.)

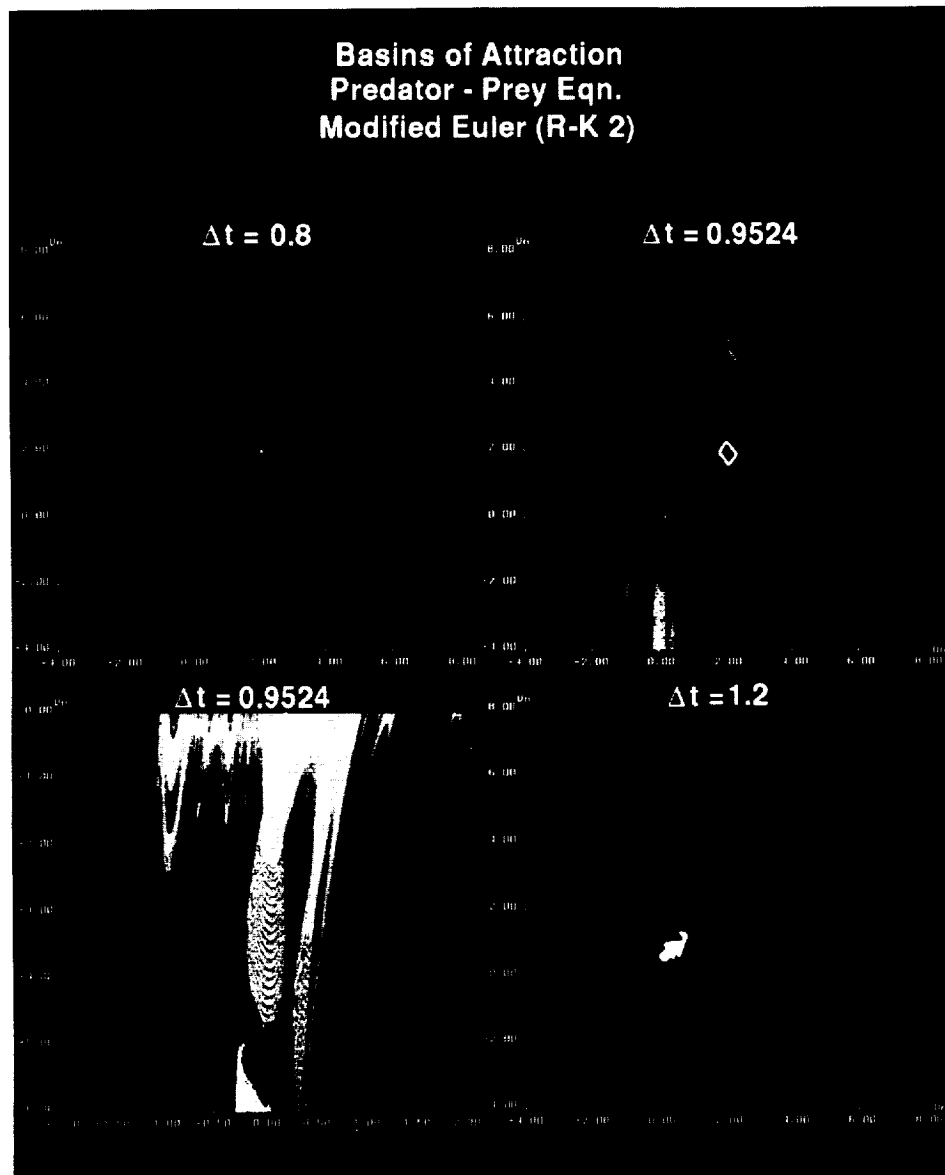


Figure 6.15 (Continued) (See Color Plate XIII at the back of this issue.)

further attempt was made. A better approach in computing these types of basins is to use interval arithmetic or the enclosure type method (Adams, 1990).

6.5 Numerical Results for the Perturbed Hamiltonian Equation

Selected results for the two representations of numerical basins of attraction of the various numerical methods for $\varepsilon = 0.1$ are shown in Figures 6.19- 6.25. Our studies

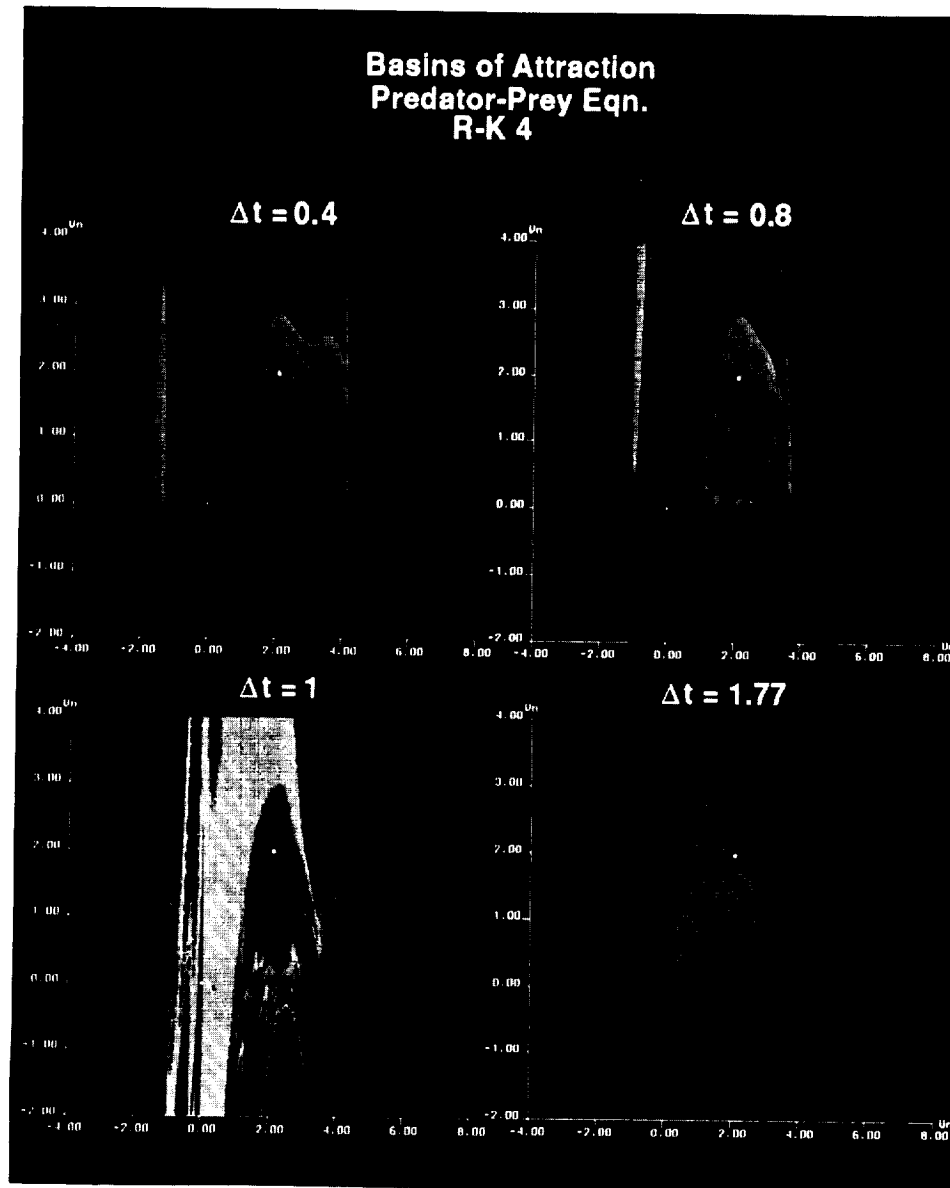


Figure 6.16 (See Color Plate XIV at the back of this issue.)

indicate that all of the studied Runge-Kutta methods exhibit spurious limit cycles and other spurious periodic solutions. For the Kutta and Heun methods, stable spurious asymptotes can occur below the linearized stability limit of the scheme. The implicit methods also exhibit spurious asymptotes. In particular, unstable spurious asymptotes were produced below the linearized stability limit by all of the studied schemes.

Although this example consists of an artificially small number of grid points, it can shed some light on the interplay between initial data, spurious stable and unstable asymptotes, basins of attraction and the time-dependent approach to the asymptotic numerical solutions. A solid understanding of this concept at the fundamental level can

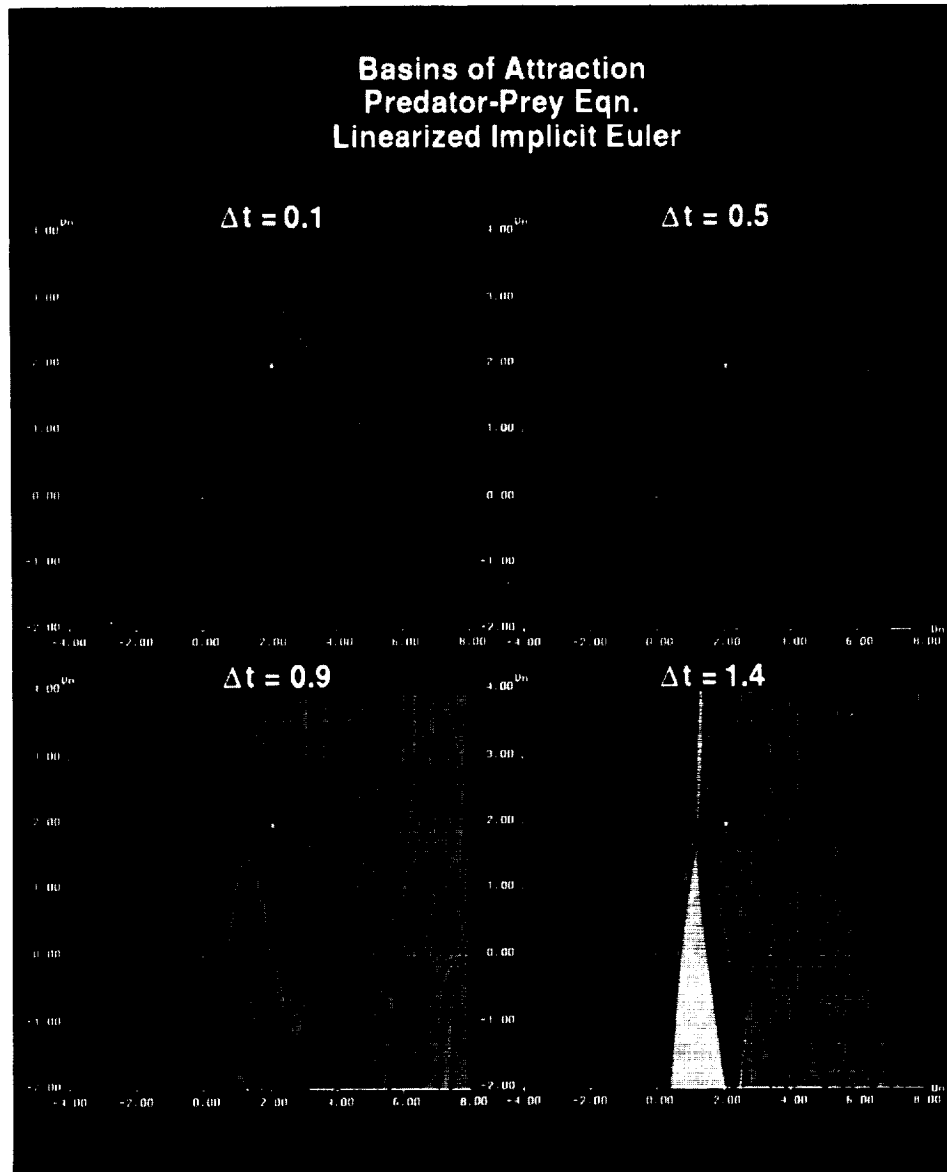


Figure 6.17 (See Color Plate XV at the back of this issue.)

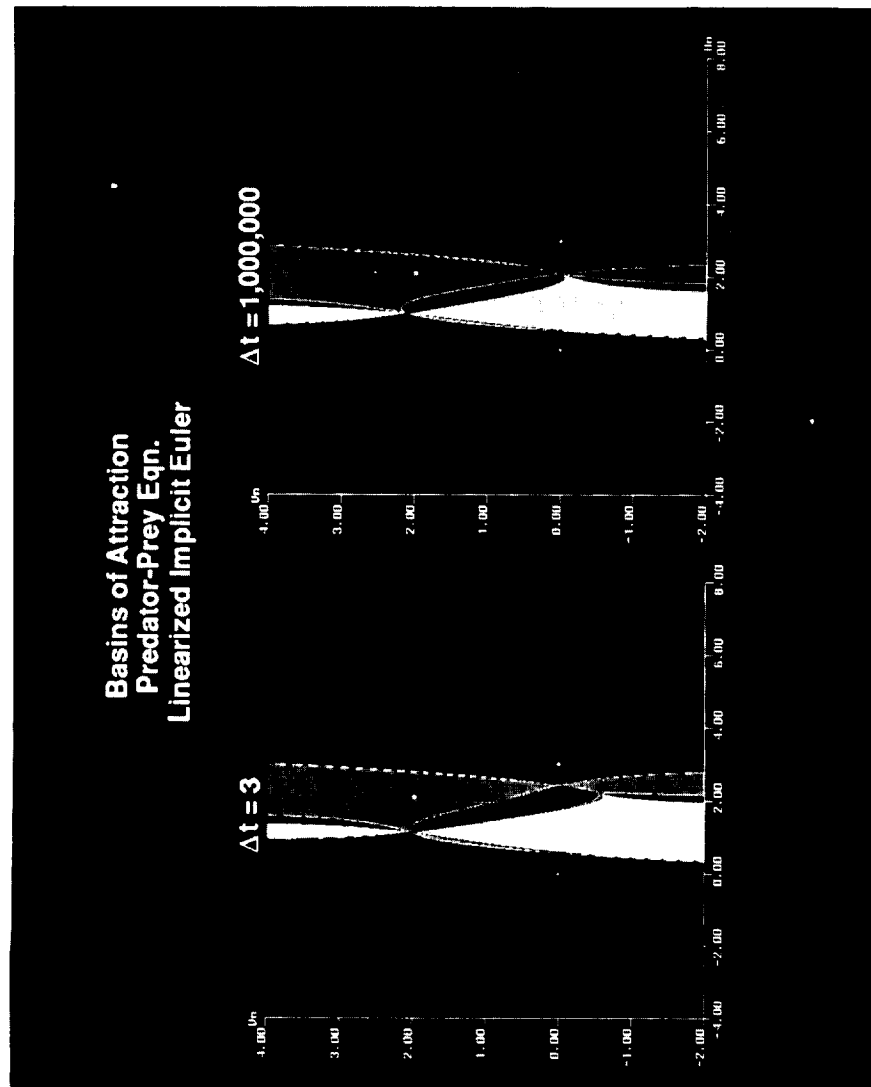


Figure 6.17 (Continued) (See Color Plate XV at the back of this issue.)

help to determine the reliability of the time-dependent approach to obtaining steady-state numerical solutions.

In all of Figures 6.19–6.25, red regions represent the numerical basins of attraction for the stable spiral $(1/3, 1/3)$ when Δt is below the linearized stability of the scheme. When Δt is above the linearized stability, some of the red regions represent the numerical basin of attraction of the stable spurious asymptotes. The numerical basins

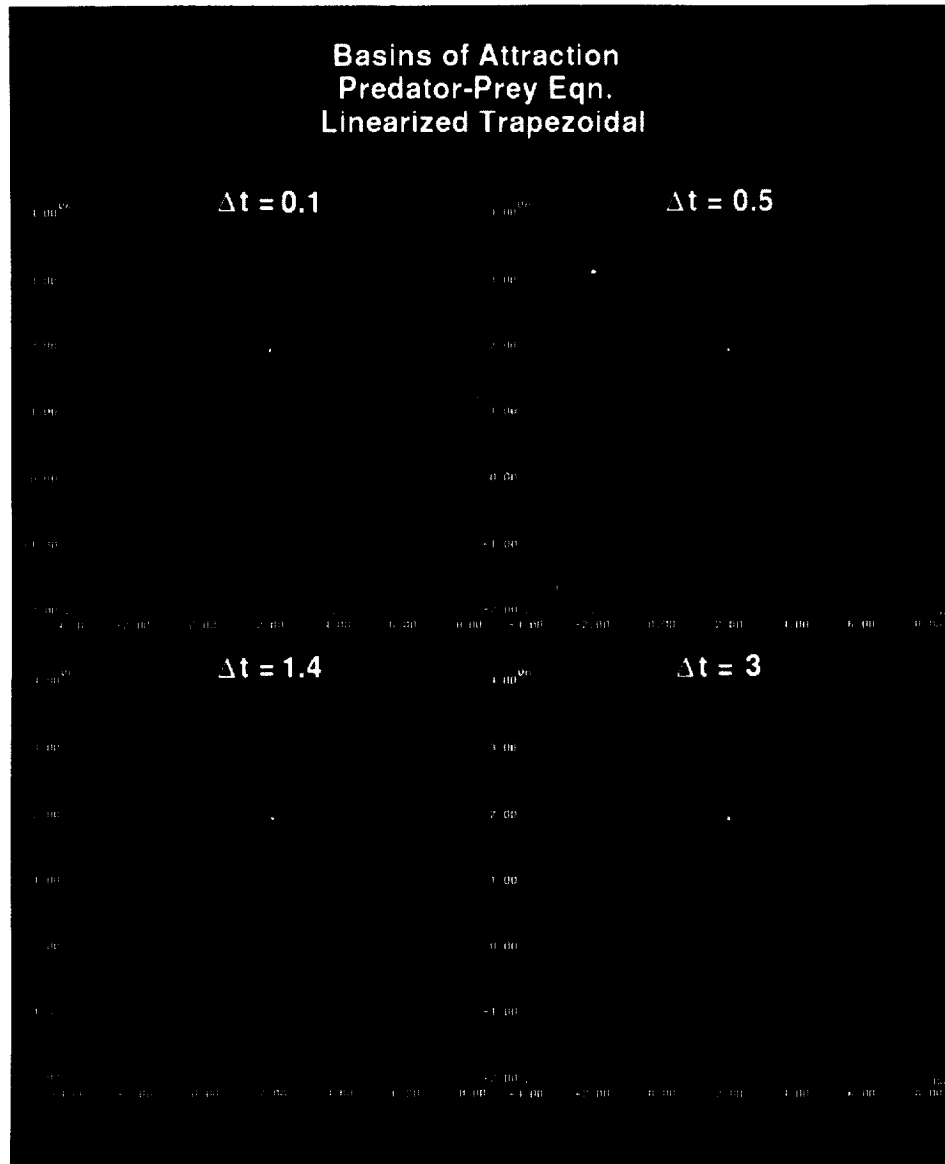


Figure 6.18 (See Color Plate XVI at the back of this issue.)

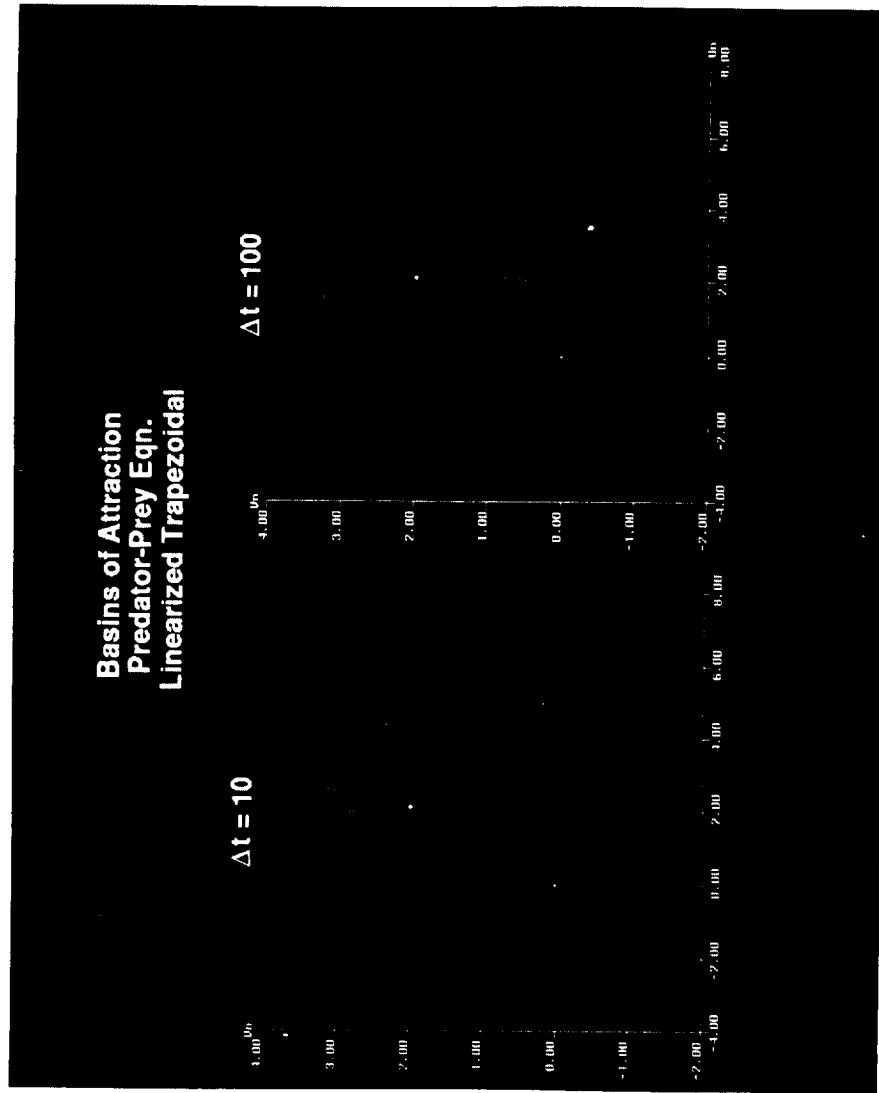


Figure 6.18 (Continued) (See Color Plate XVI at the back of this issue.)

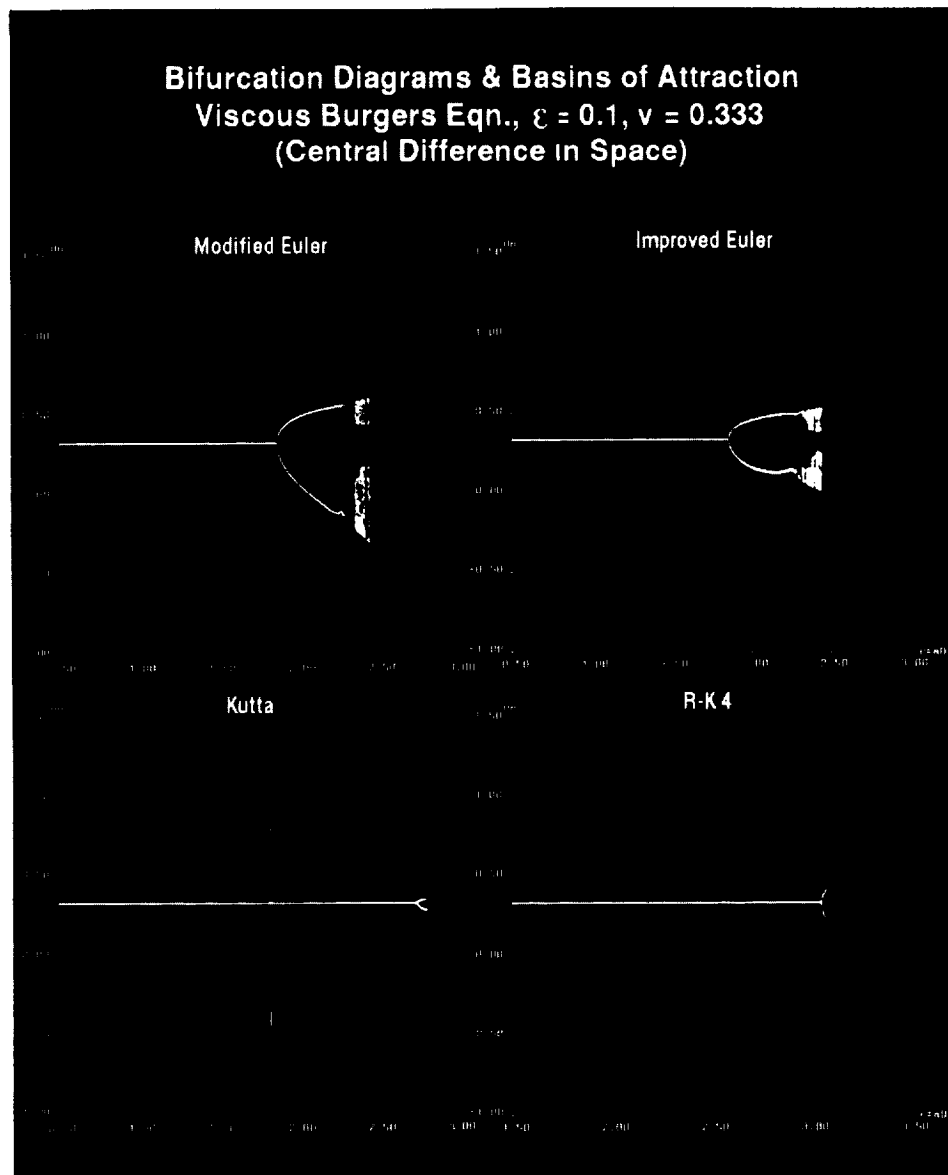


Figure 6.19 (See Color Plate XVII at the back of this issue.)

of attraction in Figures 6.21 with $\Delta t = 0.1$ appear to be the same as the exact basins of attraction. Note also that the possibility of the numerical basin of attraction being larger than the exact one does not always occur when the time step is the smallest. The numerical basin of attraction for $(1/3, 1/3)$ is larger than the corresponding exact basin of attraction for $\Delta t = 1$ by the improved Euler and Kutta methods and for $\Delta t = 0.1$ by

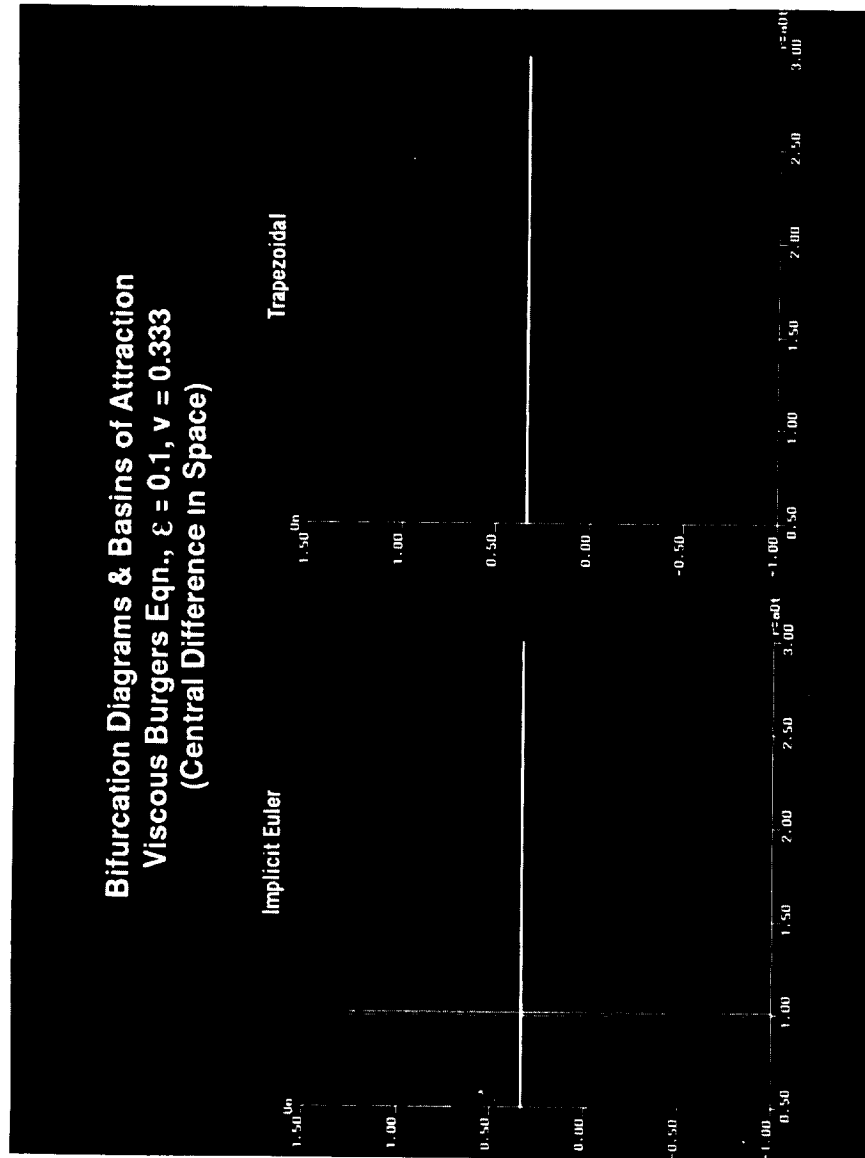


Figure 6.20 (See Color Plate XVIII at the back of this issue.)

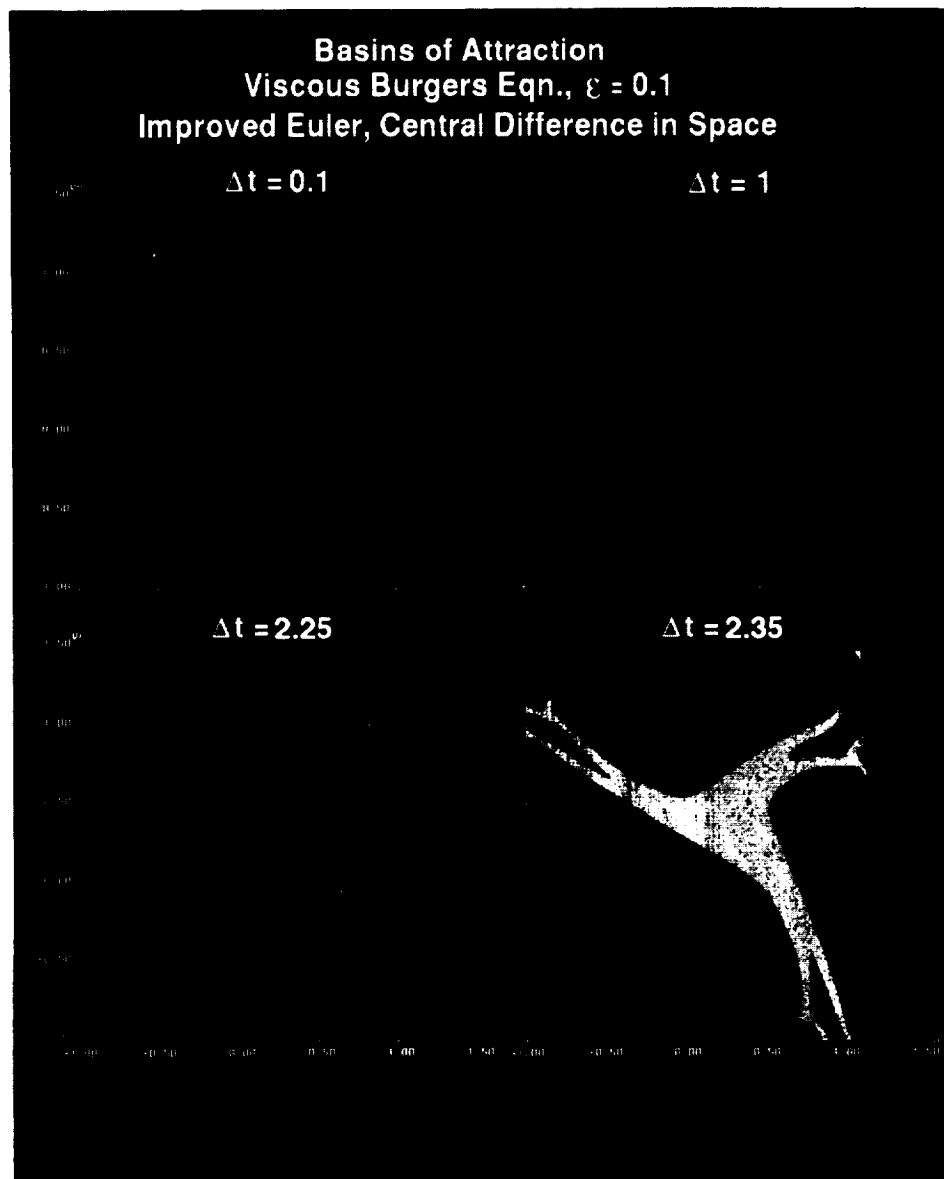


Figure 6.21 (See Color Plate XIX at the back of this issue.)

the implicit Euler and trapezoidal methods. See Figures 6.21–6.24. The following discusses results for the improved Euler, the Kutta, the implicit Euler and the trapezoidal methods.

Improved Euler Method: This example illustrates the existence of spurious limit cycles and its effect on the numerical basins of attraction for the exact steady state. Figure 6.21

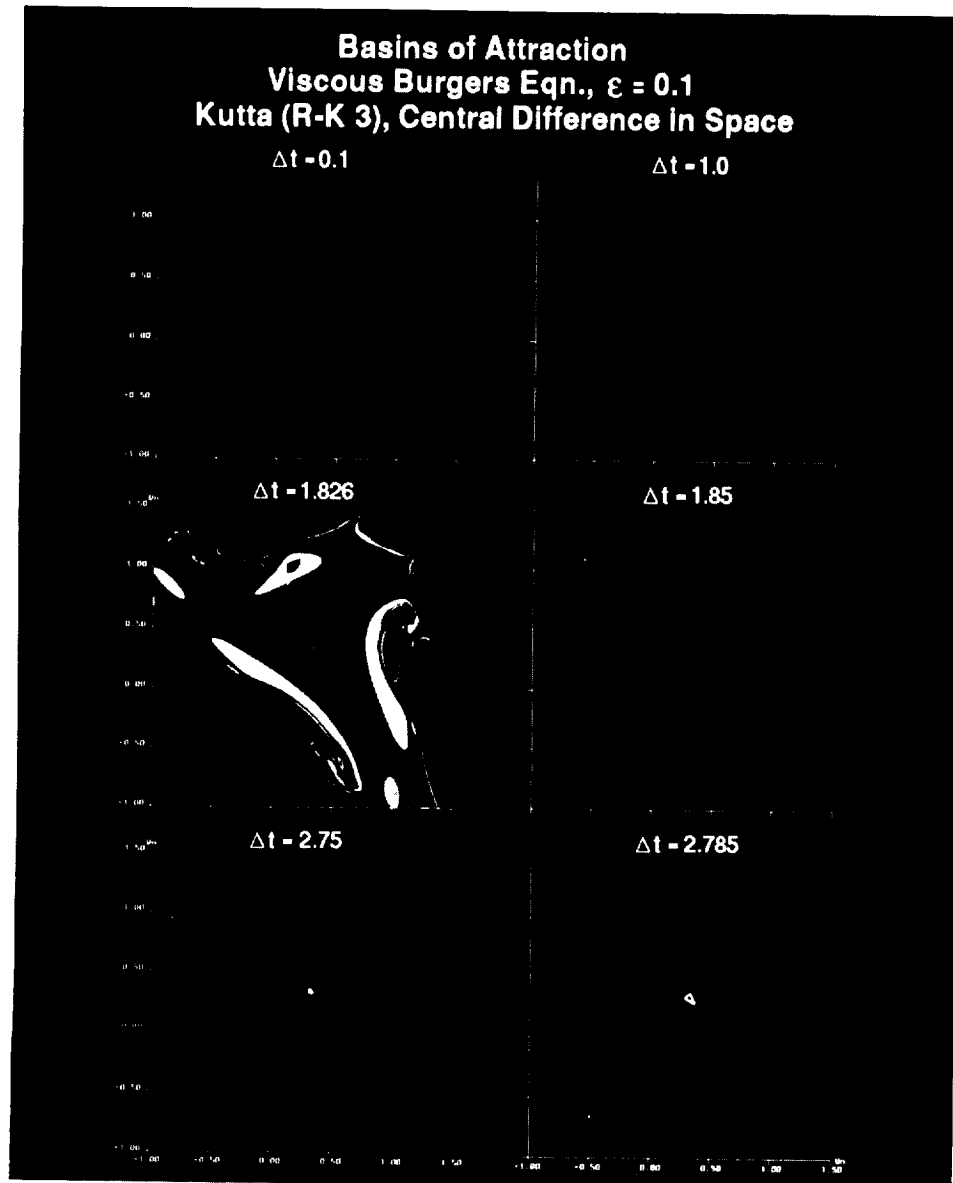


Figure 6.22 (See Color Plate XX at the back of this issue.)

shows the basins of attraction of the improved Euler method for 4 different $\Delta t = 0.1, 1, 2.25, 2.35$ with $\varepsilon = 0.1$. By a bifurcation computation shown in Figure 6.19, we found that the first two time steps are below the linearized stability limit around the exact stable steady state $(1/3, 1/3)$, and the last two time steps are above the limit.

Above the linearized stability limit spurious limit cycles and higher dimensional periodic solutions were observed. Further increasing Δt resulted in numerical chaos-type phenomena and eventually divergence (with additional increase in Δt). For $\Delta t = 2.25$ and 2.35 , the red or multicolor regions are the basins of the spurious limit cycle (the irregular white closed curve shown on Fig. 6.21) or other type of spurious

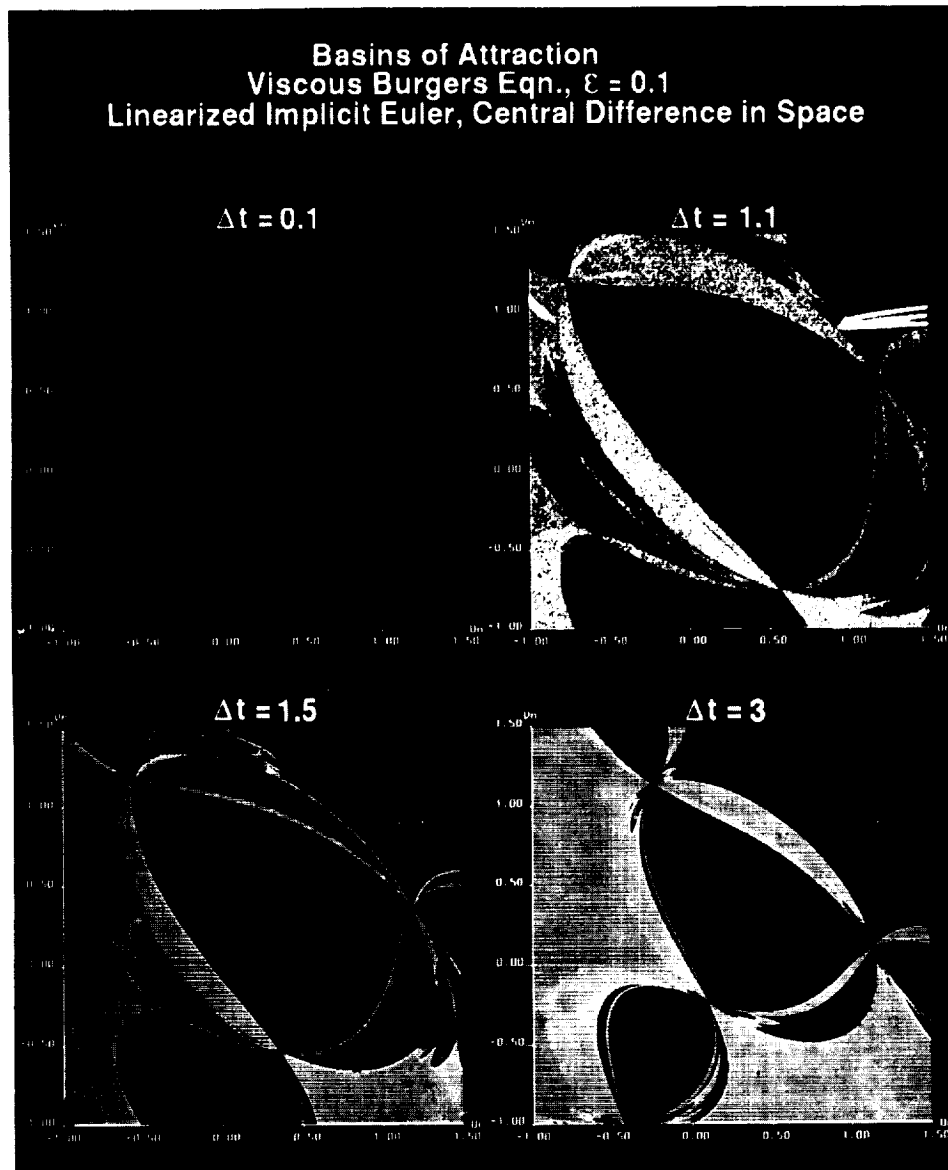


Figure 6.23 (See Color Plate XXI at the back of this issue.)

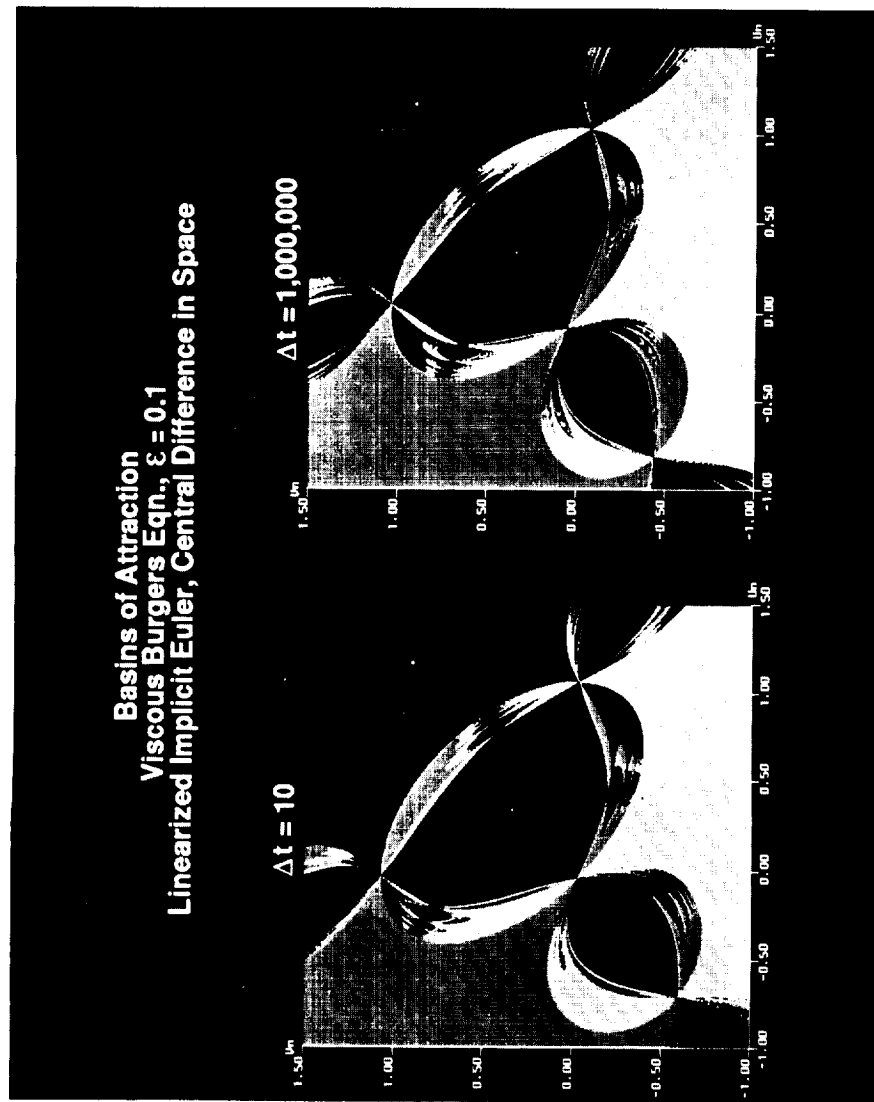


Figure 6.23 (Continued) (See Color Plate XXI at the back of this issue.)

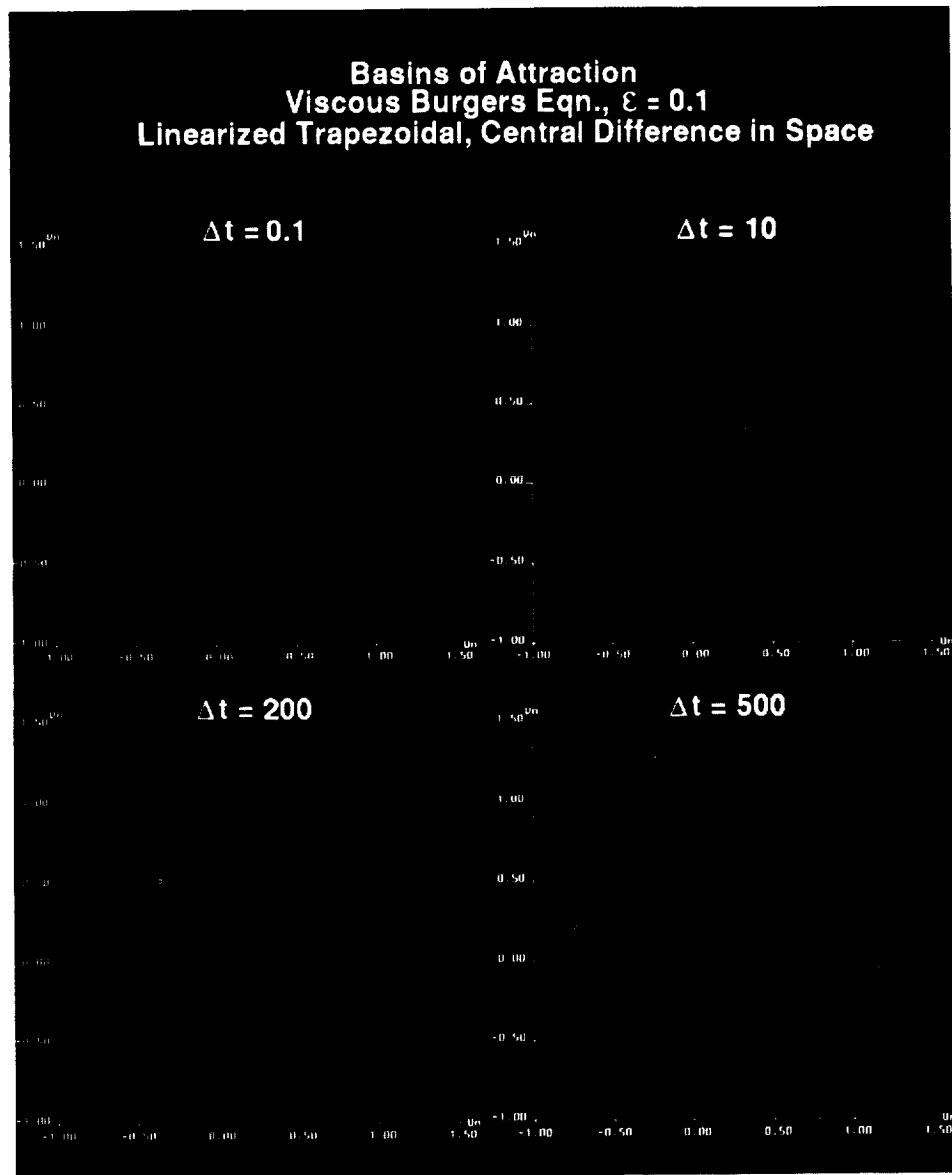


Figure 6.24 (See Color Plate XXII at the back of this issue.)

asymptote (white dots for Fig. 6.21). For these two time steps the numerical basins for the exact steady state $(1/3, 1/3)$ by the improved Euler method disappeared. However, if the initial data are in the red or multicolor region, one gets spurious solution instead of what the linearized stability predicts—divergent solution.

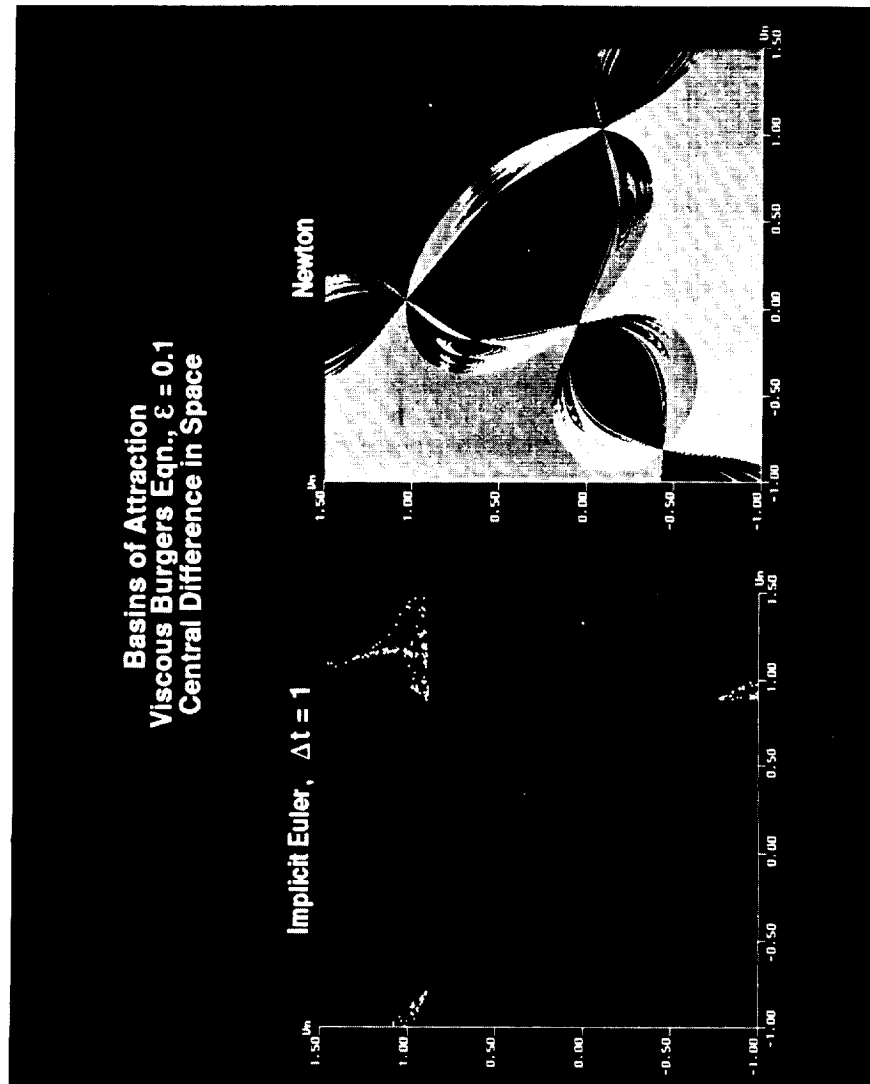


Figure 6.25 (See Color Plate XXIII at the back of this issue.)

Kutta Method: To give an example of the existence of spurious stable asymptotes below the linearized stability limit of the scheme, as well as the existence of spurious limit cycles above the linearized stability limit, Figure 6.22 shows the basins of attraction of the Kutta method for 6 different fixed time steps $\Delta t = 0.1, 1, 1.826, 1.85, 2.75$ and 2.785 (the first four below the linearized stability of the scheme) with $\varepsilon = 0.1$. For $\Delta t = 1.826$, the numerical basin for $(1/3, 1/3)$ has become fractal like with the birth of fragmented, isolated new basins of attraction due to the presence of spurious periodic solutions (the three white complicated closed curves with the associated purple, green and blue basins shown in Fig. 6.22). The last two time steps in Figure 6.22 show the disappearance of the numerical basin of attraction for the exact steady state with the birth of basins for the spurious limit cycle.

Implicit Euler Method: This is yet another interesting illustration of the use of an unconditionally stable implicit method where in practical computations, when the initial data are not known, the scheme has a higher chance of obtaining a physically correct solution if one uses a Δt restriction slightly higher than that for the stability limit of standard explicit methods (but with larger numerical basins of attraction than the explicit method counterparts). Figures 6.20 and 6.23 show the two representations of numerical basins of attraction using the implicit Euler method. These figures show the generation of stable spurious asymptotes for $\Delta t \geq 1$. As Δt increases further, the size of the same numerical basin decreases and becomes fractal like, and new numerical basins are generated. The behavior is similar to the predator-prey model (4.3) in a sense that the numerical basin of attraction for $(1/3, 1/3)$ was permanently altered for Δt near or larger than 10. Observe the fragmentation of the numerical basin of attraction for $(1/3, 1/3)$ by the basins of the spurious asymptotes.

Trapezoidal Method: Figures 6.20 and 6.24 show the two representations of numerical basins of attraction using the trapezoidal method. As in the implicit Euler case, this scheme has a higher probability of obtaining a physically correct solution if one uses a Δt similar to that of standard explicit methods (but with larger numerical basins of attraction than the explicit method counterparts). In a manner similar to the implicit Euler, the numerical basins of attraction for $(1/3, 1/3)$ are much larger than the corresponding exact basin of attraction for $\Delta t \leq 2$. Their sizes are bigger than the ones generated by the implicit Euler method with the same Δt values. The scheme becomes effectively unstable due to the fragmentation of the numerical basins of attraction. Again due to the high cost of double precision computations, no further attempts were made for Δt large. The computation of these basins requires an interval arithmetic or the enclosure-type (Adams, 1990) of mathematical operation before a more precise behavior can be revealed.

Straight Newton vs. Other Studied Methods: Figure 6.25 shows the basin of attraction using Newton method in solving the steady part of the ODE (hereafter referred to as straight Newton) compared with the implicit Euler at $\Delta t = 1$. One can see that straight Newton method has a smaller attracting basin for the stable spiral $(1/3, 1/3)$ than the implicit Euler method for small Δt . In fact its basin is the same as the implicit Euler using larger Δt . Figure 6.25 illustrates the situation where quadratic convergence by the Newton method can be achieved only if the initial data are in the red regions.

Figures 6.23 and 6.25 also illustrates the fact that using very large Δt by the (linearized) implicit Euler method has the same chance of obtaining the correct steady state as the Newton method if the initial data are not known. Comparison of Newton method with other iteration procedures for the implicit Euler and trapezoidal methods are reported in our companion paper (Yee and Sweby, 1993a).

Combining the current result with Yee and Sweby (1993a), we can conclude that contrary to popular belief, the initial data using the straight Newton method may *not* have to be close to the exact solution for convergence. Straight Newton also exhibits stable and unstable spurious asymptotes. Initial data can be reasonably removed from the asymptotic values and still be in the basin of attraction. However, the basins can be fragmented even though the corresponding exact basins of attraction are single closed domains. The cause of nonconvergence may just as readily be due to the fact that its numerical basins of attraction are fragmented.

6.6 Global Asymptotic Behavior of Iterative Implicit Schemes

The global asymptotic nonlinear behavior of some standard iterative procedures in solving nonlinear systems of algebraic equations arising from four implicit linear multistep methods (LMMs) in discretizing models (4.1), (4.3) and (4.4) is analyzed in our companion paper (Yee and Sweby, 1993a). The implicit LMMs include implicit Euler, trapezoidal, mid-point implicit and three-point backward differentiation methods. The iterative procedures include simple iteration and full and modified Newton iterations. The results are compared with standard Runge-Kutta explicit methods, a non-iterative implicit procedure, and straight Newton method. Here we give a summary of Yee and Sweby (1993a) so that the reader may get a bigger picture of implicit methods other than the ones studied in this paper.

Studies in Yee and Sweby (1993a) showed that all of the four implicit LMMs exhibit a drastic distortion but less shrinkage of the basin of attraction of the true solution than standard explicit methods studied in this paper. In some cases with smaller Δt , the implicit LMMs exhibit enlargement of the basins of attraction of the true solution. Overall, the numerical basins of attraction of a non-iterative implicit procedure mimic more closely the basins of attraction of the continuum than the studied iterative implicit procedures for the four implicit LMMs. In general the numerical basins of attraction bear no resemblance to the exact basins of attraction. The size can increase or decrease depending on the time step. Also the possible existence of the largest numerical basin of attraction that is larger than the exact one does not occur when the time step is the smallest. The dynamics of numerics of the implicit methods differ significantly from each other, and the different methods of solving the resulting non-linear algebraic equations are very different from each other since different numerical methods and solution procedures result in entirely different nonlinear discrete maps. Although unconditionally stable implicit methods allow a theoretically large time step Δt , the numerical basins of attraction (allowable initial data) for large Δt some-times are so fragmented and/or so small that the safe (or practical) choice of Δt is slightly larger or comparable to the stability limit of standard explicit methods (but with larger numerical basins of attraction than the explicit method counterparts). In general, if one uses a Δt that is a fraction of the stability limit,

one has a higher chance of convergence to the correct asymptote than the standard explicit methods.

Studies in Yee and Sweby (1993a) also showed that the variable time step control method can occasionally stabilize unstable fixed points, depending on the initial data, starting time step and the iterative tolerance value. One shortcoming is that the size of Δt needed to avoid spurious dynamics is impractical to use, especially for the explicit method.

7. CONCLUDING REMARKS

The global asymptotic nonlinear behavior and bifurcation phenomena for the explicit Euler method, five different multistage Runge-Kutta methods (modified Euler, improved Euler, Heun, Kutta and 4th-order methods), two and three-step predictor-corrector methods, Adams-Bashforth method, and implicit Euler and trapezoidal method with linearization are compared for different model nonlinear ODEs. The five multistage Runge-Kutta methods and the predictor-corrector methods are nonlinear in the discretized parameter space Δt and all LMMs are linear in Δt . With the aid of the CM-2, the complex behavior and sometimes fractal like structure of the associated numerical basins of attraction of these time discretizations are compared and revealed for the first time.

The numerical results indicate that with sufficiently small Δt and initial data close to the steady state (usually not known for the time-marching method), one can have the highest chance of convergence to the correct asymptote. In general, the initial data can be far removed from the exact steady state by the studied implicit methods provided that a fraction of the allowable time step restriction is used. Our study also indicates that bifurcation to a period two or lower order period solution is readily detectable in numerical calculations. However, bifurcation to a limit cycle will not be so obvious (without a phase portrait representation), especially in the vicinity of the bifurcation point. Indeed the phenomenon of an artificial time iteration to steady-state of a large system formed by spatial discretization which nears convergence before the residuals “plateaus out”, could actually be the result of a stable spurious limit cycle around the Hopf bifurcation point. In addition, the bifurcation of spirals to limit cycles might account in part for the phenomenon of near (but lack of) convergence in large stiff systems.

For a given initial data and two finite but different Δt 's that are below the linearized stability limit of the scheme, their numerical solutions might converge to two different solutions even if no spurious *stable* steady-state numerical solution is introduced by the scheme and the initial data are physically relevant. The source of the behavior is due to the existence of *unstable* spurious asymptotes or stable asymptotes other than steady states which have the same detrimental (in terms of robustness) effect. However, in the case of occurrence of stable spurious steady states, they can be mistaken for the true steady state in practical computations. In other words depending on the initial data, for a given Δt below the linearized stability limit, the numerical solution can (a) converge to the correct steady state, (b) converge to a different steady state, (c) converge to a spurious periodic solution, (d) yield spurious asymptotes other than (a)–(c), or (e) diverge, even though the initial data are physically relevant.

Another important finding is that unlike the scalar first-order autonomous ODE discussed in part I (Yee *et al.*, 1991), the fixed points can change types as the time step is varied even for two-time-level unconditionally stable implicit LMMs. An unstable fixed point can become a stable fixed point and can e.g., change from a saddle to a stable or unstable node (for a fixed system parameter ε). Since these implicit methods can introduce spurious asymptotes as well, thus even though LMMs preserve the same number but not the same types of fixed points as the underlying DEs, the numerical basins of attraction of LMMs (explicit or implicit) do not always coincide with the exact basins of attraction of the underlying DEs. One major consequence of this behavior is that the flow pattern can change type as the discretized parameter is varied. Another consequence of these phenomena is the fragmentation of the numerical basin of attraction. In general, unconditionally stable implicit LMMs exhibit less shrinkage of the basin of attraction of the true solution than standard explicit methods. Another interesting result is that contrary to popular belief, the initial data using the straight Newton method may not have to be close to the exact steady state for convergence. However, we believe that one cause of nonconvergence in straight Newton or implicit LMMs with large time step may be due to the fact that the numerical basins of attraction are fragmented.

In conclusion, the present results can explain some of the roots of why one cannot achieve the theoretical linearized stability limit of the typical implicit Euler and trapezoidal time discretization in practice when solving strongly nonlinear DEs, e.g. in CFD. The results can also shed some light in bridging some of the gaps between theoretical convergence criterion ($\Delta t \rightarrow 0$, as $n \rightarrow \infty$) and practical scientific computation (finite Δt as $n \rightarrow \infty$).

Acknowledgements

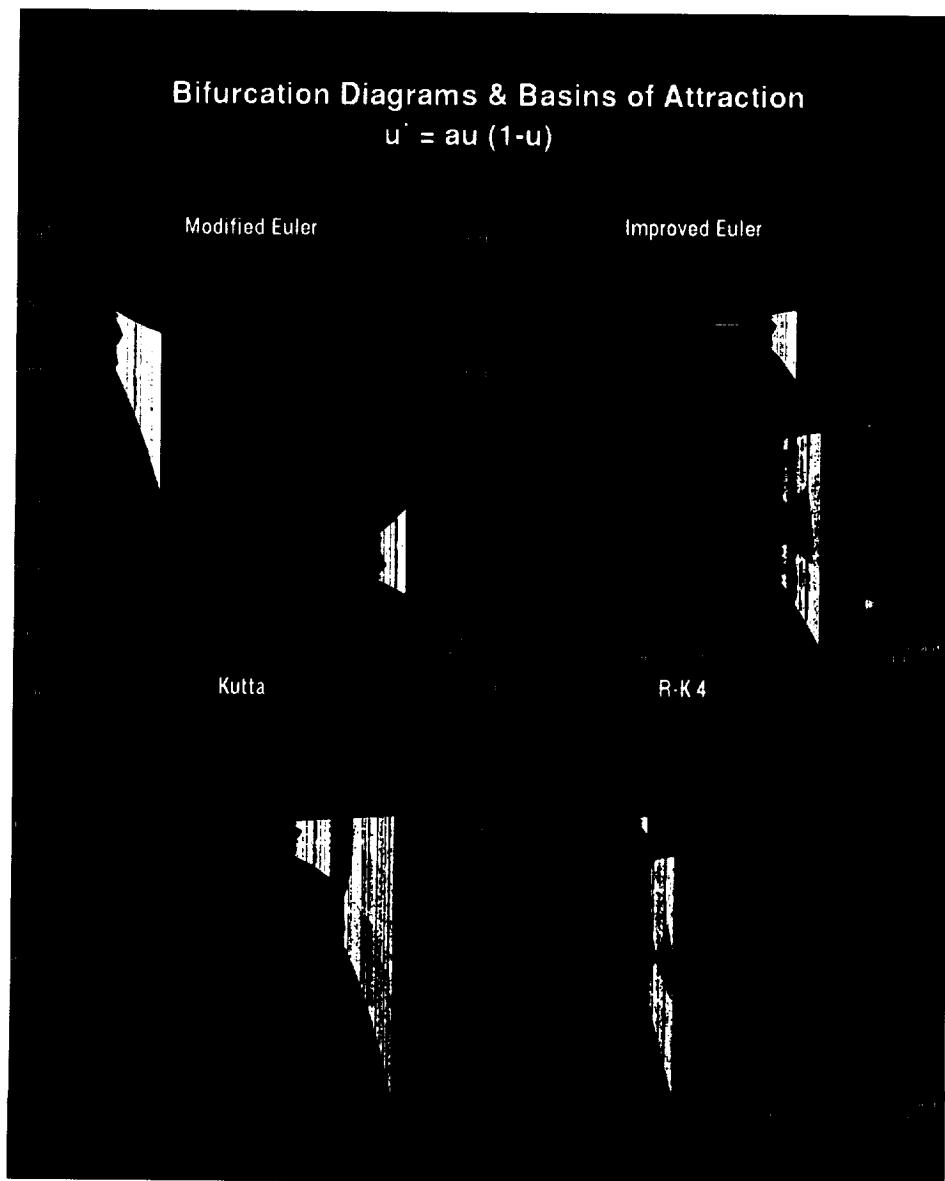
The authors wish to thank A. M. Stuart and D. F. Griffiths for their valuable discussions during the course of this research and for suggesting the model equations (4.1) and (4.4). Special thanks to A. Lafon, M. Vinokur, T. Coakley and C. Y. McNeil for their critical review of the manuscript. Financial support from T. Lasinski for the second author as a visiting scientist at NASA Ames is gratefully acknowledged.

References

- Adams, E. (1990) "Periodic Solutions: Enclosure, Verification, and Applications", *Computer Arithmetic and Self-Validating Numerical Methods*, Academic Press, 199–245.
- Beam, R. M. and Bailey, H. E. (1988) "Direct Solver for Navier-Stokes Equations", Proceedings of International Conference on Computational Engineering Science, Atlanta, GA.
- Beam, R. M. and Warming, R. F. (1976) "An Implicit Finite-Difference Algorithm for Hyperbolic Systems in Conservation Law Form", *J. Comput. Phys.*, **22**, 87–110.
- Budd, C. J., Stuart, A. M., Koomullil, G. P. and Yee, H. C. (1994) "Numerical Solution Behavior of Model Convection-Diffusion BVP with Grid Adaptation", in preparation.
- Foias, C., Sell, G. and Temam, R. (1985) "Varietes Inertielles des Equations Differentielles Dissipatives", *C.R. Acad. Sci. Paris, Ser. I Math.*, **301**, 139–141.
- Globus, A., Levit, C. and Lasinski, T. (1991) "A Tool for Visualizing the Topology of Three-Dimensional Vector Fields", NAS Applied Research Branch Report RNR-91-017, NASA Ames Research Center.
- Griffiths, D. F., Sweby, P. K. and Yee, H. C. (1992a) "On Spurious Asymptotes Numerical Solutions of Explicit Runge-Kutta Schemes", *IMA J. Numer. Anal.*, **12**, 319–338.
- Griffiths, D. F., Stuart, A. M. and Yee, H. C. (1992b) "Numerical Wave Propagation in Hyperbolic Problems with Nonlinear Source Terms", *SIAM J. of Numer. Anal.*, **29**(5), 1244–1260.

- Guckenheimer, J. and Holmes, P. (1983) *Nonlinear Oscillations, Dynamical Systems, and Bifurcations of Vector Fields*, Springer-Verlag, New York.
- Hale, J. and Kocak, H. (1991) *Dynamics and Bifurcations*, Springer-Verlag, New York.
- Hairer, E., Iserles, A. and Sanz-Serna, J. M. (1989) "Equilibria of Runge-Kutta Methods", *Numer. Math.*
- Hsu, C. S. (1987) *Cell-to-Cell Mapping*, Springer-Verlag, New York.
- Hung, C. M., Sung, C. H. and Chen, C. L. (1991) "Computation of Saddle Point of Attachment", AIAA-91-1713, AIAA 22nd Fluid Dynamics, Plasma Dynamics and Lasers Conference, Honolulu, Hawaii.
- Humphries, A. R. (1992) "Spurious Solutions of Numerical Methods for Initial Value problems", *IMA J. Num. Anal.*
- Iserles, A. (1988) "Stability and Dynamics of Numerical Methods for Nonlinear Ordinary Differential Equations", DAMTP NA1, University of Cambridge, Cambridge, England.
- Iserles, A., Peplow, A. T. and Stuart, A. M. (1990) "A Unified Approach to Spurious Solutions Introduced by Time Discretisation", Part I: Basic Theory, DAMTP 1990/NA4, Numerical Analysis Reports, University of Cambridge.
- Jameson, A. (1991) "Airfoils Admitting Nonunique Solutions to the Euler Equations", AIAA-91-1625.
- Keller, H. B. (1977) "Numerical Solution of Bifurcation and Nonlinear Eigenvalue Problems", *Applications of Bifurcation Theory*, P. H. Rabinowitz, ed., Academic Press, 359-384.
- Kwak, M. (1991) "Finite Dimensional Inertial Forms for the 3D Navier-Stokes Equations," IMA preprint Series #828.
- Lafon, A. and Yee, H. C. (1991) "Dynamical Approach Study of Spurious Steady-State Numerical Solutions for Nonlinear Differential Equations", Part III: The Effects of Nonlinear Source Terms and Boundary Conditions in Reaction-Convection Equations, NASA TM-103877, to appear in *Intern. J. CFD*.
- Lafon, A. and Yee, H. C. (1992) "Dynamical Approach Study of Spurious Steady-State Numerical Solutions of Nonlinear Differential Equations", Part IV: Stability vs. Numerical Treatment of Nonlinear Source Terms, ONERA-CERT Technical Report DERAT 45/5005.38, to appear in *Intern. J. CFD*.
- Lambert, J. D. (1973) *Computational Methods in Ordinary Differential Equations*, John Wiley, New York.
- Langford, W. F. and Iooss, G. (1980) "Interactions of Hopf and Pitchfork Bifurcations", ISNM 54, *Bifurcation Problems and Their Numerical Solution*, Workshop on Bifurcation Problems and Their Numerical Solution, Dortmund, ed. H. D. Mittelman and H. Weber, Birkhauser Verlag, Basel, 103-134.
- Panov, A. M. (1956) "Behavior of the Trajectories of a System of Finite Difference Equations in the Neighbourhood of a Singular Point", *Uch. Zap. Ural. Gos. Univ. vyp.* **19**, 89-99.
- Perron, O. (1929) "Über Stabilität und Asymptotisches Überhalten der Lösungen eines Systems endlicher Differenzgleichungen", *J. Reine Angew. Math.*, **161**, 41-64.
- Richtmyer, R. D. and Morton, K. W. (1967) *Difference Methods for Initial-Value Problems*, Interscience-Wiley, New York.
- Sanz-Serna, J. M. (1990) "Numerical Ordinary Differential Equations vs. Dynamical Systems," Applied Math. Comput. Report 1990/3, Universidad de Valladolid.
- Schecter, S. and Shearer, M. (1990) "Undercompressive Shocks for Nonstrictly Hyperbolic Conservation Laws", IMA Preprint Series #619.
- Shearer, M., Schaeffer, D. G., Marchesin, D. and Paes-Leme, P. (1987) "Solution of the Riemann Problem for a Prototype 2×2 System of Non-Strictly Hyperbolic Conservation Laws", *Arch. Rat. Mech. Anal.*, **97**, 299-320.
- Strang, G. (1968) "On the Construction and Comparison of Difference Schemes", *SIAM J. Num. Anal.*, **5**, 506-517.
- Sweby, P. K., Yee, H. C. and Griffiths, D. F. (1990) "On Spurious Steady-State Solutions of Explicit Runge-Kutta Schemes", University of Reading, Department of Mathematics, Numerical Analysis Report 3/90, also NASA TM 102819, April 1990.
- Sweby, P. K. and Yee, H. C. (1991) "On Spurious Asymptotic Numerical Solutions of 2×2 Systems of ODEs", Numerical analysis Report 7/91, University of Reading, England.
- Sweby, P. K. and Yee, H. C. (1994) "On the Dynamics of Some Grid Adaptation Schemes", Proceedings of the 4th International Conference on Numerical Grid Generation in CFD and Related Fields, University College of Swansea, UK, also RIACS Technical Report 94.02, Feb. 1994.
- Temam, R. (1989) "Do Inertial Manifolds Apply to Turbulence?", *Physica D*, **37**, 146-152.
- Warner, B. (1980) "Turning Points of Branches of Positive Solutions", ISNM 54, *Bifurcation Problems and Their Numerical Solution*, Workshop on Bifurcation Problems and Their Numerical Solution, Dortmund, ed. H. D. Mittelman and H. Weber, Birkhauser Verlag, Basel, 211-226.
- Yee H. C. (1989) "A Class of High-Resolution Explicit and Implicit Shock-Capturing Methods", VKI Lecture Series 1989-04 March 6-10, 1989, also NASA TM-101088, Feb. 1989.
- Yee, H. C. (1991) "A Nonlinear Dynamical Approach to Algorithm Development in Hypersonic CFD", Proceedings of the 4th International symposium on Computational Fluid Dynamics, Davis, Calif.

- Yee, H. C., Klopfer, G. H. and Montagne, J.-L. (1990) "High-Resolution shock-capturing Schemes for Inviscid and Viscous Hypersonic Flows", *J. Comput. Phys.*, **88**, 31 - 61.
- Yee, H. C., Sweby, P. K. and Griffiths, D. F. (1991) "Dynamical Approach Study of Spurious Steady-State Numerical Solutions for Nonlinear Differential Equations", Part I: The Dynamics of Time Discretizations and Its Implications for algorithm Development in Computational Fluid Dynamics, NASA TM-102820, April 1990, also *J. Comput. Phys.*, **97**, 249 - 310.
- Yee, H. C., Sweby, P. K. and Lafon, A. (1992) "Basins of Attraction and the Time-Dependent Approach to Obtaining Steady-State Numerical Solutions", Proceedings of the ICFD Conference on Numerical Methods for Fluid Dynamics, Reading England.
- Yee, H. C. and Sweby, P. K. (1993a) "Global Asymptotic Behavior of Iterative Implicit Schemes", RIACS Technical Report 93.11, NASA Ames Research Center, to appear in International J. of Bifurcation and Chaos, Dec., 1994.
- Yee, H. C. and Sweby, P. K. (1993b) "On the Dynamics of Some Iterative Implicit schemes", Proceedings of the Chaotic Numerics Workshop, Deakin University, Geelong, Australia.



Color Plate I

Figure 6.1 (See H.C. Yee and P. K. Sweby.)

Bifurcation Diagrams & Basins of Attraction

$$u' = au(1-u)(0.5-u)$$

Modified Euler



Improved Euler



Kutta



R-K 4



Color Plate II

Figure 6.2 (See H.C. Yee and P. K. Sweby.)

Bifurcation Diagrams & Basins of Attraction
Dissipative Complex Eqn.. $\varepsilon = 1, \nu = 0.0$

Modified Euler

Improved Euler



Kutta



R-K 4



Color Plate III

Figure 6.3 (See H.C. Yee and P. K. Sweby.)

Bifurcation Diagrams & Basins of Attraction
Dissipative Complex Eqn.: $\mu = 1, v = 0.0$

Hogg

Adams-Bashforth



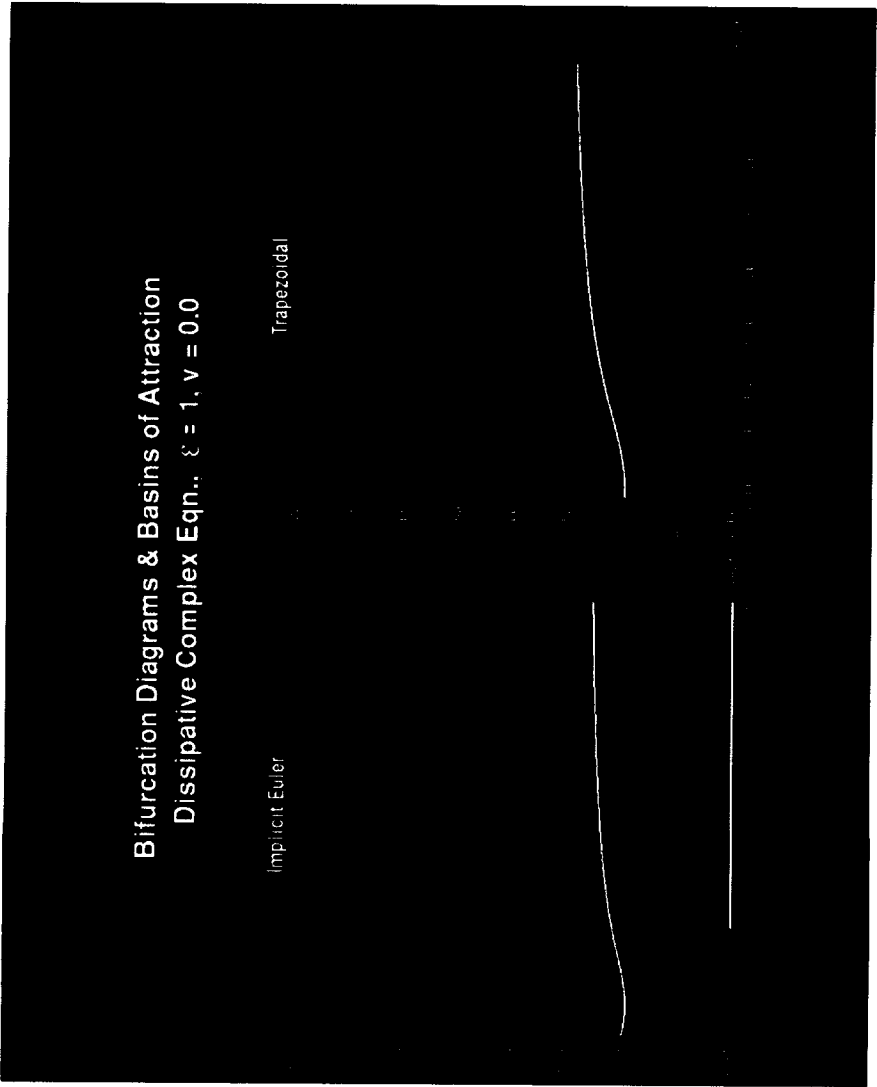
PC2

$\mu = 1.0$

PC3

Color Plate IV

Figure 6.4 (See H.C. Yee and P. K. Sweby.)



Color Plate V **Figure 6.5** (See H.C. Yee and P. K. Sweby.)

Basins of Attraction
Dissipative Complex Eqn., $\beta = 1$
R-K 4

$\lambda t = 0.5$



$\lambda t = 1.5$



$\lambda t = 1.75$

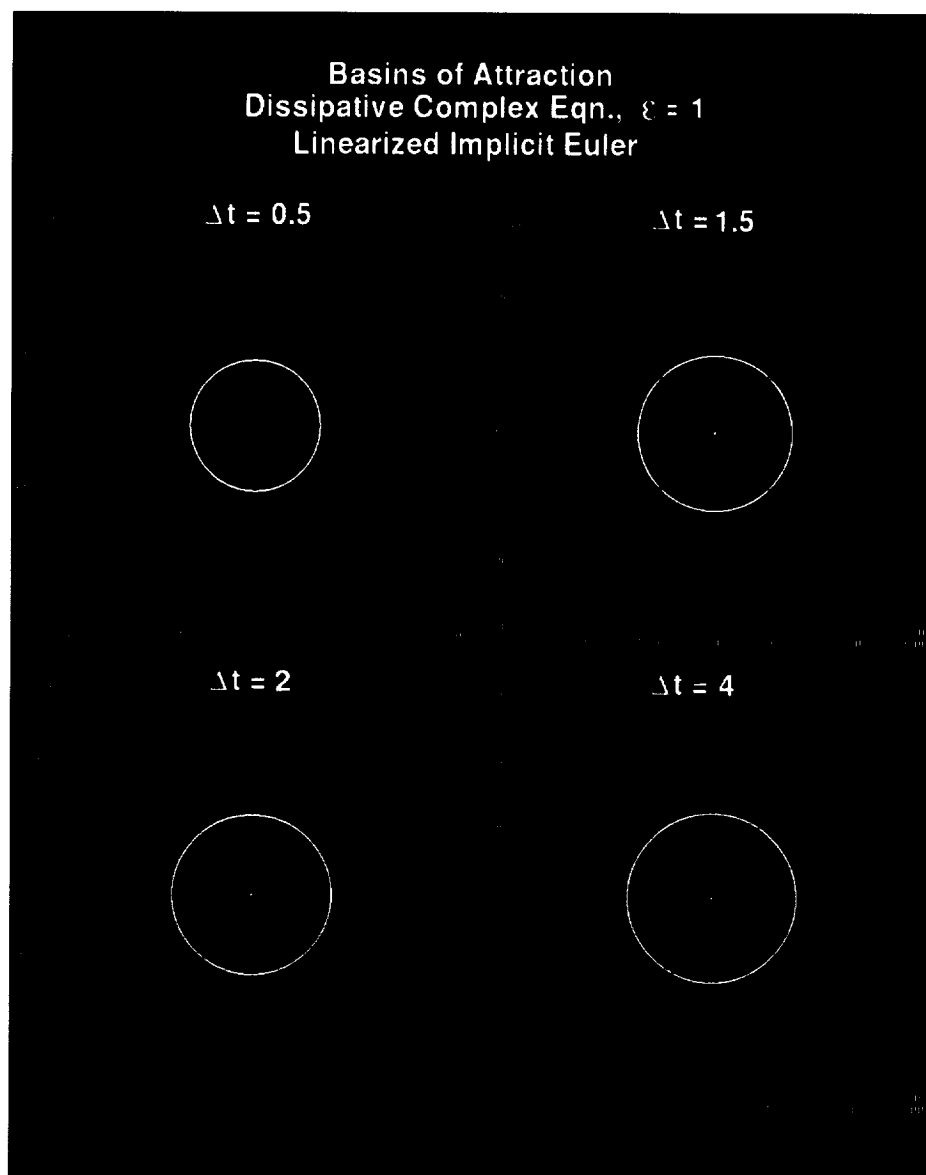


$\lambda t = 2$

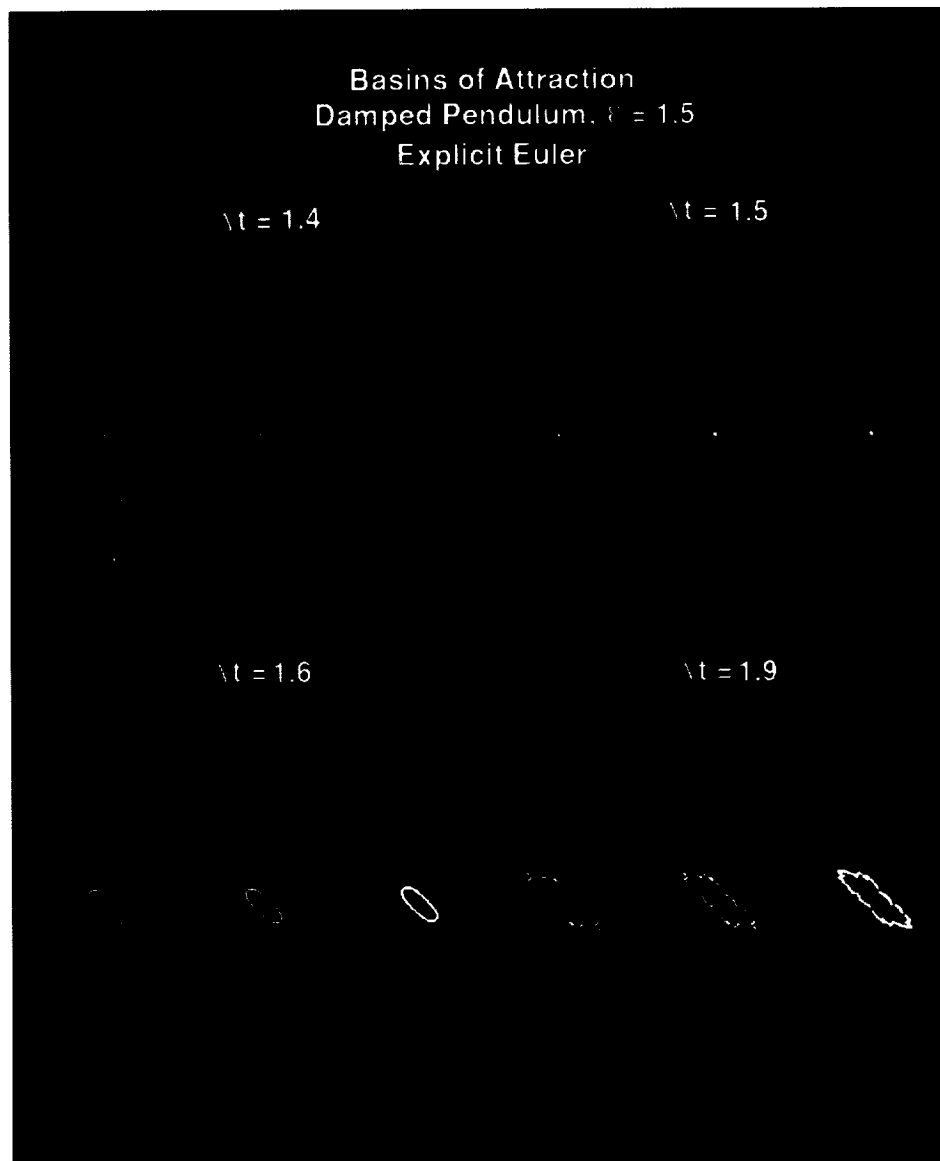


Color Plate VI

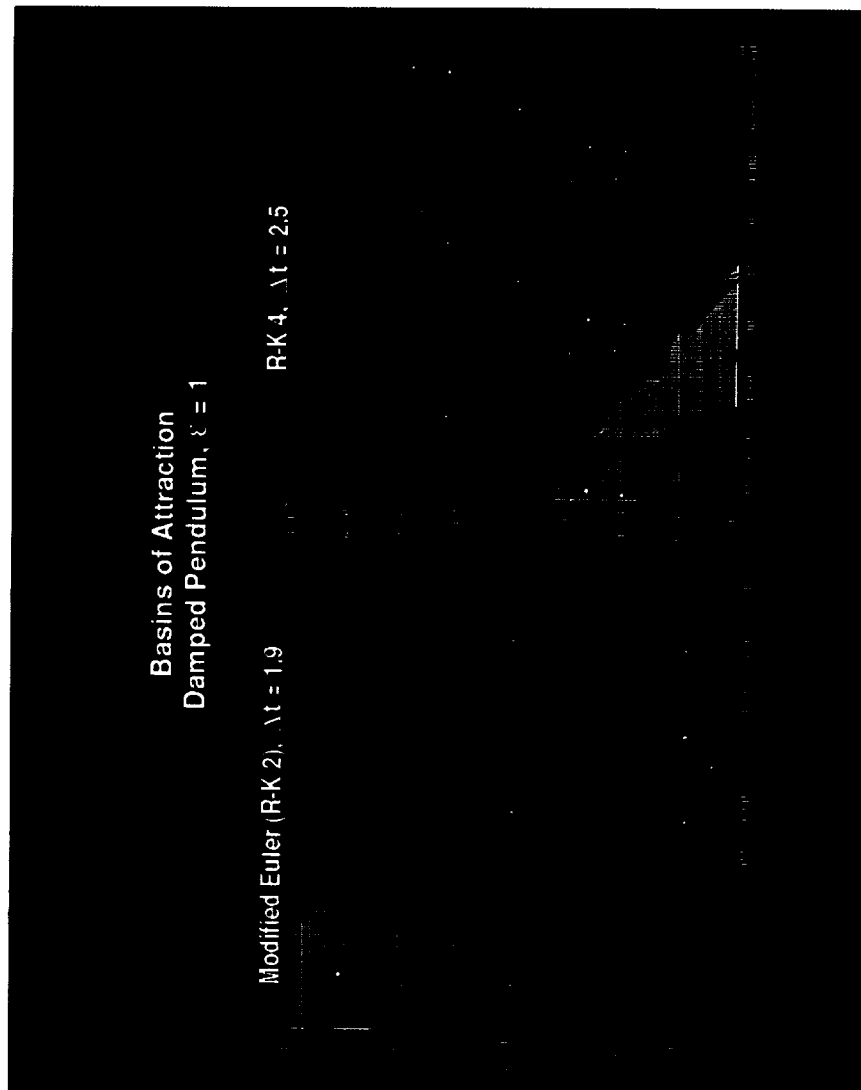
Figure 6.8 (See H.C. Yee and P. K. Sweby.)



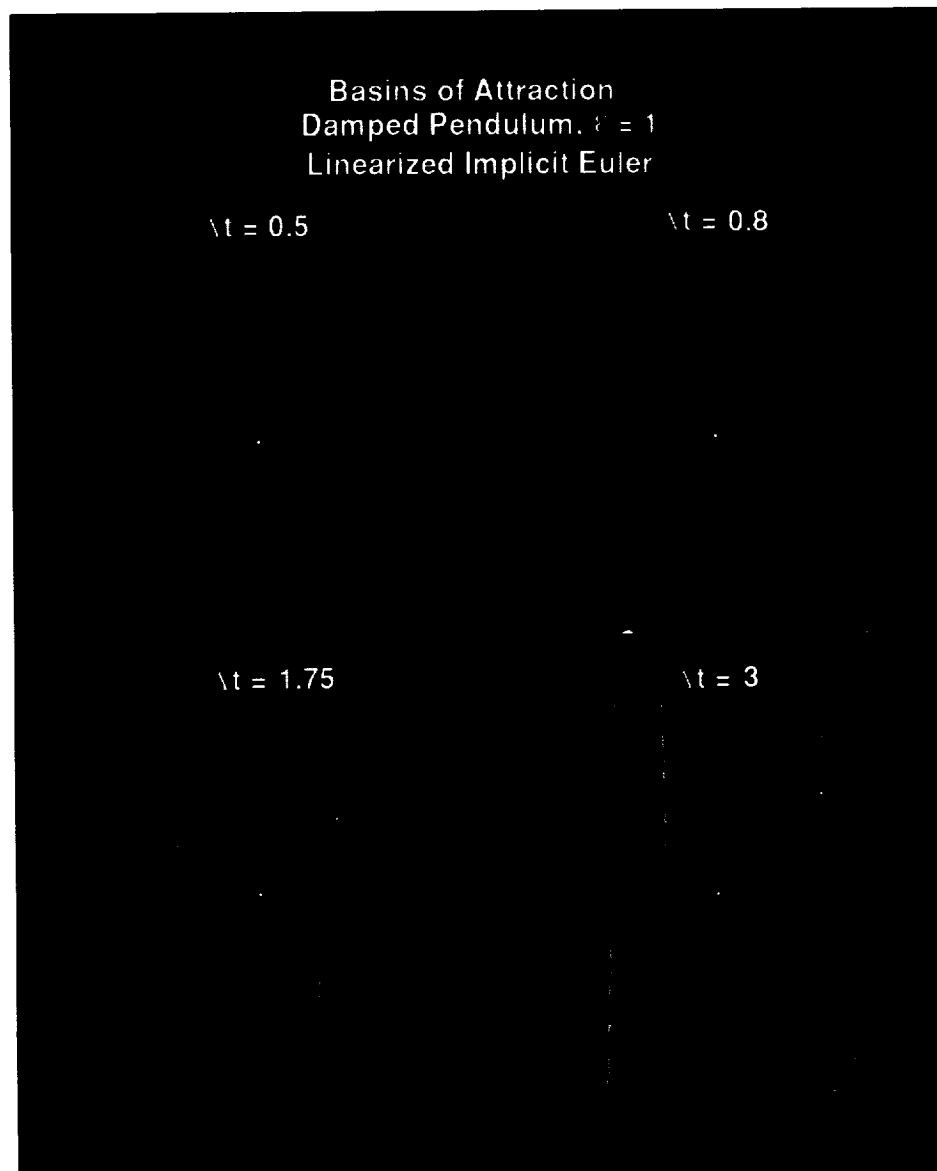
Color Plate VII **Figure 6.9** (See H.C. Yee and P. K. Sweby.)



Color Plate VIII **Figure 6.10** (See H.C. Yee and P. K. Sweby.)

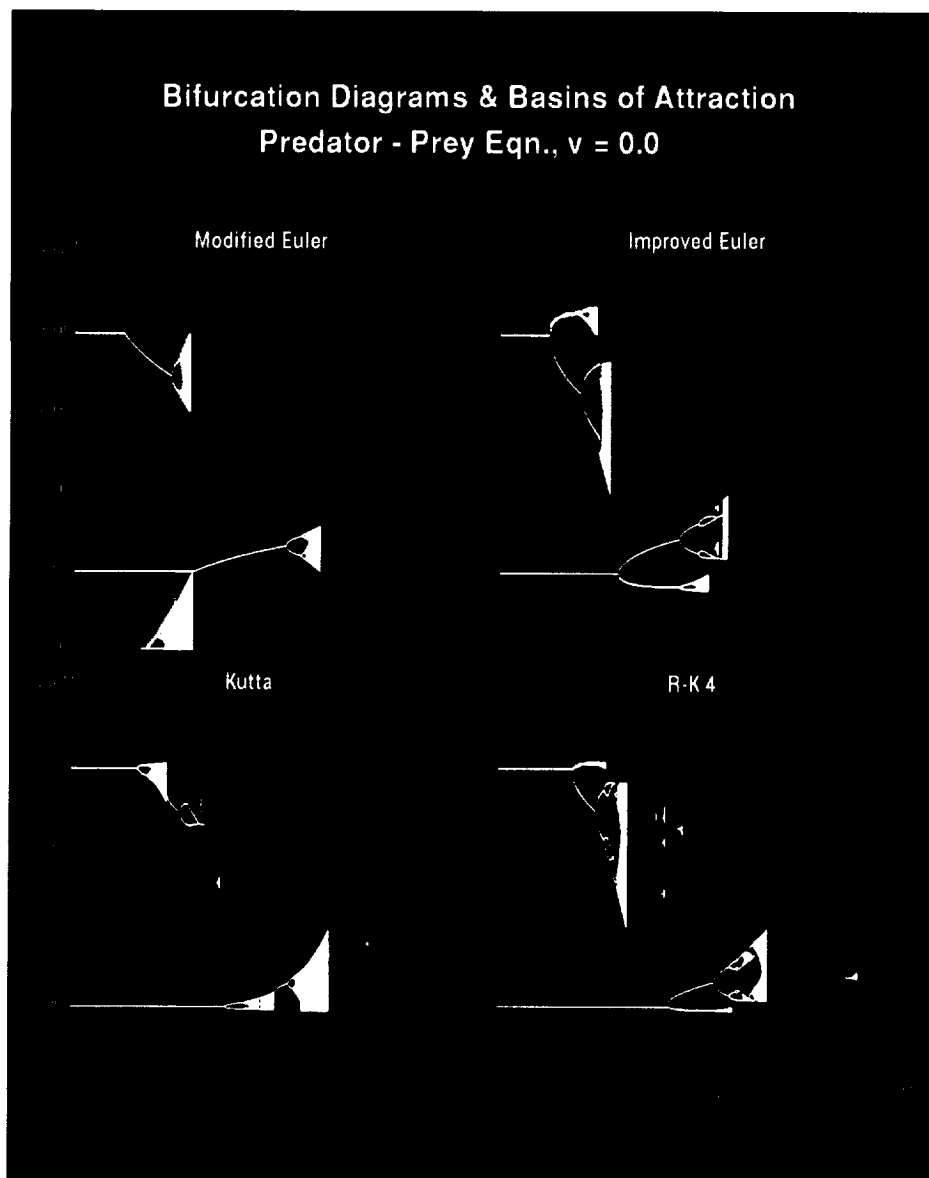


Color Plate IX **Figure 6.11** (See H.C. Yee and P. K. Sweby.)



Color Plate X

Figure 6.12 (See H.C. Yee and P. K. Sweby.)

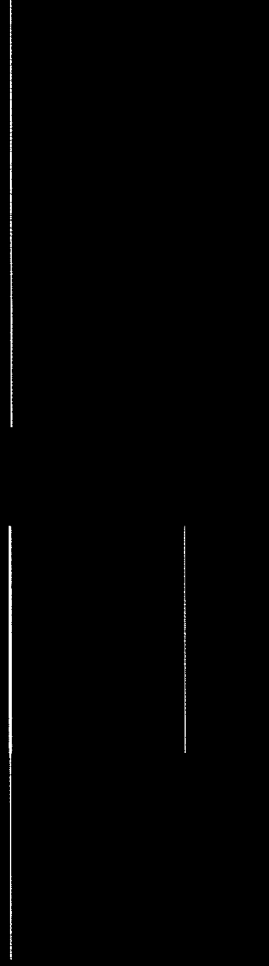


Color Plate XI **Figure 6.13** (See H.C. Yee and P. K. Sweby.)

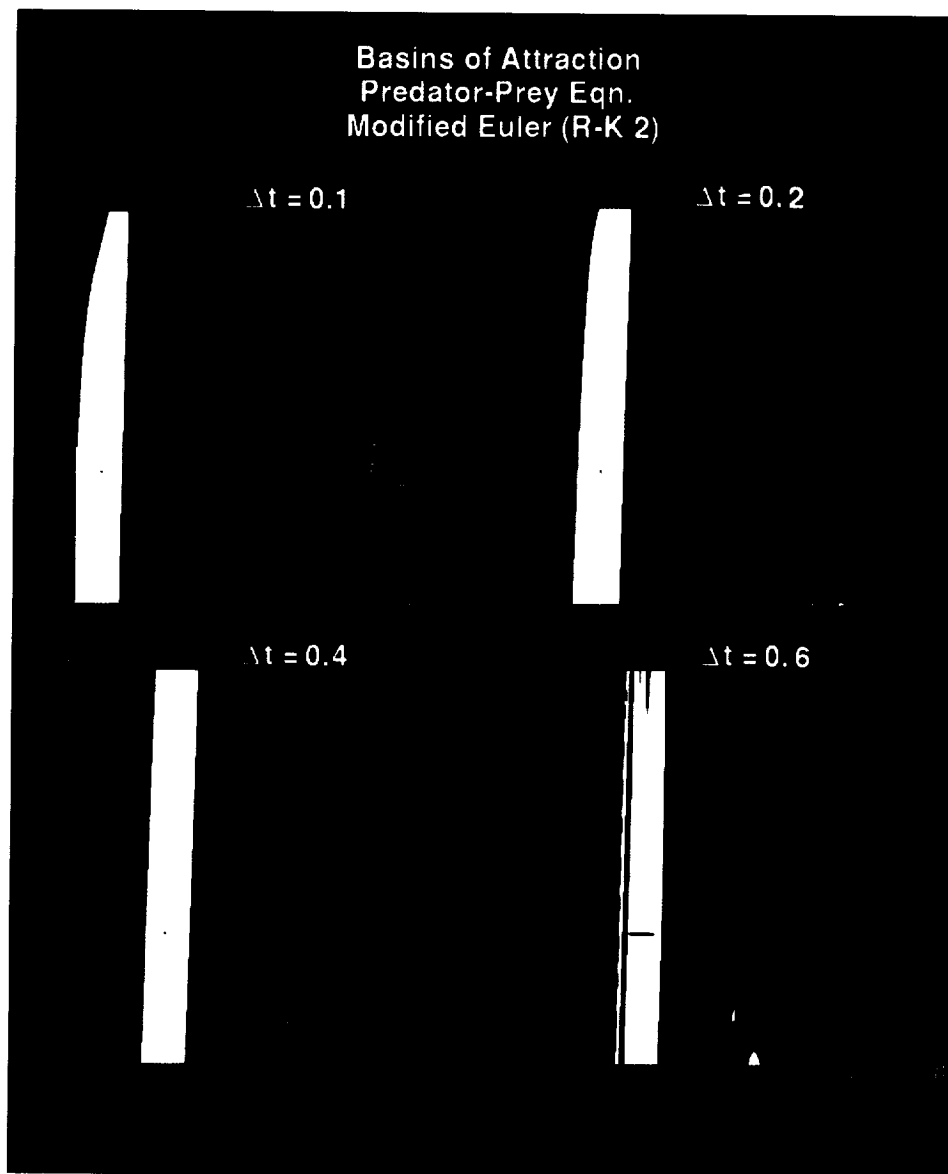
Bifurcation Diagrams & Basins of Attraction Predator-Prey Eqn., $\nu = 0.0$

Implicit Euler

Trapzoidal



Color Plate XII **Figure 6.14** (See H.C. Yee and P. K. Sweby.)



Color Plate XIII **Figure 6.15** (See H.C. Yee and P. K. Sweby.)

Basins of Attraction
 Predator - Prey Eqn.
 Modified Euler (R-K 2)

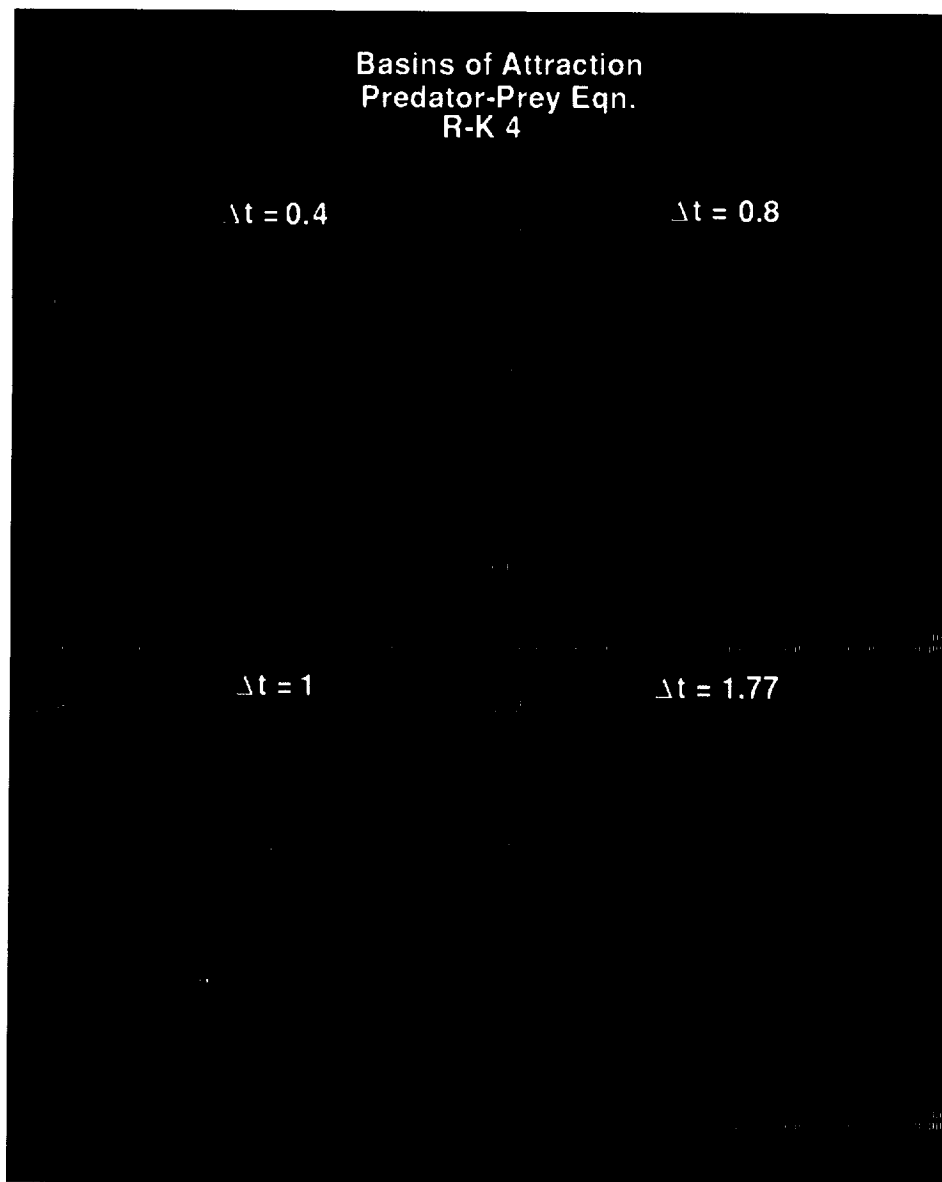
$\lambda t = 0.8$

$\lambda t = 0.9524$

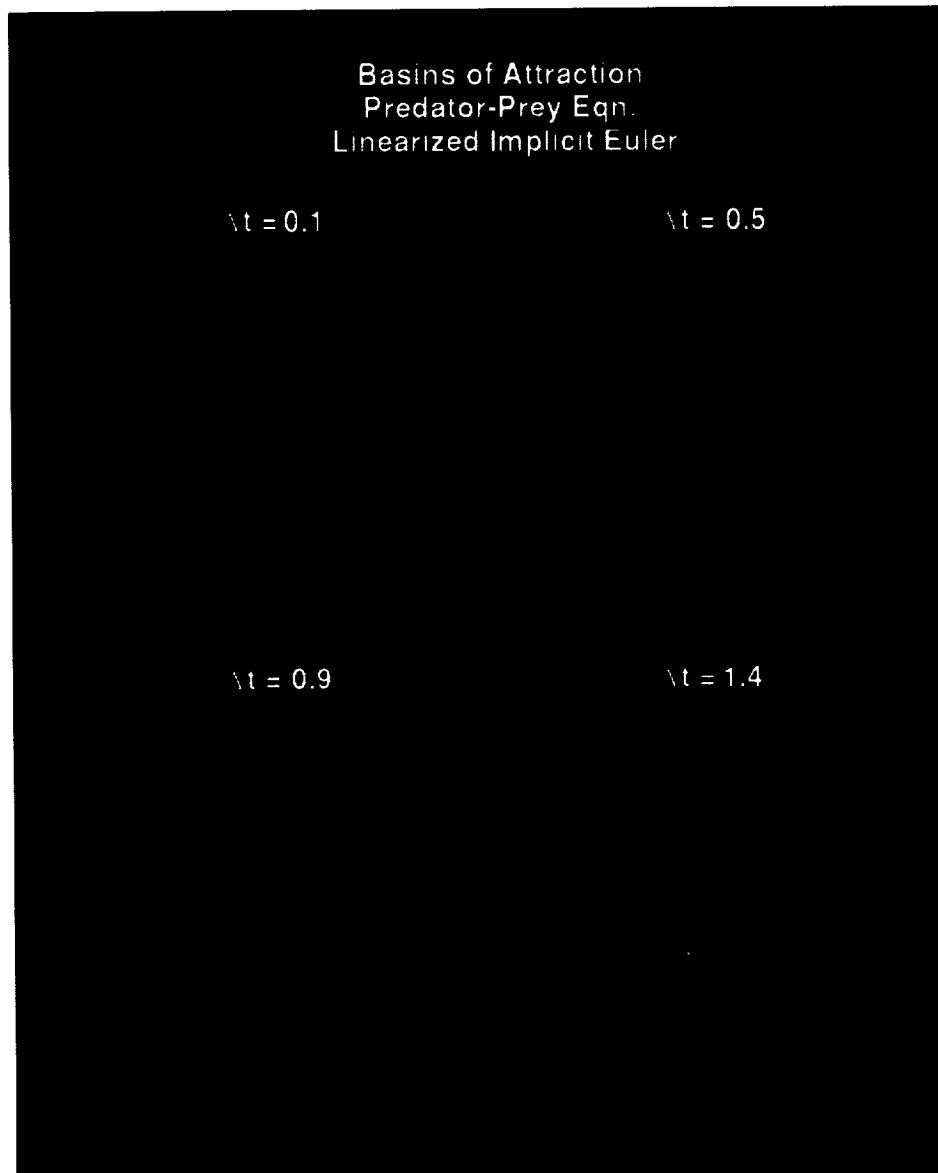
$\lambda t = 0.9524$

$\lambda t = 1.2$

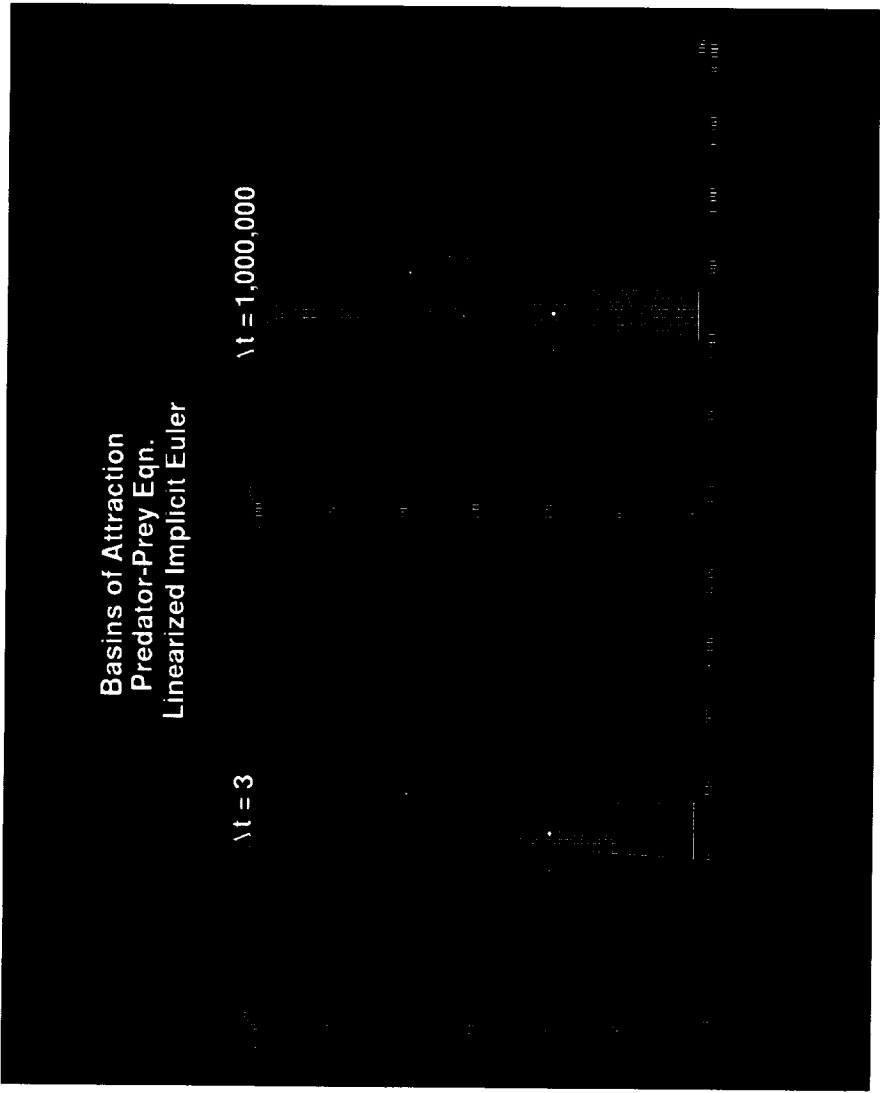
Color Plate XIII **Figure 6.15** (Continued) (See H.C. Yee and P. K. Sweby.)



Color Plate XIV Figure 6.16 (See H.C. Yee and P. K. Sweby.)



Color Plate XV **Figure 6.17** (See H.C. Yee and P. K. Sweby.)



Color Plate XV **Figure 6.17 (Continued)** (See H.C. Yee and P. K. Sweby.)

Basins of Attraction
Predator-Prey Eqn.
Linearized Trapezoidal

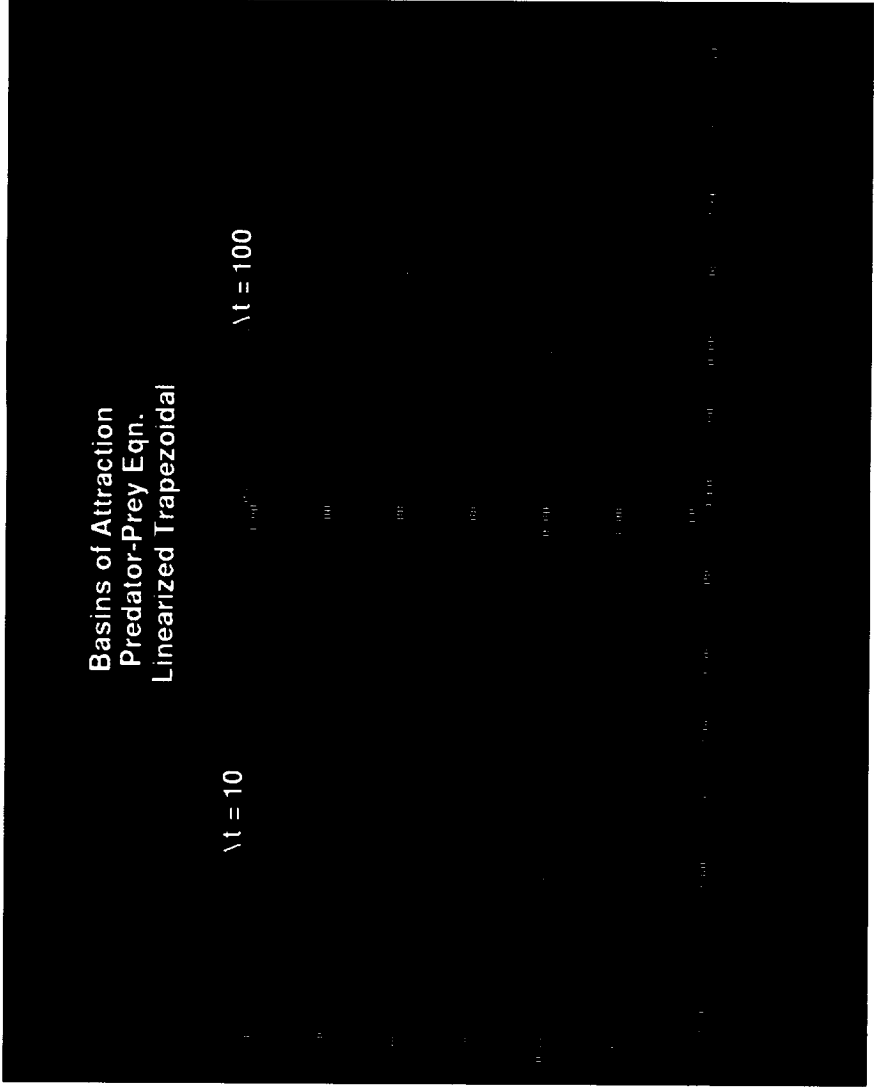
$\lambda t = 0.1$

$\lambda t = 0.5$

$\lambda t = 1.4$

$\lambda t = 3$

Color Plate XVI Figure 6.18 (See H.C. Yee and P. K. Sweby.)

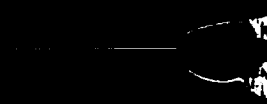


Color Plate XVI Figure 6.18 (Continued) (See H.C. Yee and P. K. Sweby.)

Bifurcation Diagrams & Basins of Attraction
Viscous Burgers Eqn., $\varepsilon = 0.1$, $\nu = 0.333$
(Central Difference in Space)

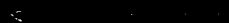
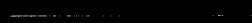
Modified Euler

Improved Euler



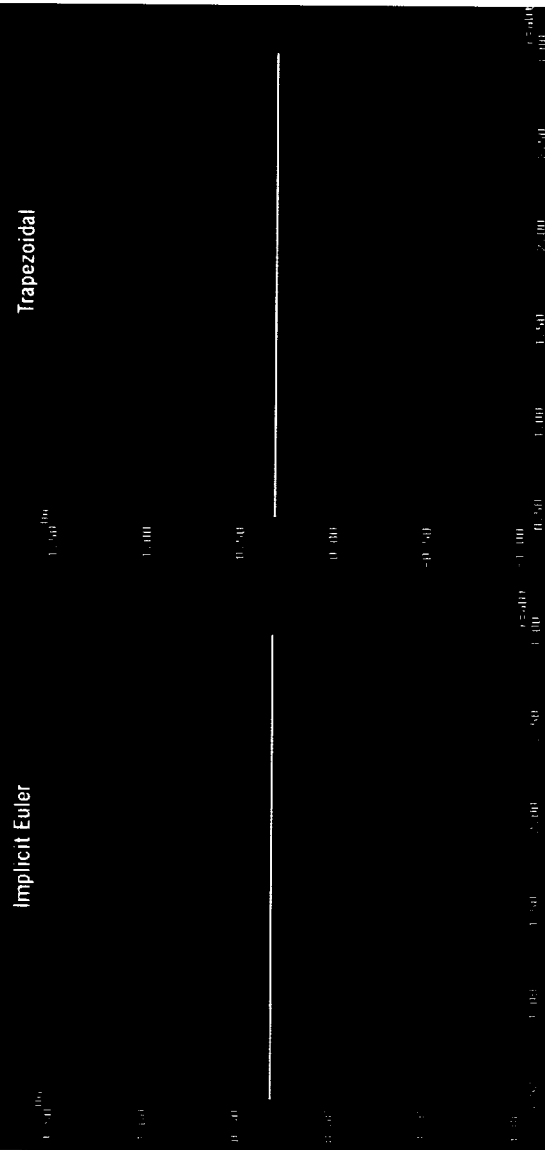
Kutta

R-K 4

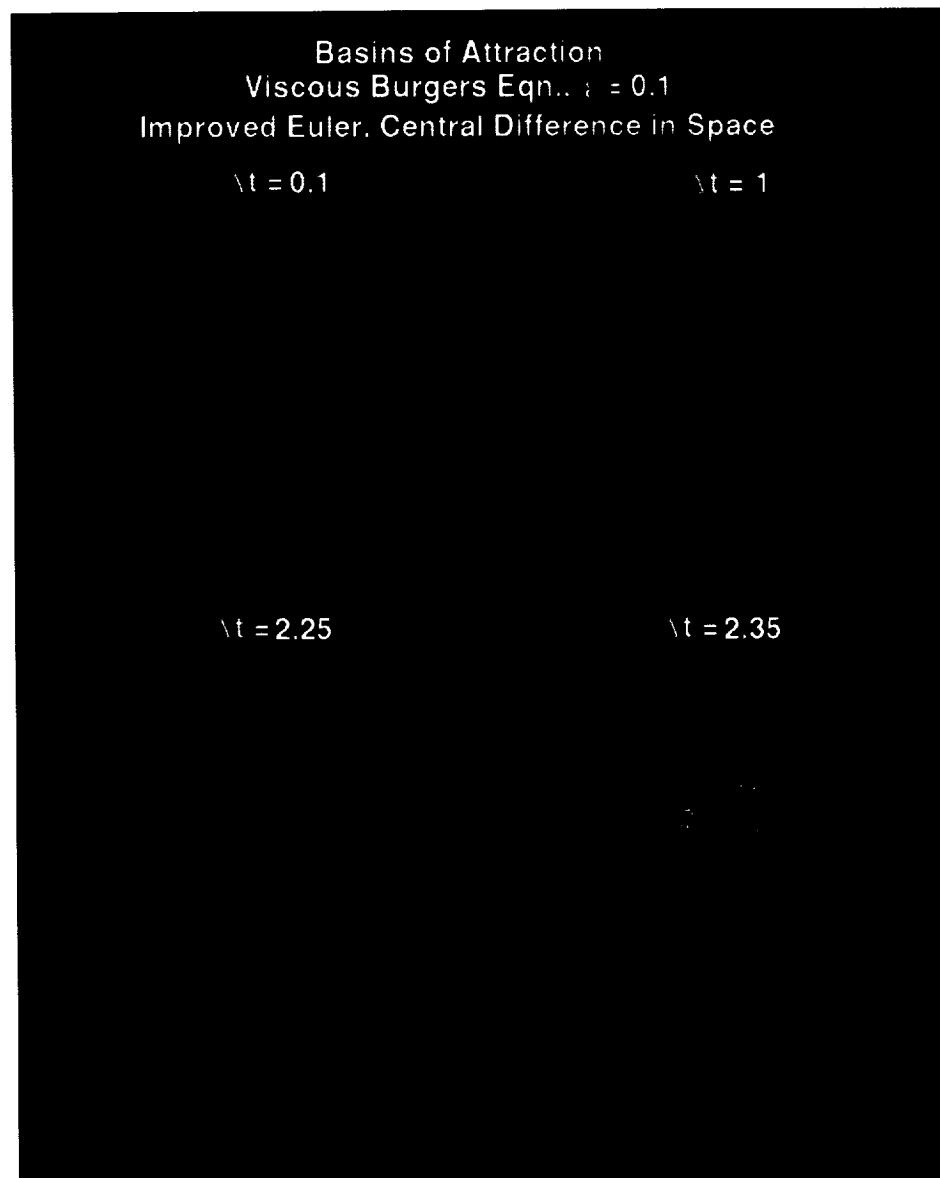


Color Plate XVII Figure 6.19 (See H.C. Yee and P. K. Sweby.)

Bifurcation Diagrams & Basins of Attraction Viscous Burgers Eqn., $\varepsilon = 0.1$, $\nu = 0.333$ (Central Difference in Space)



Color Plate XVIII Figure 6.20 (See H.C. Yee and P. K. Sweby.)



Color Plate XIX **Figure 6.21** (See H.C. Yee and P. K. Sweby.)

Basins of Attraction
Viscous Burgers Eqn., $\varepsilon = 0.1$
Kutta (R-K 3), Central Difference in Space

$\Delta t = 0.1$

$\Delta t = 1.0$

$\Delta t = 1.826$

$\Delta t = 1.85$

$\Delta t = 2.75$

$\Delta t = 2.785$

Color Plate XX

Figure 6.22 (See H.C. Yee and P. K. Sweby.)

Basins of Attraction
Viscous Burgers Eqn., $\nu = 0.1$
Linearized Implicit Euler, Central Difference in Space

$\Delta t = 0.1$

$\Delta t = 1.1$

$\Delta t = 1.5$

$\Delta t = 3$

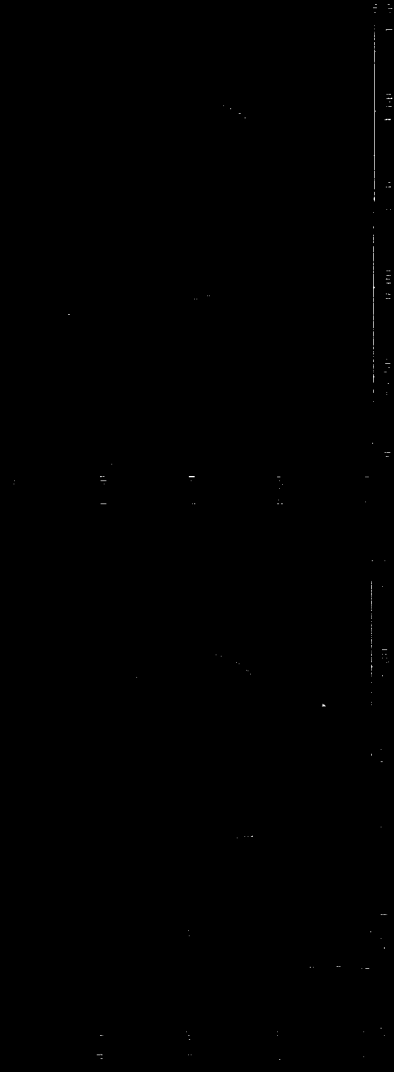
Color Plate XXI

Figure 6.23 (See H.C. Yee and P. K. Sweby.)

Basins of Attraction
Viscous Burgers Eqn., $\epsilon = 0.1$
Linearized Implicit Euler, Central Difference in Space

$\Delta t = 10$

$\Delta t = 1,000,000$



Color Plate XXI Figure 6.23 (Continued) (See H.C. Yee and P. K. Sweby.)

Basins of Attraction
Viscous Burgers Eqn., $\nu = 0.1$
Linearized Trapezoidal, Central Difference in Space

$\Delta t = 0.1$

$\Delta t = 10$

$\Delta t = 200$

$\Delta t = 500$

Color Plate XXII

Figure 6.24 (See H.C. Yee and P. K. Sweby.)

Basins of Attraction
Viscous Burgers' Eqn., $\epsilon = 0.1$
Central Difference in Space

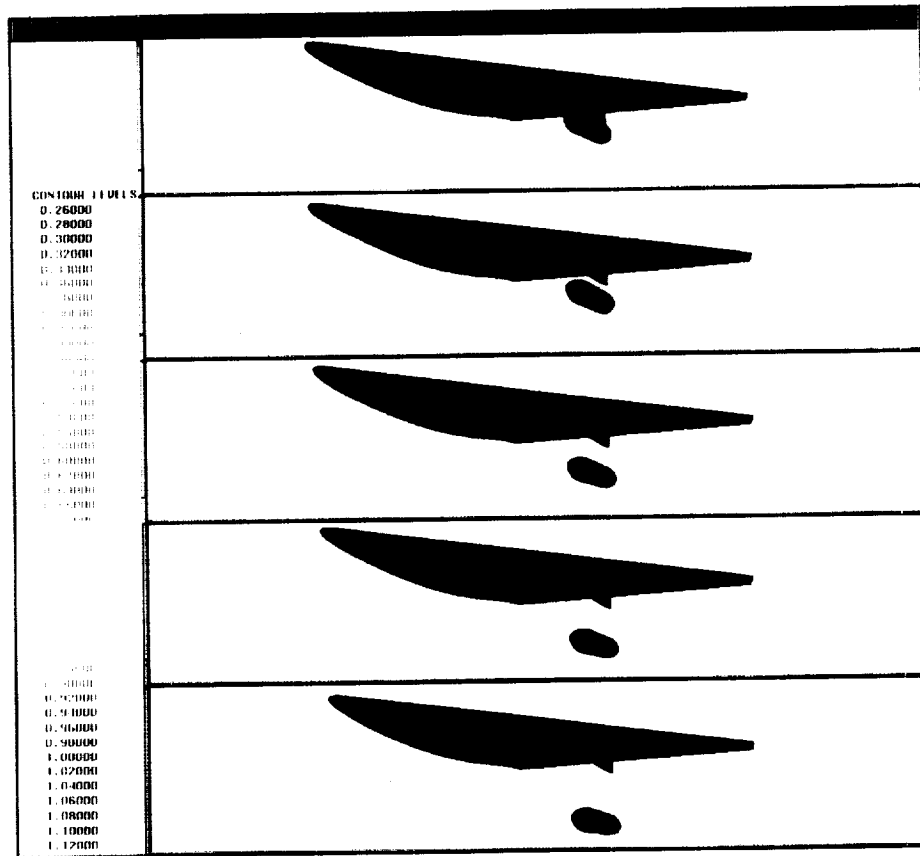
Implicit Euler, $\Delta t = 1$

Newton



Color Plate XXIII

Figure 6.25 (See H.C. Yee and P. K. Sweby.)



Color Plate XXIV

Figure 10 Computed surface pressure contours with store located in captive position and moving through 0.6, 1.0, 1.6, and 2.0 store diameters below the pylon. (See A. Arabshahi and D. L. Whitfield)